NASA Technical Memorandum 101058

The Acoustics of a Small-Scale Helicopter Rotor in Hover

Cahit Kitaplioglu

April 1989

National Aeronautics and
Space Administration

NASA Technical Memorandum 101058

The Acoustics of a Small-Scale Helicopter Rotor in Hover

Cahit Kitaplioglu, Ames Research Center, Moffett Field, California

April 1989

National Aeronautics and
Space Administration

Ames Research Center
Moffett Field, California 94035

SYMBOLS

B	number of blades
c	blade chord (cm)
c_s, CSOUND	speed of sound (m/s)
D	rotor diameter (m)
dBA	A-weighted sound pressure level (SPL) (with respect to 2×10^{-5} N/m^2)
M_{tip}	tip Mach number in hover
OASPL	overall sound pressure level (with respect to 2×10^{-5} N/m^2)
Q	rotor torque (N-m)
r	microphone distance (m)
R	rotor radius (m)
S_R	rotor blade area (m^2)
T	rotor thrust (N)
V_{tip}	tip velocity in hover (m/sec)
ρ	air density (kg/m^3)
$\sigma = \frac{S_R}{R^2}$	rotor solidity
ψ	azimuth angle (deg), measured from downstream direction, positive in direction of rotor rotation
θ,THETA	elevation angle (deg), measured from rotor plane, positive in direction of wake
θ_c, COLL	collective pitch angle (deg)
$\Omega = RPM * \frac{\pi}{30}$	rotor rotational speed (sec^{-1})

$$C_T = \frac{T}{\rho \pi R^2 (\Omega R)^2}$$ rotor thrust coefficient

$$C_Q = \frac{Q}{\rho \pi R^2 (\Omega R)^2 R}$$ torque coefficient

$$FMERIT = \frac{C_T^{3/2}}{\sqrt{2} C_Q}$$ rotor figure of merit

SUMMARY

A 2.1-m diameter, 1/6-scale model helicopter main rotor was tested in hover in the test section of the NASA Ames 40- by 80-Foot Wind Tunnel. The primary objective of the test was to obtain performance and noise data on a small-scale rotor at various thrust coefficients and tip Mach numbers for comparison with existing data on similar full-scale helicopter rotors. These data form part of a data base to permit the estimation of scaling effects on various rotor noise mechanisms. A secondary objective was to contribute to a data base that will permit the estimation of facility effects on acoustic testing. Acoustic 1/3-octave-band spectra are presented, together with variation of overall acoustic levels with rotor performance, microphone distance, and directivity angle.

INTRODUCTION

There are advantages in using small-scale instead of full-scale rotors for exploratory research in rotor aerodynamics and acoustics. Small-scale models are less costly to fabricate and generally require less time and manpower to test. Small-scale wind tunnels are also widely available. However, small-scale models have a minimum size that will yield accurate aerodynamic and acoustic information. This restriction arises from limitations in geometric and dynamic scaling, fabrication, and hardware and instrumentation size requirements. In addition, geometrical scaling will require that proportionately higher acoustic frequencies be dealt with, although it is not presently known whether all sources of rotor noise scale geometrically. Therefore, microphone and tape-recorder frequency response limitations also restrict the smallest practical scale. Rotor systems that are about 1/5- to 1/7-scale are widely used in aerodynamic, dynamic, and acoustic testing. In general, these scale models are compatible with existing test facilities. Because of these limitations, it is important to quantify scale effects on rotor aerodynamics and performance, and on the different noise generation mechanisms before small-scale test results can be used to infer full-scale behavior with confidence. An extensive, consistent data base will permit a definitive evaluation of scaling effects.

Several studies of the scaling of helicopter rotor acoustics have been reported. Schmitz and his coworkers (refs. 1-3) made extensive scaling studies on two-bladed rotors. Their main focus was on impulsive noise arising from both compressibility and blade-vortex interaction effects.

The work of Shenoy et al. (ref. 4) deals with very small-scale models. As pointed out earlier, aside from scaling questions, there are practical disadvantages to testing at such small scales. Shenoy's results indicate that 1/20-scale is too small to yield consistent data, except for relative trends at high tip Mach numbers.

Sternfeld and Schaeffer (ref. 5) report on the scaling of acoustic data obtained in hard-walled tunnels. The unique contribution of this study was the comparison of small-scale and full-scale data for tandem

rotors, as well as presenting data on single rotors. Sternfeld and Schaeffer's data reduction and analysis technique involves extensive corrections to data to account for differences in microphone location, reverberation effects, the effect of tunnel velocity, and differences in tip speed. The results indicate that even when the scaled 1/2-peak-to-peak levels agree quite closely, the waveforms and spectra of tandem rotors show radical differences. Since the full-scale and small-scale data used in this study were obtained in different facilities, environmental and installation effects undoubtedly play an important role and may help explain some of the differences. For single rotors, whereas there are large differences in peak amplitudes, the waveforms show similarities at high thrust but differ markedly at low thrust. The spectra differ significantly in all cases. Clearly, the 1/2-peak-to-peak level is not a good characteristic for comparing acoustic data.

This brief review of previous work indicates that there are still significant questions about the validity of extrapolating small-scale data up to full scale for all acoustic generation and propagation mechanisms of modern helicopter rotors. The facilities of the National Full-Scale Aerodynamic Complex (NFAC) provide the unique capability of testing both full-scale and small-scale rotors in the same facility as well as the capability of testing a given rotor in facilities of different sizes. A series of tests is being conducted to evaluate the extent to which small-scale experiments can reproduce full-scale effects. This report presents acoustic data from a hover test recently conducted in the test section of the 40- by 80-Foot Wind Tunnel. A 1/6-scale, four-bladed rotor with a current-generation airfoil was utilized. Future tests in this series will include hover experiments at the Ames Outdoor Aerodynamic Research Facility and forward flight tests in the 7- by 10-Foot Wind Tunnel and the 40- by 80- /80- by 120-Foot Wind Tunnel. These tests will utilize both small-scale and full-scale models as appropriate.

DESCRIPTION OF TEST

The primary objective of the test was to obtain hover performance and acoustic data on a 1/6-scale rotor that can then be compared to data obtained during future, planned tests of a similar full-scale rotor. A secondary objective of the test was to contribute to a data base which can be used to evaluate the relative effect of a specific facility on rotor acoustic data.

The small-scale rotor hover test was performed in the test section of the NASA Ames 40- by 80-Foot Wind Tunnel. Use of the large tunnel test section as a hover chamber has several advantages. First, the environment is easily controlled, obviating the need to wait for calm wind conditions as in outdoor testing. In addition, the tunnel test section has an acoustic lining which proved to do a good job in minimizing floor and wall reflections.

A 2.1-m diam four-bladed rotor (table 1 gives the characteristics) was mounted approximately 3 m above the tunnel floor on the Ames Rotor Test Rig (RTR) (fig. 1). The rotor is representative of the Sikorsky S-76 rotor. The carbon-and-fiberglass blades are geometrically and dynamically similar to the full-scale rotor but have rectangular tips. The fully articulated rotor head has remotely actuated collective and cyclic pitch controls. Lead-lag, coning, and cyclic flapping are measured with variable potentiometers. All data were obtained with the rotor trimmed to minimize cyclic flapping.

The RTR incorporates a six-component internal strain-gauge balance to measure steady-state rotor forces and moments. In addition, the rotor torque is measured by a load cell. Several sets of blade strain gauges and a number of accelerometers on both the metric and nonmetric portions of the RTR are used to monitor loads and vibration levels during testing to ensure safe operation. All the performance and safety data were appropriately filtered, digitized, and recorded on the data-acquisition-system computer. Important parameters, such as rotor rotational tip Mach number and thrust (C_T/σ) were displayed in real time, permitting test conditions to be accurately established.

The rotor was tested in a thrust-down/wake-up configuration, eliminating ground-effect influences and allowing the test stand to be located on the low-velocity inflow side of the rotor disk. The wake exhausted to a large unobstructed space above the model (more than four rotor diameters in extent). The clamshell overhead doors of the test section were closed.

The acoustic field of the rotor was measured over a matrix of operating conditions by an array of microphones located at distances of 1, 1.5, and 2 rotor diam and at angles of 10°, 30°, and 45° "below" the rotor plane (fig. 2 and table 2), which actually correspond to physical locations above the rotor plane for the thrust-down mode. One microphone was placed "above" the rotor to check for asymmetry of acoustic propagation for sources radiating near the plane of the rotor. Two microphones were placed on either side of the main array to check for azimuthal symmetry of the acoustic field in hover.

The microphone placement scheme was chosen to include the estimated directional locations appropriate for major hover noise-generation mechanisms. Thickness noise is radiated mostly near the rotor plane. Thus the two image microphones above and below the rotor plane allow an evaluation of asymmetrical radiation patterns in thickness noise. The microphones placed at larger angles measured rotational loading noise caused by thrust and torque. Turbulence ingestion noise, which is important in hover, is expected to have a broad directivity "below" the rotor and was expected to be adequately captured by the 45° microphone. The latter is also well placed for detecting blade-vortex interaction noise, if present.

Acoustic signals were measured with 1.27-cm, free-field response-type microphones (B&K Type 4133/2619), mounted such that their axes were parallel with the tunnel axis and facing the rotor. Since the exact locations of the noise sources were not known, this setup provides standardized orientations for comparison with other experiments. Standard protective grids were placed over the microphone cartridges. Windscreens were not used because no appreciable wake flow was estimated to be present at the microphone positions.

Microphone outputs were recorded on a 14-track, FM-instrumentation tape recorder (Ampex 1300A), set up to IRIG Wideband I standards at 30 in./sec (76.2 cm/sec). Approximately 60 sec of data were recorded at each run condition. The system frequency response was good to approximately 20 kHz as determined by an extensive set of measurements during test setup by electronically injecting a wide-band white noise signal into each cathode follower. During testing, a piston-phone calibration was performed on each microphone every day before starting any runs. The microphone signals were not filtered in any way. Time code, 1/rev, and 1024/rev signals were also recorded. Test conditions and amplifier information were annotated on the edge track. Figure 3 is a sketch of the acoustic data acquisition system.

The 40- by 80-Foot Wind Tunnel test section has an acoustic lining installed on the floor (10 cm thick), and ceiling and sides (15 cm thick), consisting of fiberglass batting and cloth covered with

perforated steel decking. Pulse reflection measurements (ref. 6) indicate that with no flow through the test section and at incidence angles less than 45° (this is the case of interest for this test geometry) absorption coefficients greater than 0.8 are obtained at frequencies above approximately 200 Hz, decreasing to a value of approximately 0.7 at 125 Hz (fig. 4). Absorption coefficients greater than 0.9 were measured above 1 kHz at all directivity angles.

The lining performed well in absorbing mid- and high-frequency wall reflections, as determined by a series of impulsive source measurements made before rotor testing began. This measurement procedure consisted of firing a starter pistol and recording the impulsive transient waveform. The pistol was fired from several positions corresponding to different source locations. For most microphones and source positions, only a single pulse corresponding to the incident wave was observed; there were no significant secondary pulses. For a few of the microphones, a secondary pulse having a relatively high amplitude was also observed, indicating the presence of a reflective surface. From the measured delay times, the probable reflection points were identified as localized flat areas such as the bases of some of the microphone stands and the RTR mount. After those areas were covered with 7.5-cm-thick absorptive foam, these reflections were eliminated. Figure 5 shows typical time traces before and after local treatment with absorptive foam. We judged the final test setup to be acoustically quite good. No attempt was made to measure the reverberation characteristics of the tunnel test section using steady sources.

TEST MATRIX

The primary variables during the hover test were tip Mach number and collective pitch. Operating conditions were chosen to cover a wide range of performance parameters. Table 3 is a compilation of test conditions for each data run point.

RESULTS

After completion of the test, the acoustic data recorded on tape were reduced using a GenRad GR 1995 1/3-Octave Band Analyzer. The analyzer was calibrated for each microphone and each run by making use of the calibrated piston-phone signal of known amplitude recorded during testing. The integration time was set to 60 sec for a majority of the data points to make use of as much of the recorded data as possible (however, care was taken to avoid tape start/stop transients). A relatively long averaging time was chosen because a preliminary review of the data indicated the presence of non-stationary characteristics, a common feature of hover acoustic data. Averaging the data over a long time record was deemed the best method for characterizing the signal without resorting to much more sophisticated statistical techniques. Such techniques are presently under evaluation. As indicated on each plot in appendix A, some data points required shorter integration times because of shorter available record lengths.

The nonstationarity is related primarily to the recirculation patterns existing in the confined environment of the test section, even though its dimensions are large compared to model size. Piziali and Felker (ref. 7) have shown the sensitivity of rotor aerodynamics to flow circulation patterns in a hover chamber and Amiet et al. (refs. 8 and 9) have demonstrated the sensitivity of rotor acoustics to inflow unsteadiness in hover. The postulated mechanism is the stretching of turbulent eddies leading to a blade/eddy encounter,

highly correlated blade-to-blade in hover. The resulting acoustic radiation is phase additive (coherent), producing high amplitudes.

Table 4 lists the operating conditions, rotor performance parameters, and corresponding OASPL and dBA values for microphones in the main array (i.e., not including the sideline microphones) for the two data runs for which data have been reduced.

Appendix A contains a representative set of 1/3-octave band plots (as well as integrated unweighted OASPL and A-weighted dBA values) for the test parameters covered during runs 16 and 19, for microphones 5, 7, 8, and 9 (figs. A1-A4). These cover the range of distances and directivity angles studied during the test.

Appendix B contains plots of OASPL and dBA trends as functions of test parameters. The thrust and figure-of-merit trend plots include polynomial curve fits of second- and third-order, respectively (figs. B1-B12). The order of the polynomials were chosen by trial and error on the basis of the maximum correlation coefficient at minimum order. Curve fits are not included for the tip Mach number trend plots because data were obtained at only two values.

Appendix C contains plots of acoustic levels at several frequency bands as functions of distance and directivity angle for various operating conditions (figs. C1-C4). Each of these plots also includes a curve, proportional to $(r/D)^{-1}$, which indicates free-field decay. The SPL level of this curve is arbitrary and was chosen for convenient comparison with the data.

DISCUSSION

The trend plots indicate a small increase in acoustic levels with tip Mach number. This is as expected since the tip Mach numbers during the test were relatively low, below the drag divergence Mach number of 0.76. On the other hand, because a wide range of thrust conditions were set during the test, more variation in acoustic levels is seen with thrust changes, especially for $C_T/\sigma > 0.05$.

The acoustic radiation pattern is frequency dependent, as expected. At the blade passage frequency (112 -128 Hz depending on rpm, which is within the 125-Hz 1/3-octave band) the acoustic directivity is quite broad at the lower tip speed but becomes noticeably more directional near the plane of the rotor at the higher tip speed. As thrust is increased, however, this directionality is somewhat moderated. At higher frequencies, on the other hand, acoustic radiation is distinctly greater at an angle 45° to the rotor plane. This is most pronounced at the low-tip-speed, low-thrust condition.

From these trends one can infer that thickness noise even at these low tip Mach numbers contributes significantly to the overall acoustic radiation. Loading noise, as expected, increases in amplitude away from the rotor plane and is more directional at $\theta = 45°$. The directivity lobe of loading noise grows "fatter" at higher thrust levels (i.e., there is less difference in acoustic levels with directivity change). This can be attributed to the increase in the induced drag dipole noise-component at higher thrust conditions, which is confirmed by the high sensitivity of acoustic levels to variations in rotor figure of merit for $FM > 0.5$.

The plots in appendix C show the behavior of the acoustic field near the rotor plane as a function of distance. The 5-kHz data exhibit a noticeable reverberation effect (they have a shallower slope than $(r/D)^{-1}$) at the lower tip Mach number. This is absent at the higher tip Mach number. The two lowest frequencies, approximately the first two blade passage harmonics, have considerably steeper slopes than free-field behavior, indicating that the measurement of these low frequencies were not made far enough from the source.

Further discussion of the data, including comparison to some full-scale data, can be found in reference 10.

CONCLUSIONS

Acoustic 1/3-octave band spectra were presented, followed by acoustic levels in terms of OASPL and dBA as functions of rotor operating conditions, and acoustic levels at several 1/3-octave band frequencies as functions of distance and directivity angle.

The data displayed nonstationary characteristics related to wake recirculation effects. The acoustic levels were more sensitive to thrust variations than to tip speed variations because the data were obtained at below the drag divergence Mach number. Some of the data displayed reverberant effects. Also, there were indications that the lower frequencies were not measured under far-field conditions even though several microphones were placed at distances of two rotor diameters from the hub.

REFERENCES

1. Schmitz, F.H.; Boxwell, D.A.; Lewy, S.; and Dahan, C.: A Note on the General Scaling of Helicopter Blade-Vortex Interaction Noise. Presented at the 38th Annual National Forum of the American Helicopter Society, Anaheim, CA, May 1982.

2. Boxwell, D.A.; Schmitz, F.H.; Splettstoesser, W.R.; and Schultz, K.J.: Helicopter Model Rotor Blade Vortex Interaction Impulsive Noise: Scalability and Parametric Variations. Presented at the 10th European Rotorcraft Forum, the Hague, Netherlands, Aug. 1984.

3. Schmitz, F.H.; Boxwell, D.A.; Splettstoesser, W.R.; and Schultz, K.J.: Model-Rotor High Speed Impulsive Noise: Full-Scale Comparisons and Parametric Variations. Vertica, vol. 8, no. 4, 1984, pp. 395-422.

4. Shenoy, R.K.; Kohlhepp, F.W.; and Leighton, K.P.: Acoustic Characteristics of 1/20-Scale Model Helicopter Rotors. NASA CR-177355, Aug. 1986.

5. Sternfeld, H.; and Schaeffer, E.G.: An Investigation of Rotor Harmonic Noise by the Use of Small Scale Wind Tunnel Models. NASA CR-166337, Jan. 1982.

6. Soderman, P.T.: Oblique Incidence Sound Absorption of Porous Materials Covered by Perforated Metal and Exposed to Tangential Airflow. Internoise 82 Proceedings, San Francisco, 1982, pp. 401-404.

7. Piziali, R.A.; and Felker, F.F.: Reduction of Unsteady Circulation in Hovering Model Helicopter Rotor Testing, J. American Helicopter Society, Jan. 1987.

8. Paterson R.W.; and Amiet, R.K.: Noise of a Model Helicopter Rotor Due to Ingestion of Turbulence. NASA CR-3213, Nov. 1979.

9. Simonich, J.; Schlinker, R.; and Amiet, R.: Experimental Assessment of a Turbulence Ingestion Noise Theory. Presented at the 44th Annual Forum of the American Helicopter Society, Washington, DC, June 1988.

10. Kitaplioglu, C.; and Shinoda, P.: Hover and Forward Flight Acoustics and Performance of a Small-Scale Helicopter Rotor System. NASA TM-86786, Dec. 1985.

TABLE 1.– MODEL ROTOR CHARACTERISTICS

Radius, R	1.07 m
Chord, c	6.3 cm
Airfoil	SC1095
Number of blades, B	4
Twist	–10° linear
Solidity, σ	0.075

TABLE 2.– MICROPHONE ARRAY

Microphone No.	r/D	ψ	θ
1	1.0	135°	–45°
2	1.0	210°	–10°
3	1.0	150°	–10°
4	1.0	180°	–10°
5	1.0	180°	+10°
6	1.5	180°	+10°
7	2.0	180°	+10°
8	2.0	180°	+30°
9	2.0	180°	+45°

TABLE 3.– TEST MATRIX

Run No.	Point	M_{tip}	θ_c
16	1 - 4	Zero and calibration points	
	5	0.55	1.0
	6	0.55	3.0
	7	0.55	5.0
	8	0.55	7.0
	9	0.55	9.0
	10	0.55	11.0
	11	0.55	12.9
	12	0.55	10.9
	13	0.55	9.0
	14	0.55	6.9
	15	0.55	5.1
	16	0.55	2.9
	17	0.55	1.1
	18	Zero point	
18	1-4	Zero and calibration points	
	5	0.63	1.6
	6	0.63	3.1
	7	0.63	5.0
	8	0.63	7.0
	9	0.63	9.0
	10	0.63	11.0
	11	0.63	12.0
	12	0.63	11.0
	13	0.63	9.0
	14	0.63	7.0
	15	0.63	5.0
	16	0.63	3.1
	17	0.63	1.5
	18	Zero point	
19	1 - 4	Zero and calibration points	
	5	0.63	1.5
	6	0.63	3.1
	7	0.63	5.0
	8	0.63	7.0
	9	0.63	9.0
	10	0.63	11.0
	11	0.63	12.0
	12	0.63	11.0
	13	0.63	9.0
	14	0.63	7.0
	15	0.63	5.0
	16	0.63	3.1
	17	0.63	1.5
	18	Zero point	

TABLE 4.– RTR/40 × 80 HOVER TEST DATA

Rotor test conditions									Microphone No. 4 r/D = 1.0, θ = –10.0	
Run	Point	M_{tip}	V_{tip} (m/s)	RPM	Coll (deg)	CT/S	CQ/S	FMERIT	dBA	OASPL
16	5	0.55	188.8	1690	1.0	0.00	0.001	0.02	91.1	94.1
16	6	0.55	188.8	1690	3.0	0.01	0.002	0.18	93.0	95.7
16	7	0.55	188.2	1685	5.0	0.03	0.002	0.42	90.5	95.8
16	8	0.55	188.5	1687	7.0	0.05	0.004	0.59	89.5	96.5
16	9	0.55	188.5	1687	9.0	0.07	0.006	0.68	93.4	98.3
16	10	0.55	188.0	1683	11.0	0.10	0.008	0.73	95.5	100.1
16	11	0.55	188.1	1684	12.9	0.12	0.011	0.71	104.0	107.6
16	12	0.55	188.8	1690	10.9	0.10	0.008	0.72	95.0	99.7
16	13	0.55	188.4	1686	9.0	0.07	0.006	0.68	91.8	97.8
16	14	0.55	188.6	1688	6.9	0.05	0.004	0.60	91.5	97.0
16	15	0.55	188.4	1686	5.1	0.03	0.002	0.41	90.1	95.9
16	16	0.55	188.6	1688	2.9	0.01	0.002	0.16	93.6	96.0
16	17	0.55	188.7	1689	1.1	0.00	0.001	0.01	90.8	93.8
19	5	0.63	215.3	1927	1.5	0.01	0.001	0.07	95.5	100.0
19	6	0.63	215.3	1927	3.1	0.02	0.002	0.25	95.2	101.0
19	7	0.63	215.3	1927	5.0	0.04	0.003	0.48	96.0	102.0
19	8	0.63	215.3	1927	7.0	0.06	0.004	0.64	96.0	102.9
19	9	0.63	215.3	1927	9.0	0.08	0.007	0.70	99.1	104.0
19	10	0.63	215.2	1926	11.0	0.11	0.009	0.71	104.2	107.8
19	11	0.63	214.9	1924	12.0	0.12	0.011	0.70	108.0	110.2
19	12	0.63	215.4	1928	11.0	0.11	0.010	0.72	104.3	107.6
19	13	0.63	215.2	1926	9.0	0.08	0.006	0.69	99.8	104.9
19	14	0.63	215.3	1927	7.0	0.06	0.004	0.66	96.7	102.3
19	15	0.63	215.2	1926	5.0	0.03	0.003	0.48	94.0	101.7
19	16	0.63	215.3	1927	3.1	0.02	0.002	0.26	95.0	100.6
19	17	0.63	215.1	1925	1.5	0.01	0.001	0.07	95.9	99.8

TABLE 4.– CONCLUDED

Microphone No. 5 r/D = 1.0, θ = 10.0		Microphone No. 6 r/D = 1.5, θ = 10.0		Microphone No. 7 r/D = 2.0, θ = 10.0		Microphone No. 8 r/D = 2.0, θ = 30.0		Microphone No. 9 r/D = 2.0, θ = 45.0	
dBA	OASPL	dBA	OASPL	dBA	OASPL	dBA	OASPL	dBA	OASPL
91.0	94.2	86.6	89.3	84.1	86.5	87.8	88.5	90.6	91.0
94.0	95.5	89.3	90.6	86.8	87.8	90.0	90.0	93.0	92.4
91.9	94.9	87.3	90.0	85.1	87.5	87.8	89.0	90.8	91.1
91.0	96.0	86.3	91.0	84.0	87.8	86.1	88.5	89.0	90.1
96.0	100.8	91.6	96.0	88.8	92.1	90.5	93.0	92.8	94.0
98.0	104.0	93.0	98.2	90.0	94.0	91.0	94.7	93.0	96.0
107.6	111.9	103.2	107.6	100.0	104.0	100.8	105.1	101.7	106.0
98.1	103.8	93.5	98.3	90.5	94.7	91.8	94.9	94.0	96.0
94.5	99.6	90.0	94.9	87.2	91.2	89.0	92.4	91.2	93.1
93.1	96.8	89.0	92.6	87.0	89.8	89.0	91.0	92.0	92.9
91.0	93.8	87.0	90.0	85.1	87.1	88.0	89.0	91.7	92.0
95.1	96.1	90.2	91.2	88.0	88.8	91.5	91.5	94.5	94.1
90.4	95.3	86.0	88.7	84.0	86.3	87.4	88.1	90.8	91.0
97.6	100.3	93.0	95.5	90.7	93.5	93.7	94.0	96.0	96.2
96.8	99.4	92.0	95.4	89.1	93.2	91.1	91.8	94.2	94.2
97.2	100.0	92.0	95.9	89.2	93.6	91.9	93.0	96.4	96.4
96.7	103.0	92.8	98.8	90.4	96.0	92.0	96.0	94.0	96.3
100.9	107.0	96.3	102.0	94.0	99.0	94.9	98.9	96.1	98.3
106.2	110.9	101.8	105.8	99.0	102.3	99.7	102.3	100.5	102.3
110.6	114.0	106.0	109.1	103.0	106.2	104.0	106.5	104.6	107.0
106.3	111.3	101.6	106.3	98.9	103.0	99.6	102.5	100.7	102.4
101.0	106.9	97.0	102.0	94.3	98.6	95.2	99.1	96.4	98.7
98.0	103.0	93.6	98.6	91.1	95.2	92.8	96.0	94.3	95.6
95.0	99.2	89.7	95.0	87.6	92.9	89.7	91.7	93.5	94.0
96.0	99.0	91.0	94.7	89.0	93.0	91.0	91.6	94.0	94.0
98.0	100.5	93.0	95.7	91.0	93.7	94.0	94.2	96.3	96.5

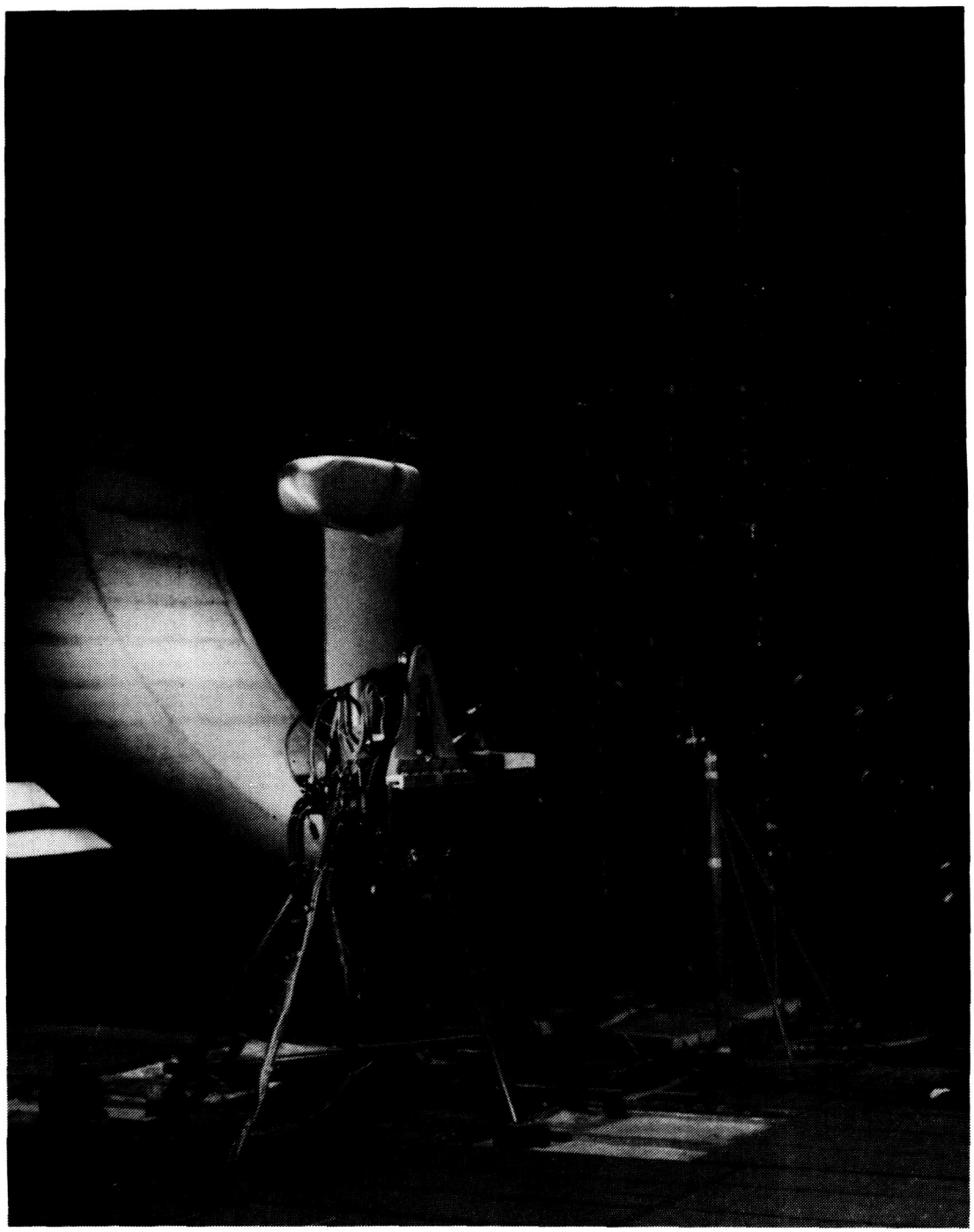

Figure 1.– Rotor test rig (RTR) in Ames 40- by 80-Foot Wind Tunnel test section.

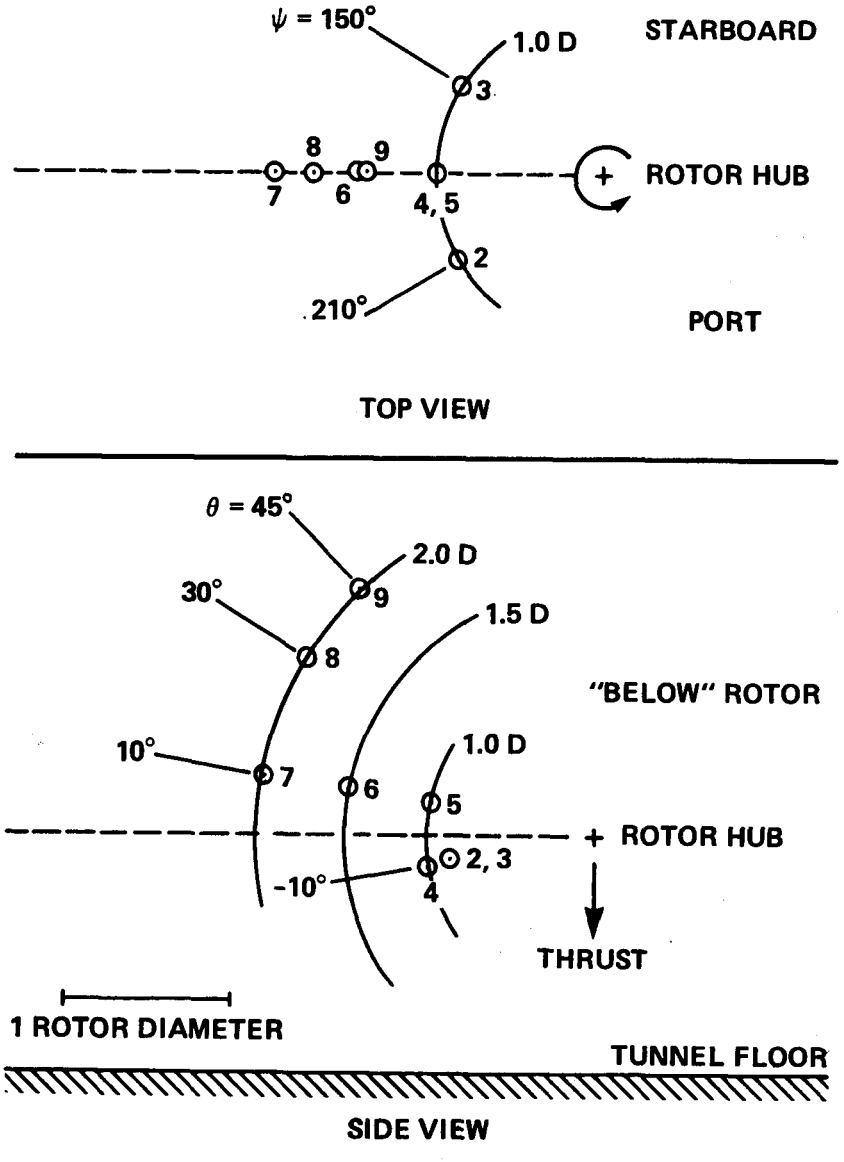

Figure 2.– Microphone array for hover test.

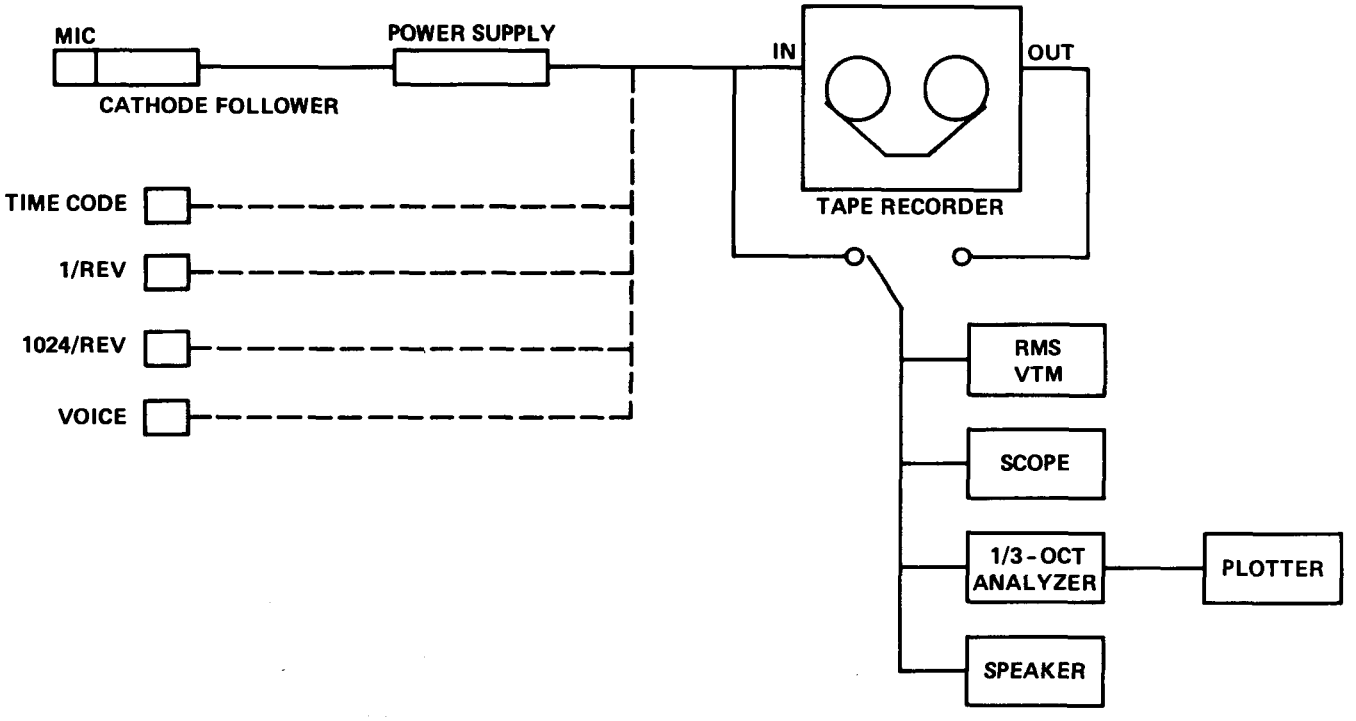

Figure 3.– Acoustic data acquisition and reduction system.

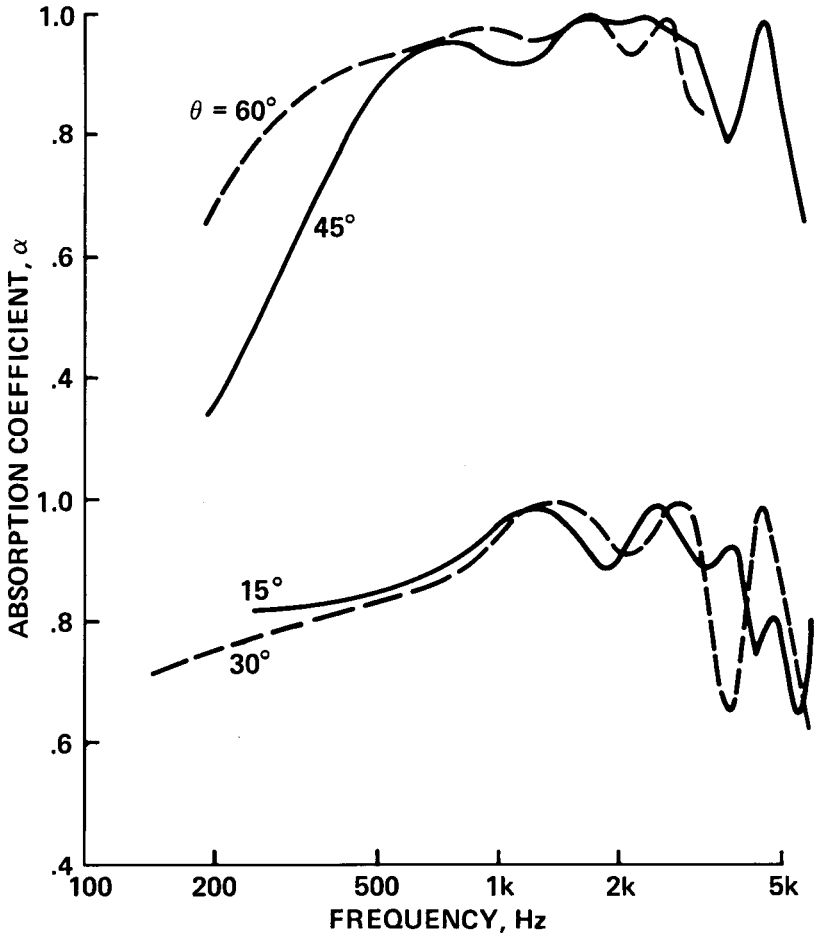

Figure 4.– Ames 40- by 80-Foot Wind Tunnel wall acoustic absorption characteristics at incidence angle θ in zero wind (from ref. 6).

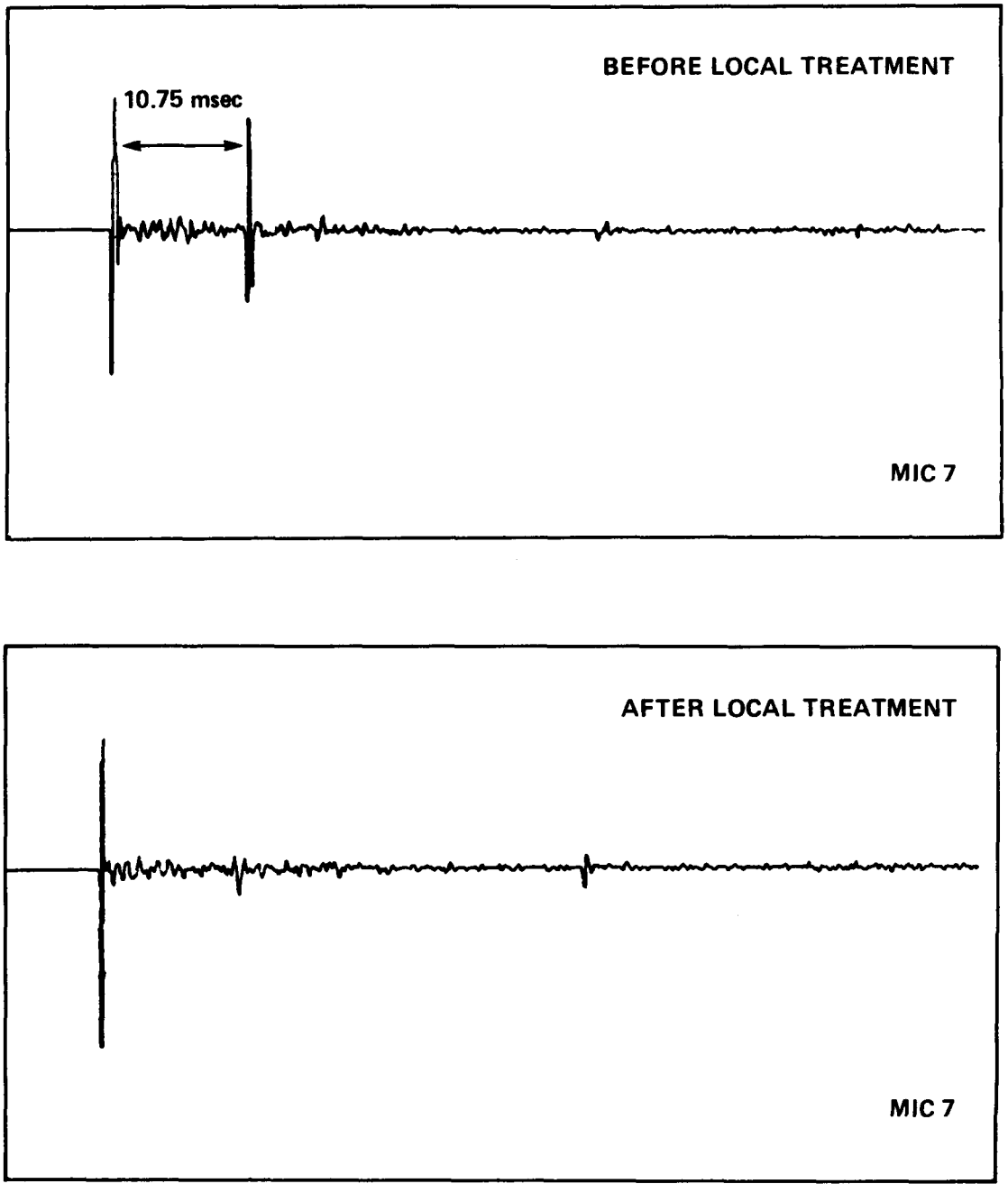

Figure 5.– Example of time delay measurements before and after local foam treatment to eliminate local acoustic reflections.

APPENDIX A

ONE-THIRD-OCTAVE BAND ACOUSTIC SPECTRA

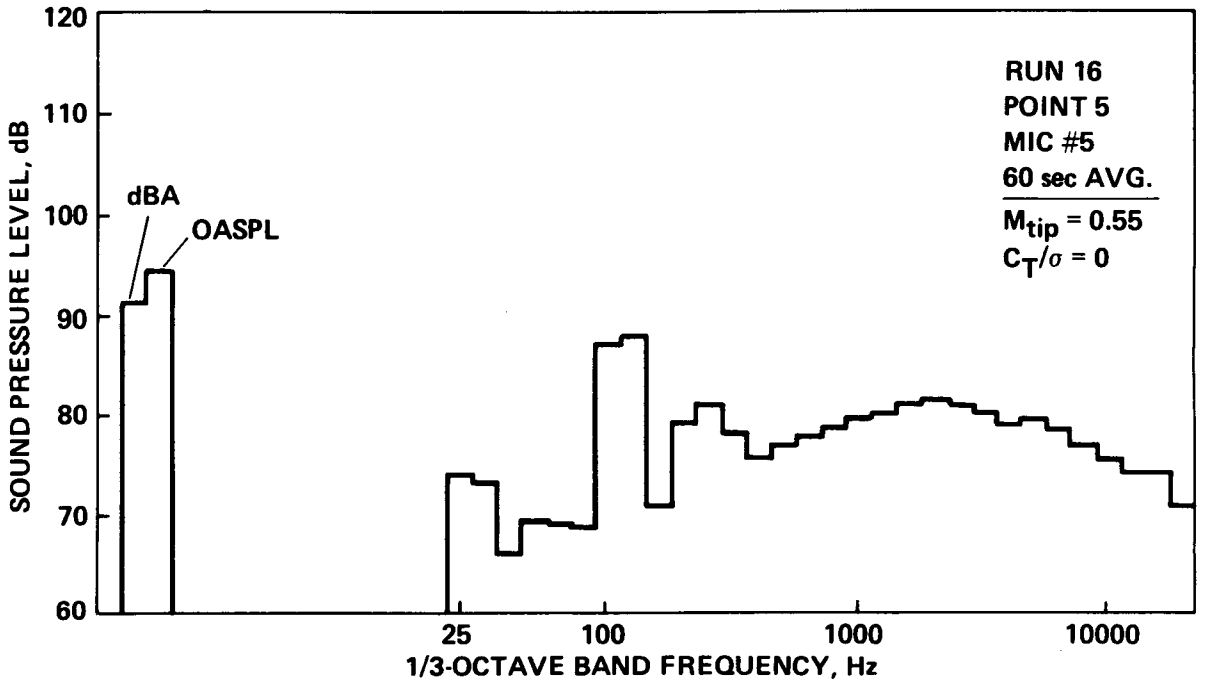

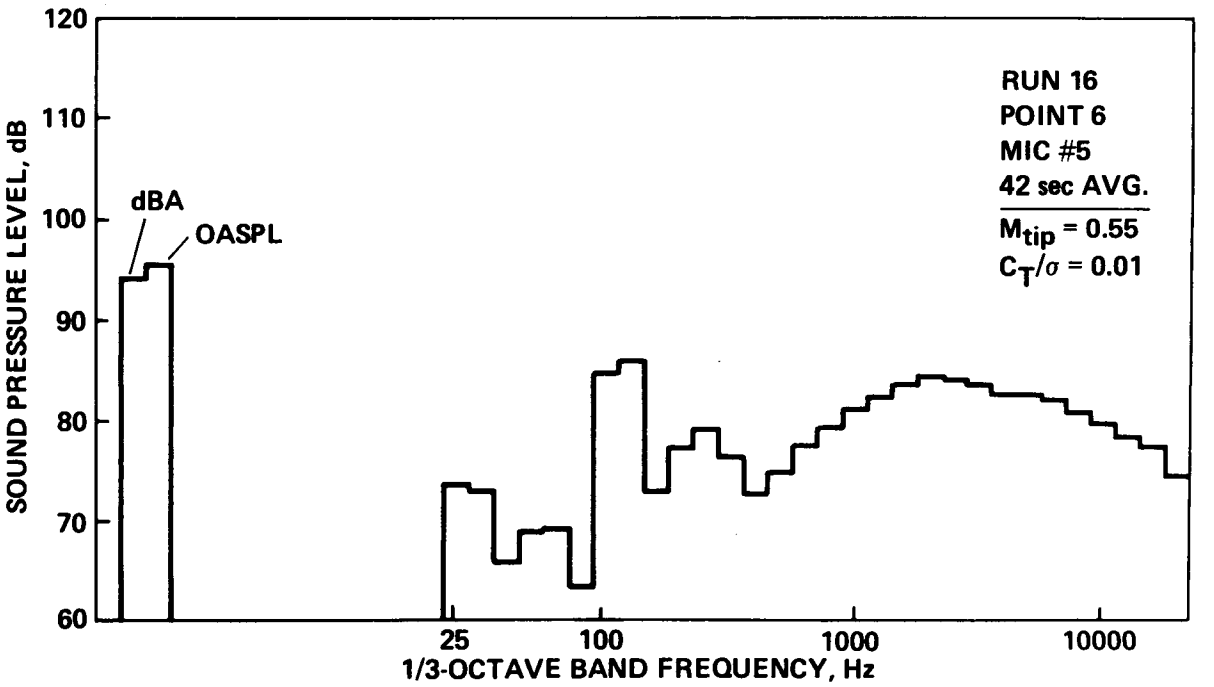

Figure A1.– 1/3-octave band acoustic spectra—Microphone No. 5: r/D = 1.0, ψ = 180°, θ = +10°.

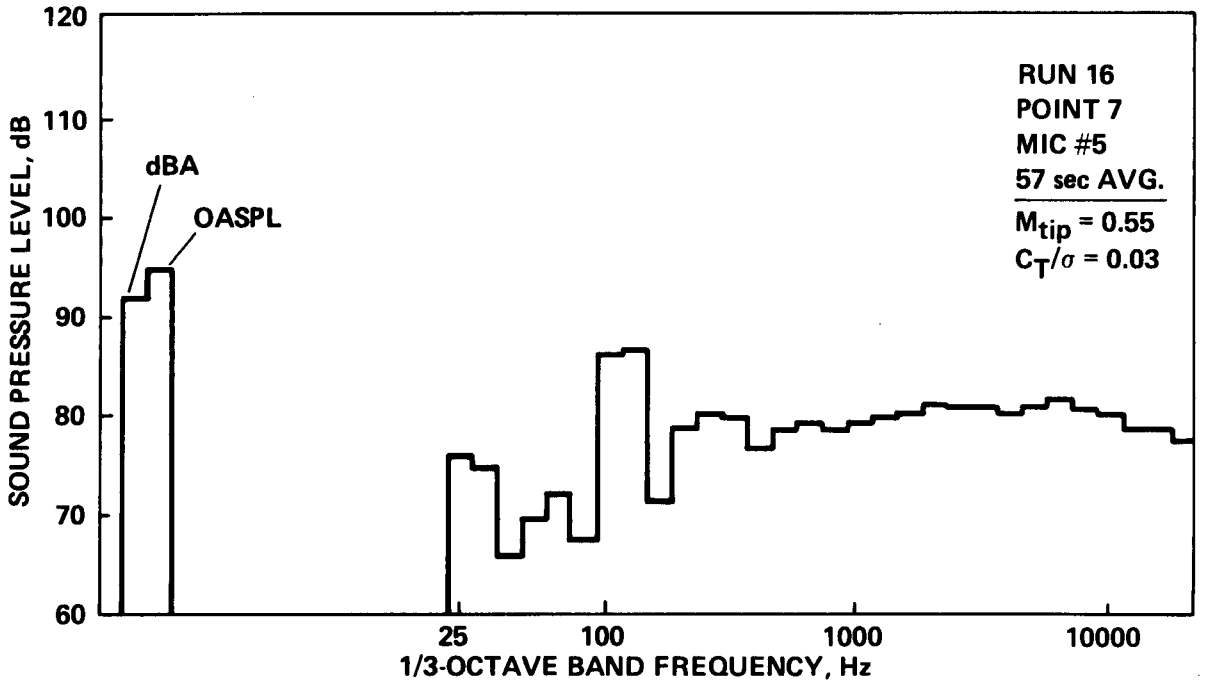

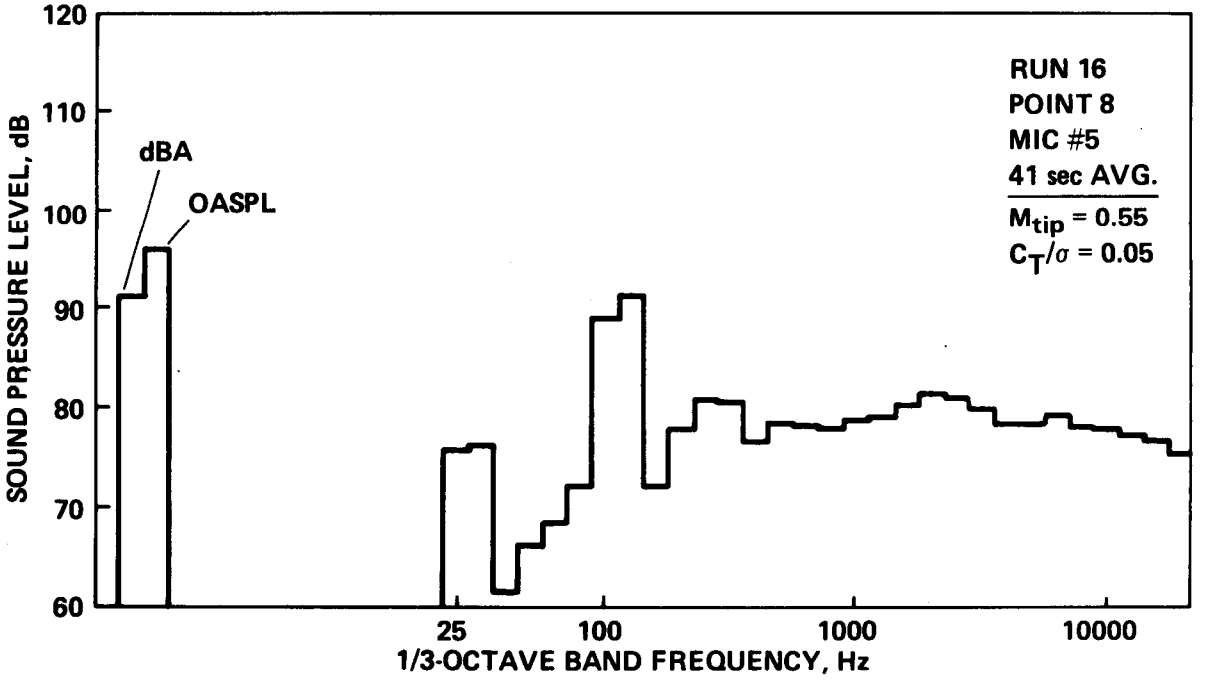

Figure A1.– Continued.

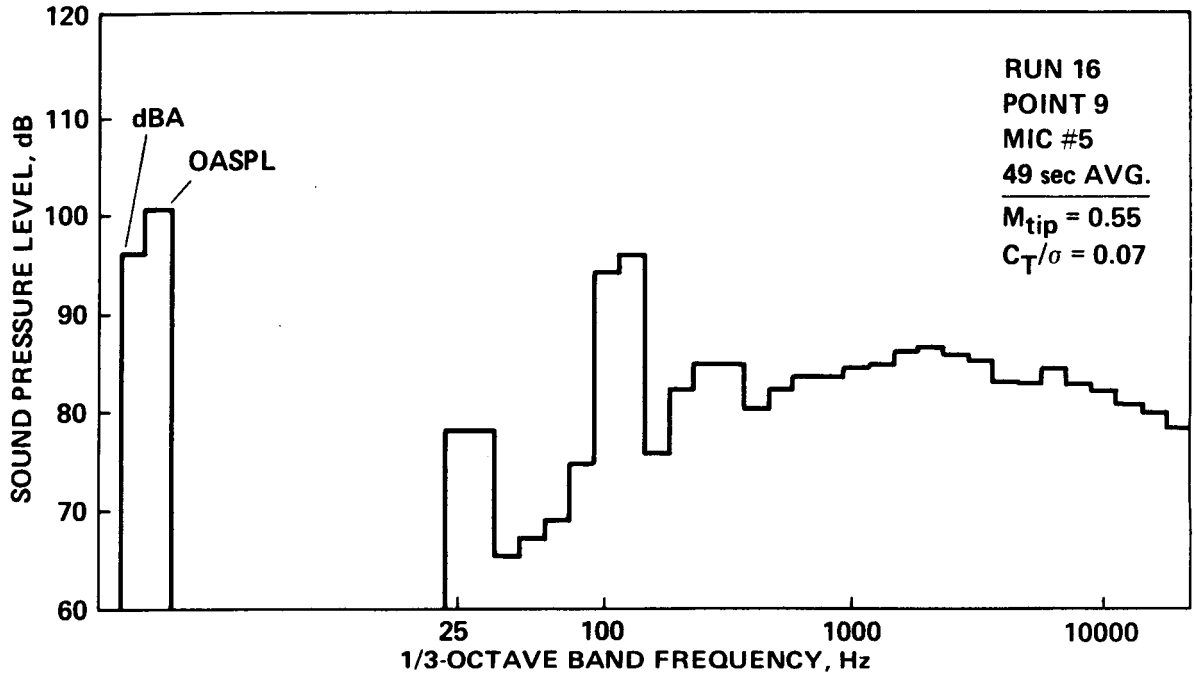

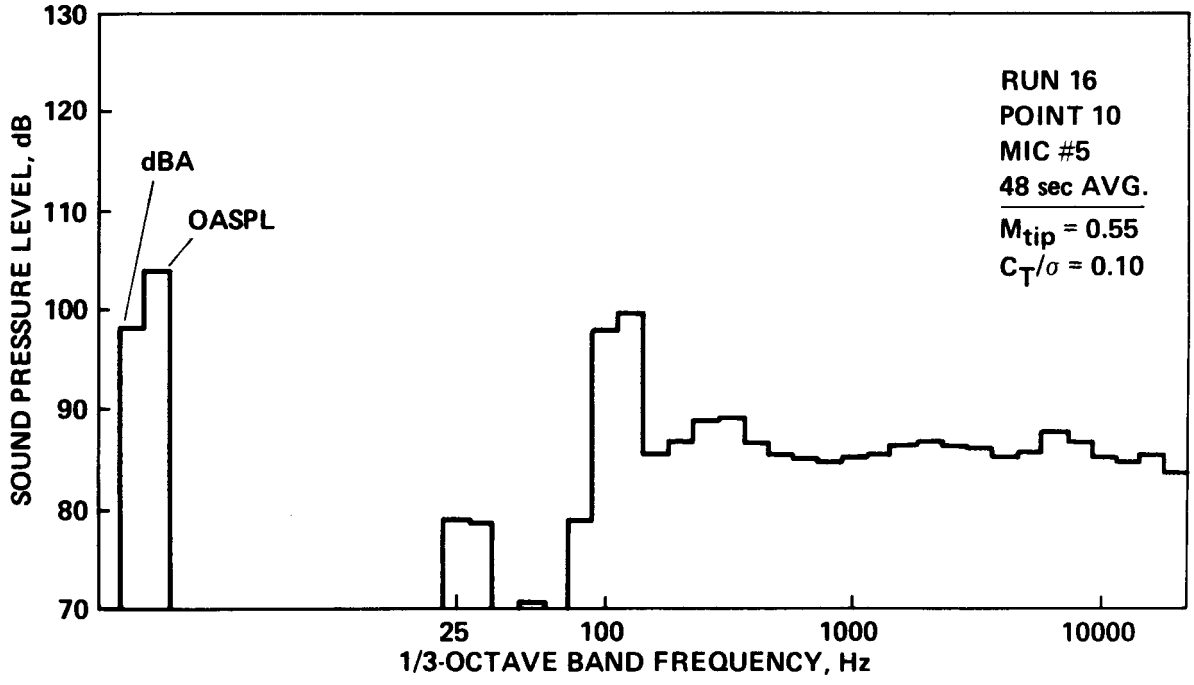

Figure A1.– Continued.

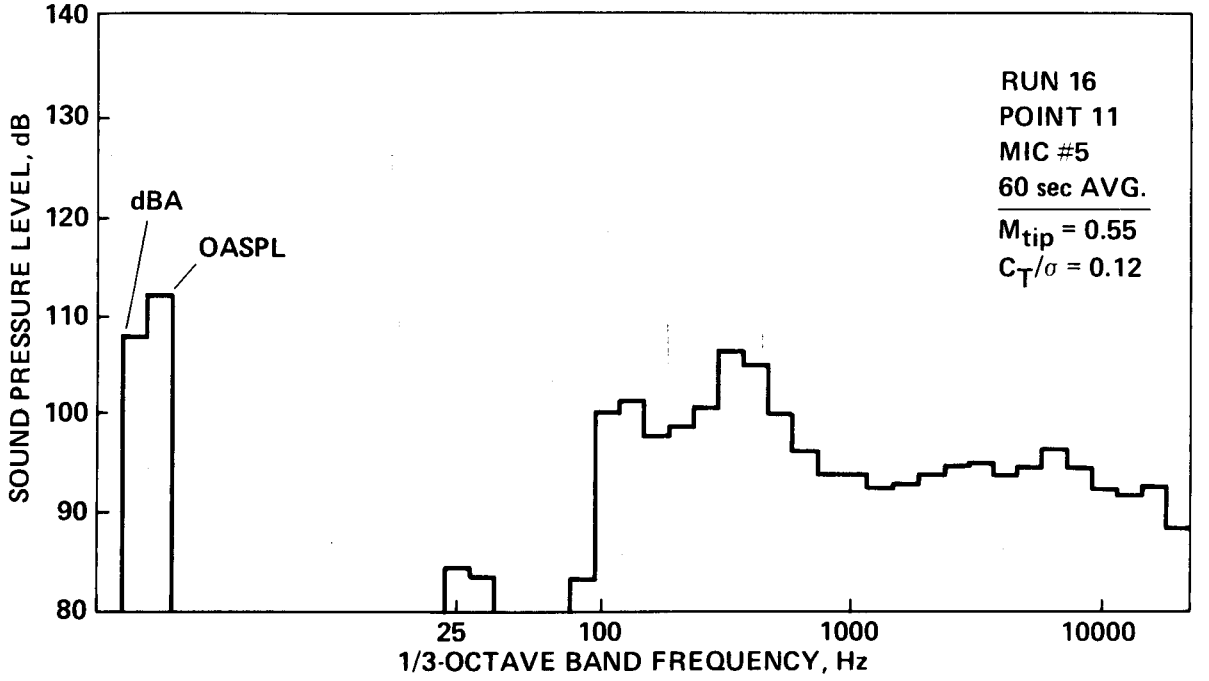

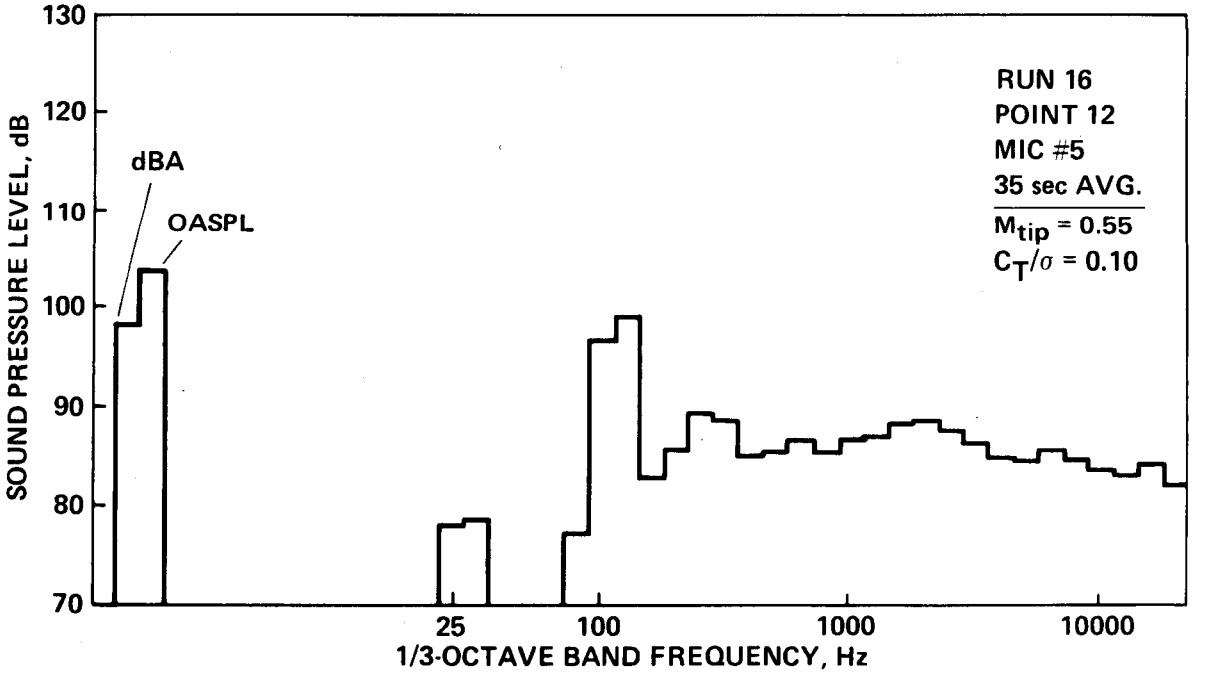

Figure A1.– Continued.

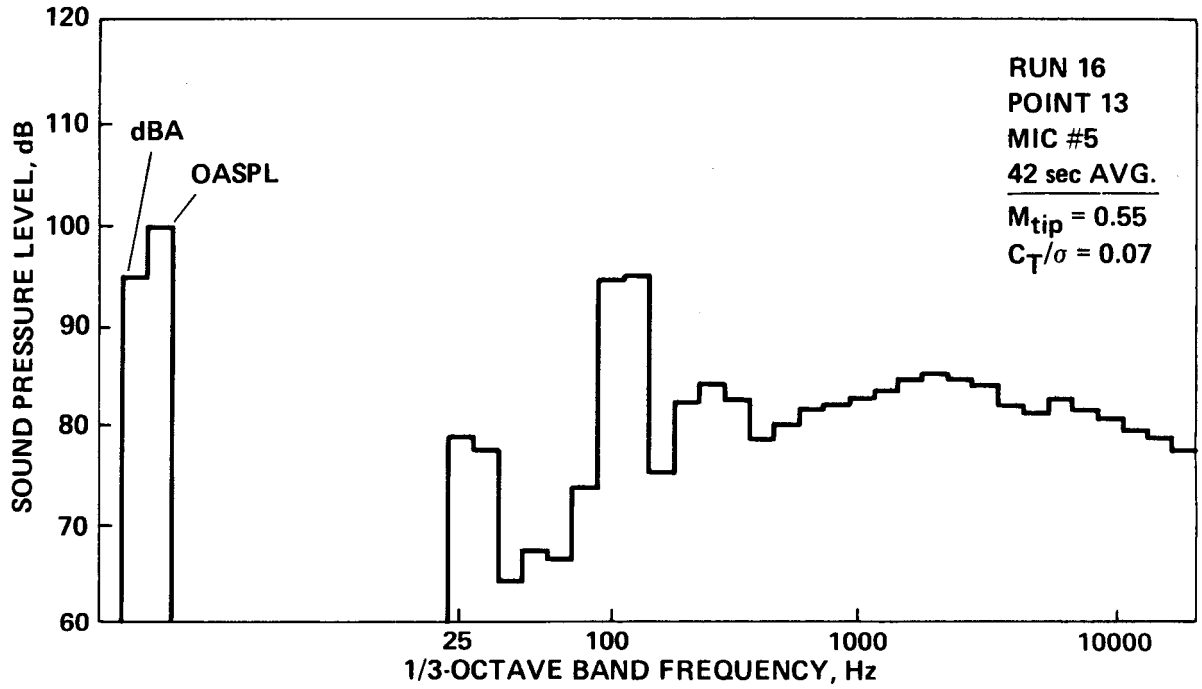

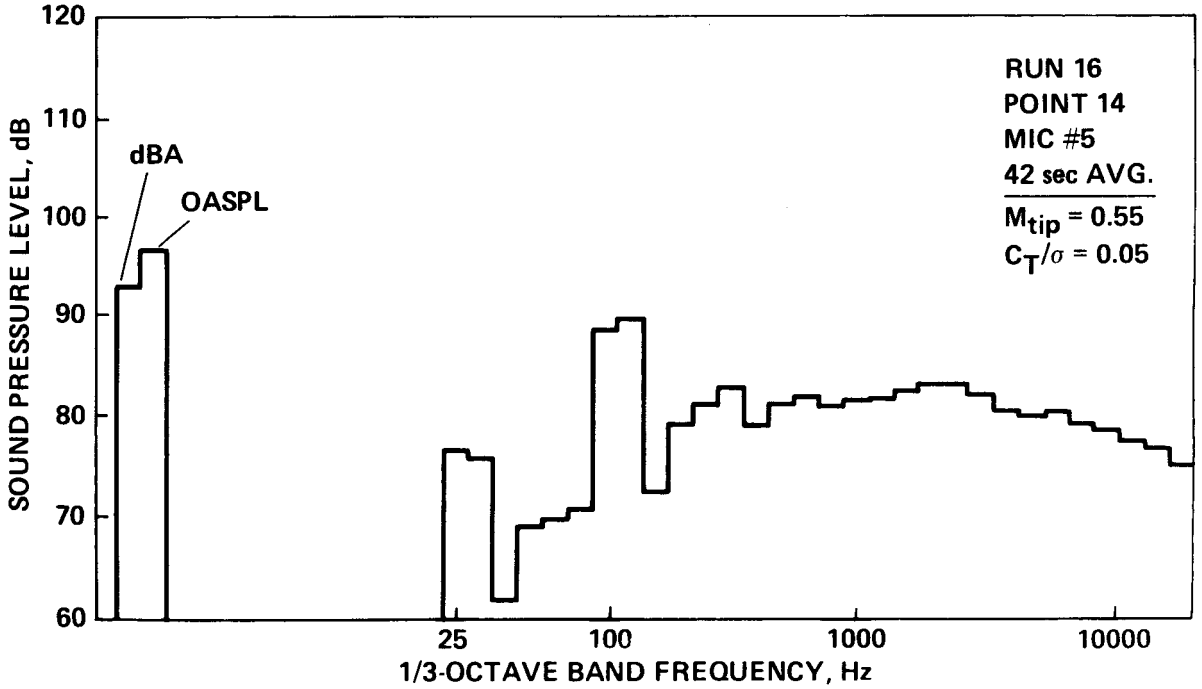

Figure A1.– Continued.

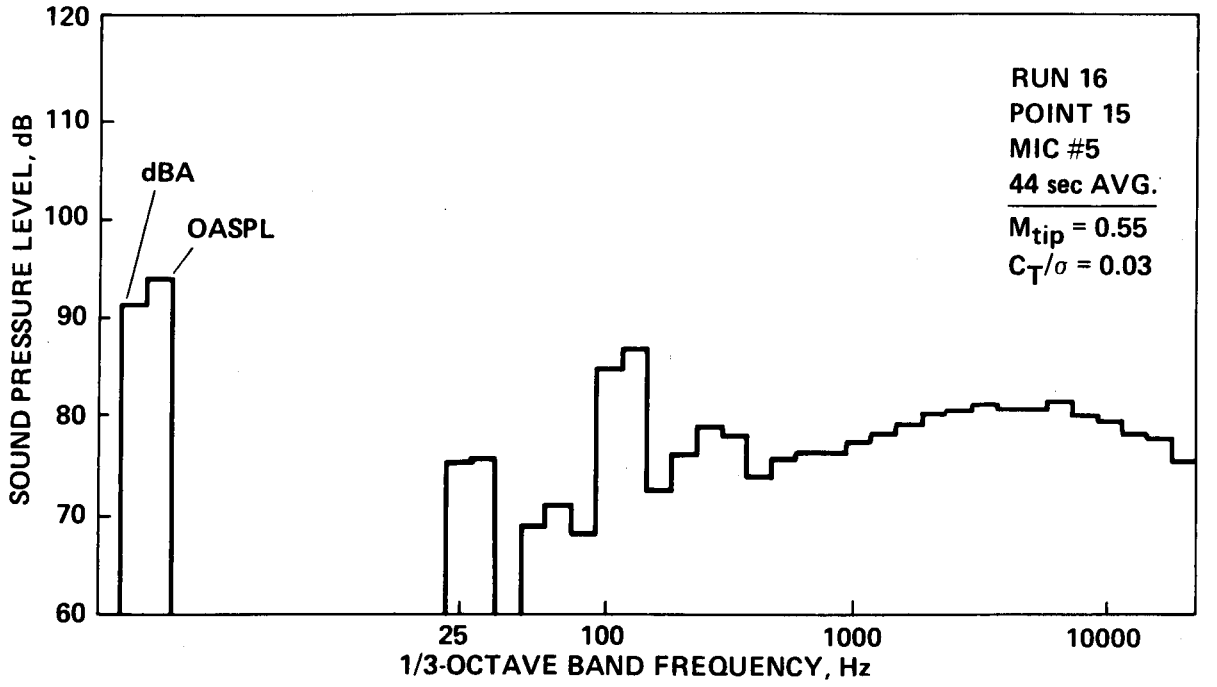

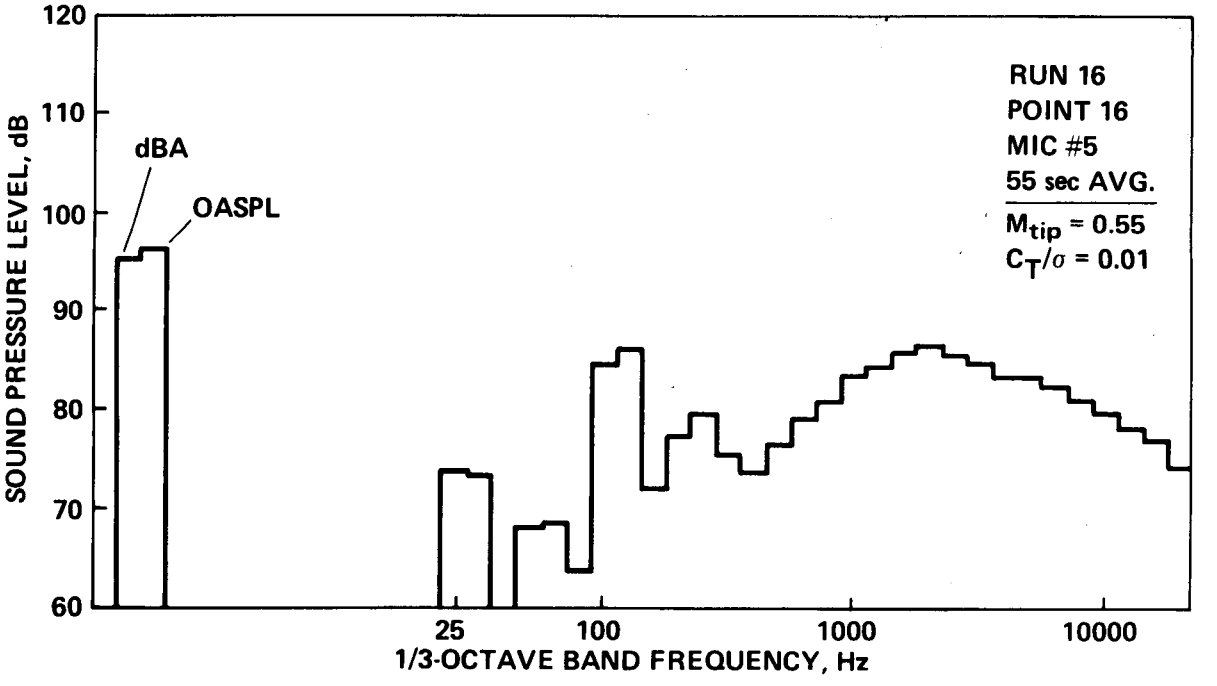

Figure A1.– Continued.

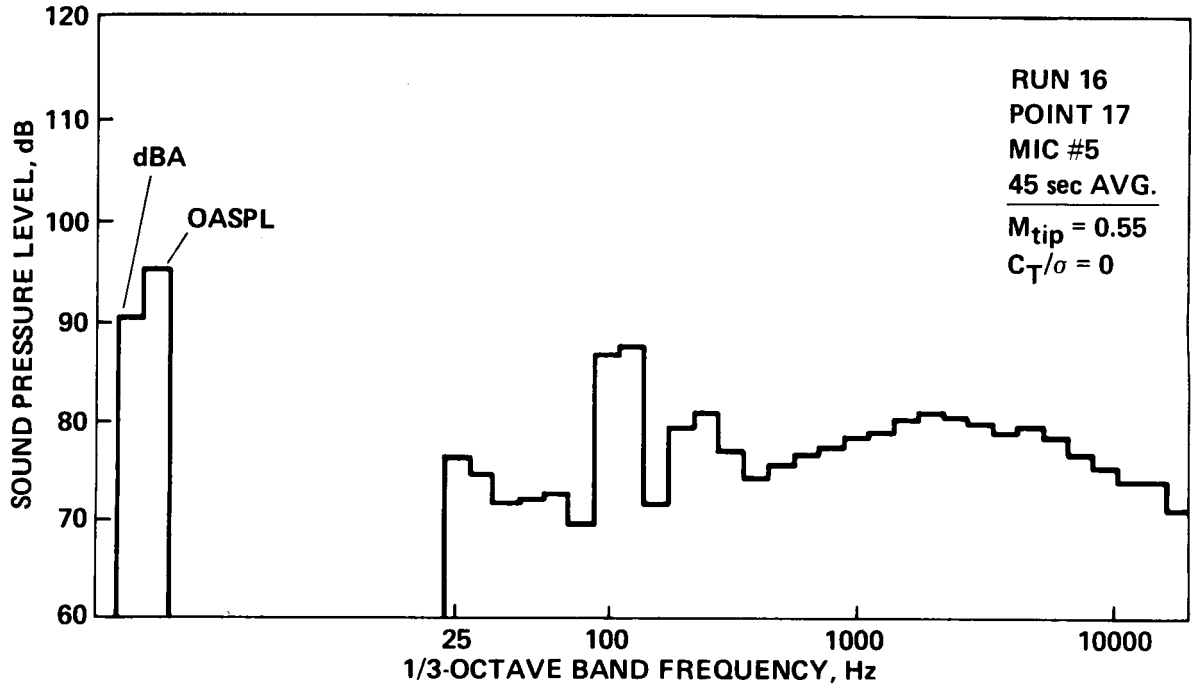

Figure A1.– Continued.

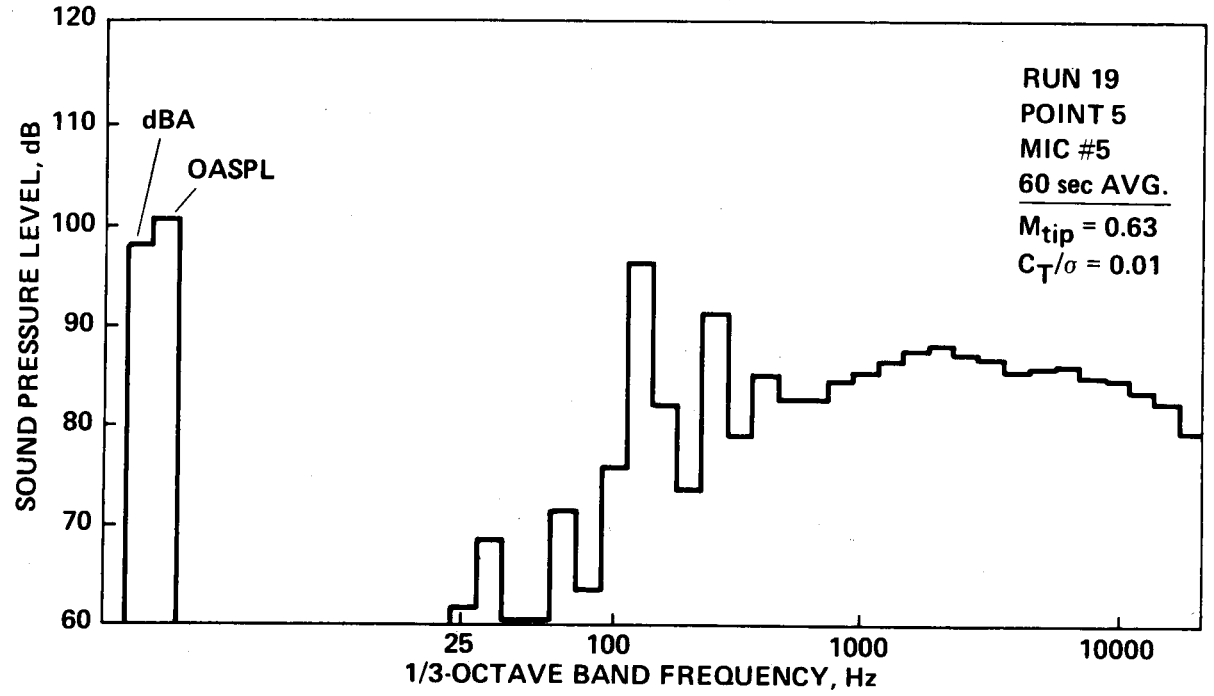

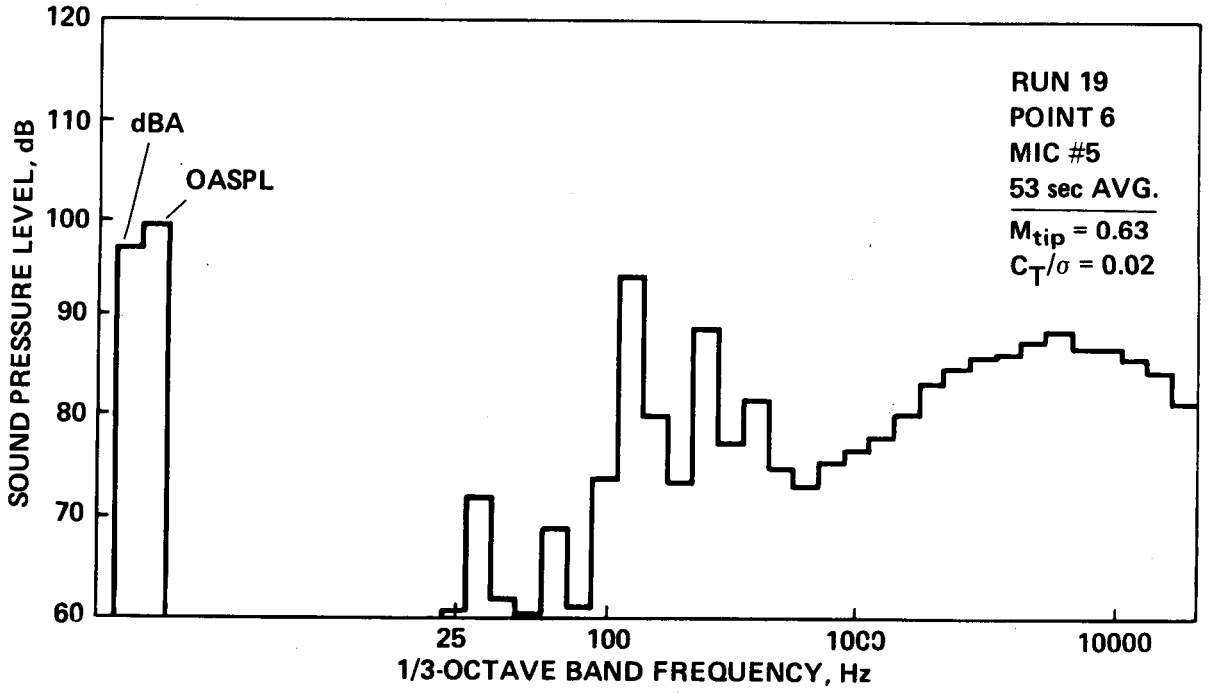

Figure A1.– Continued.

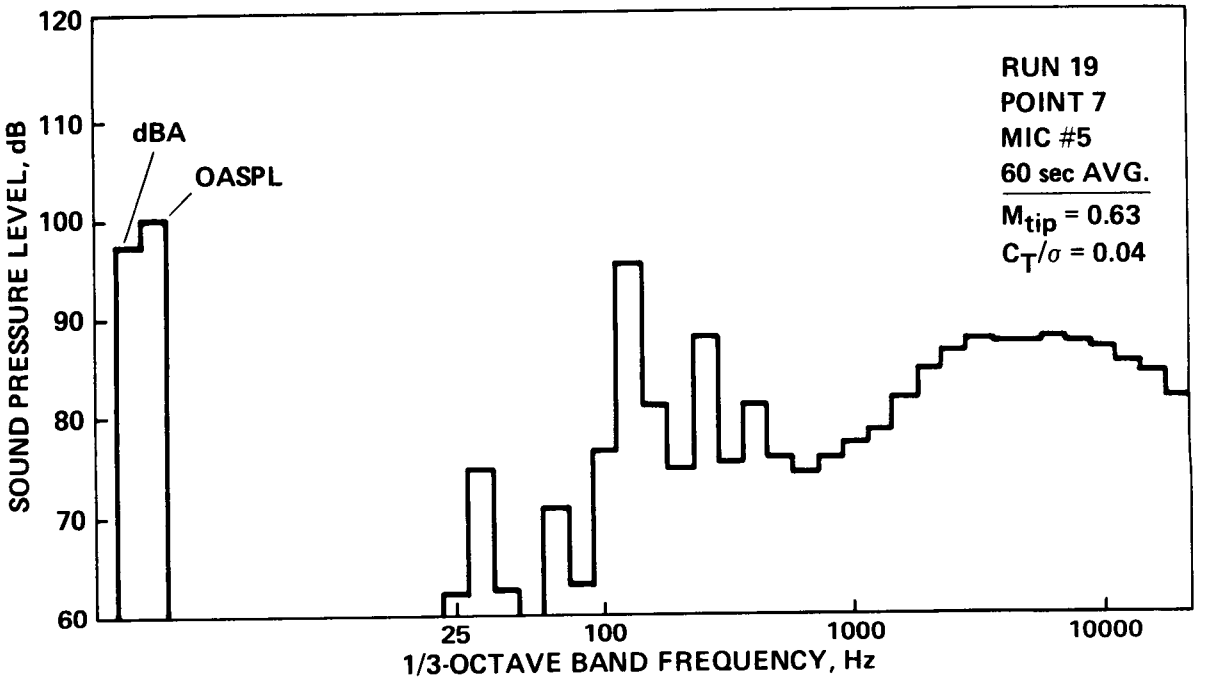

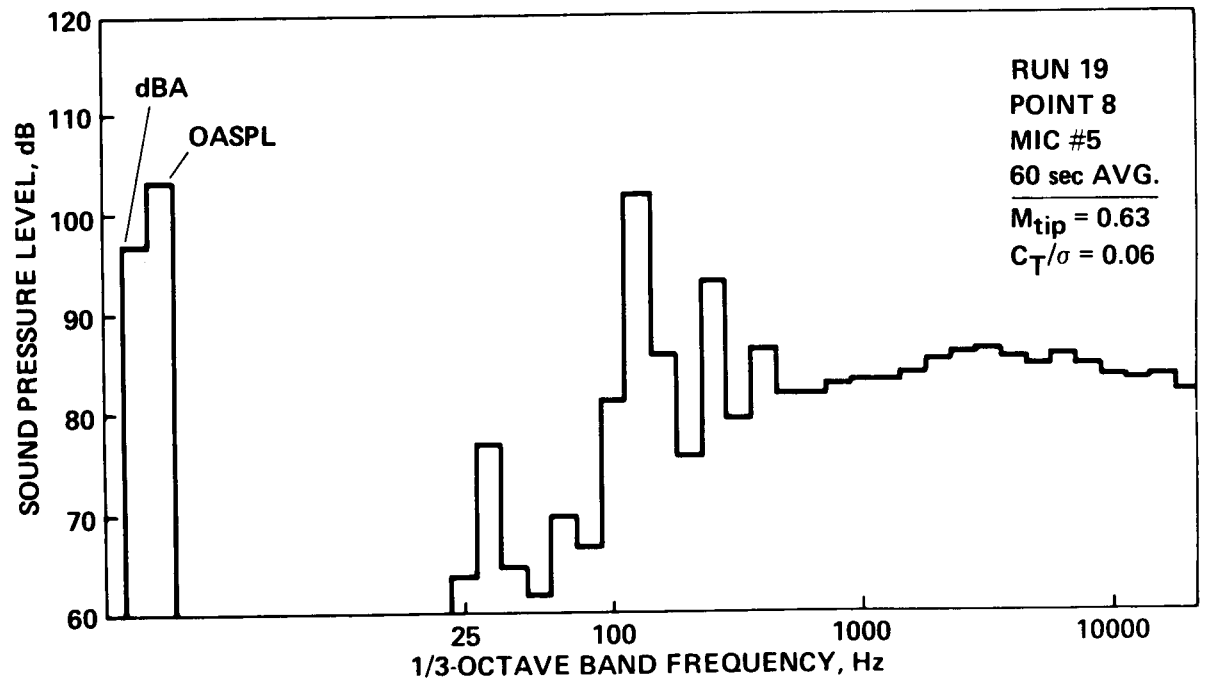

Figure A1.– Continued.

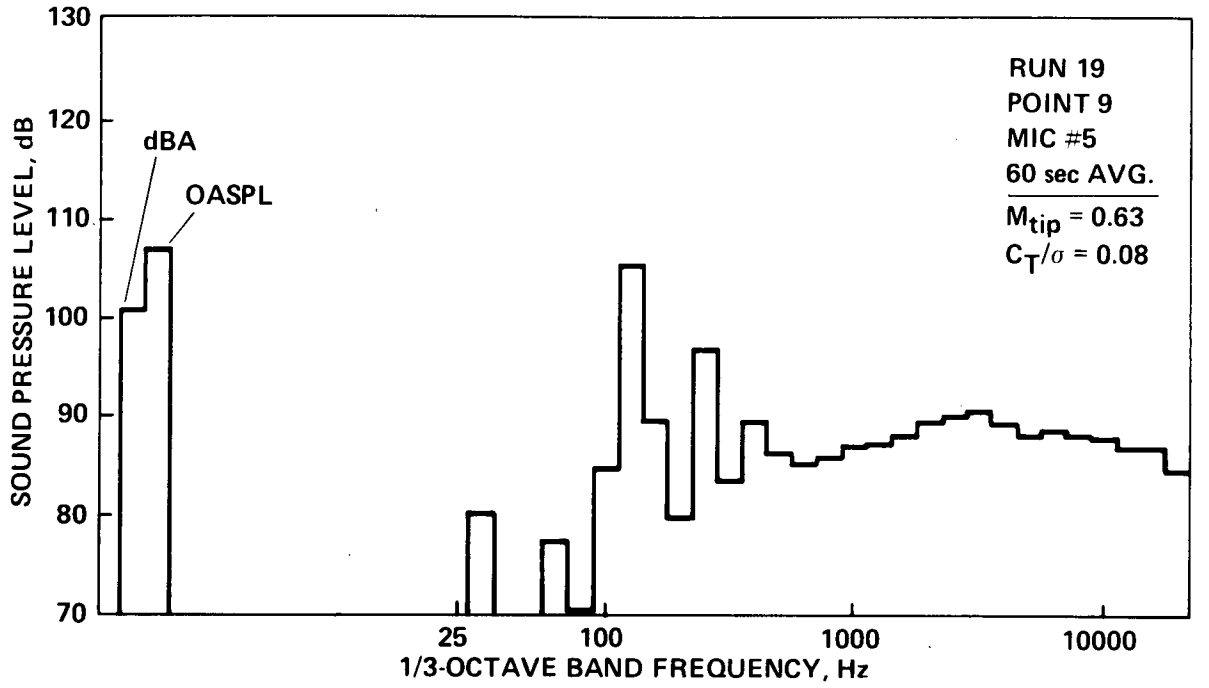

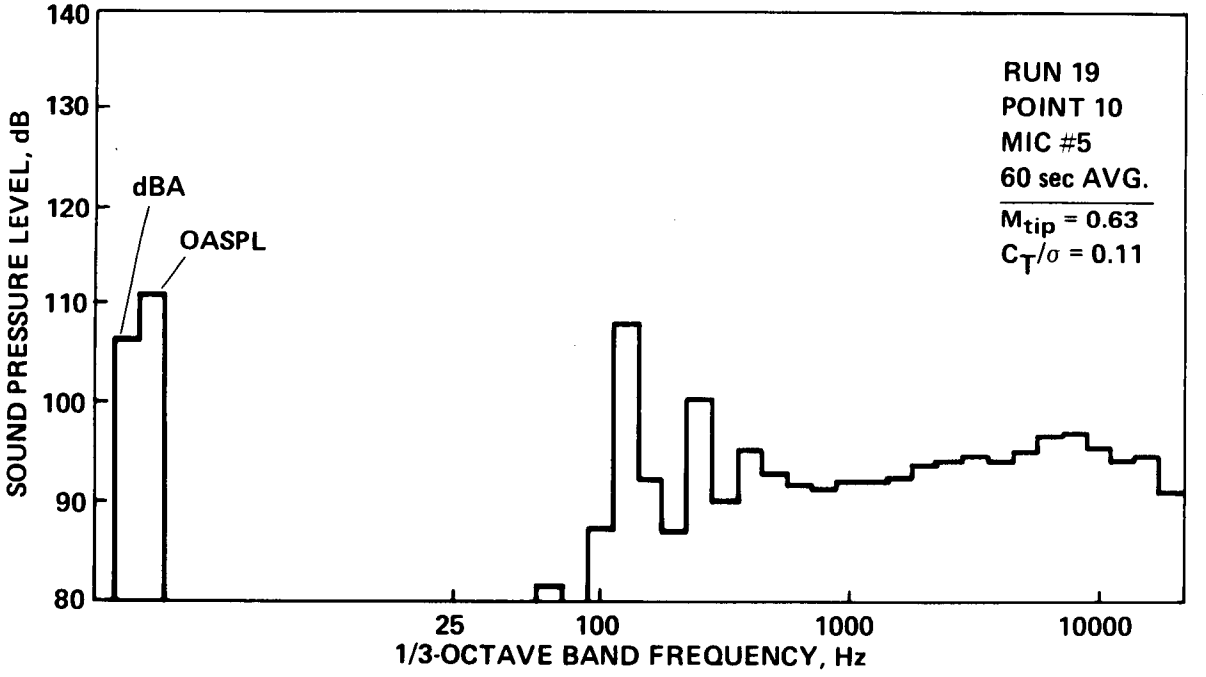

Figure A1.– Continued.

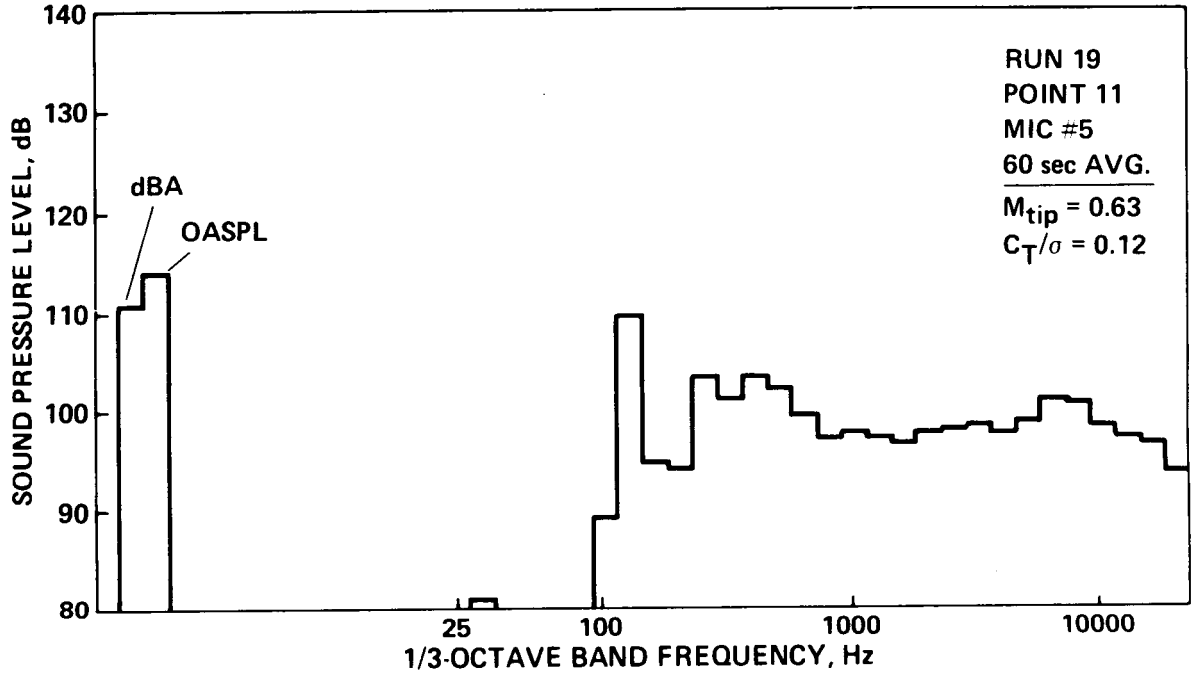

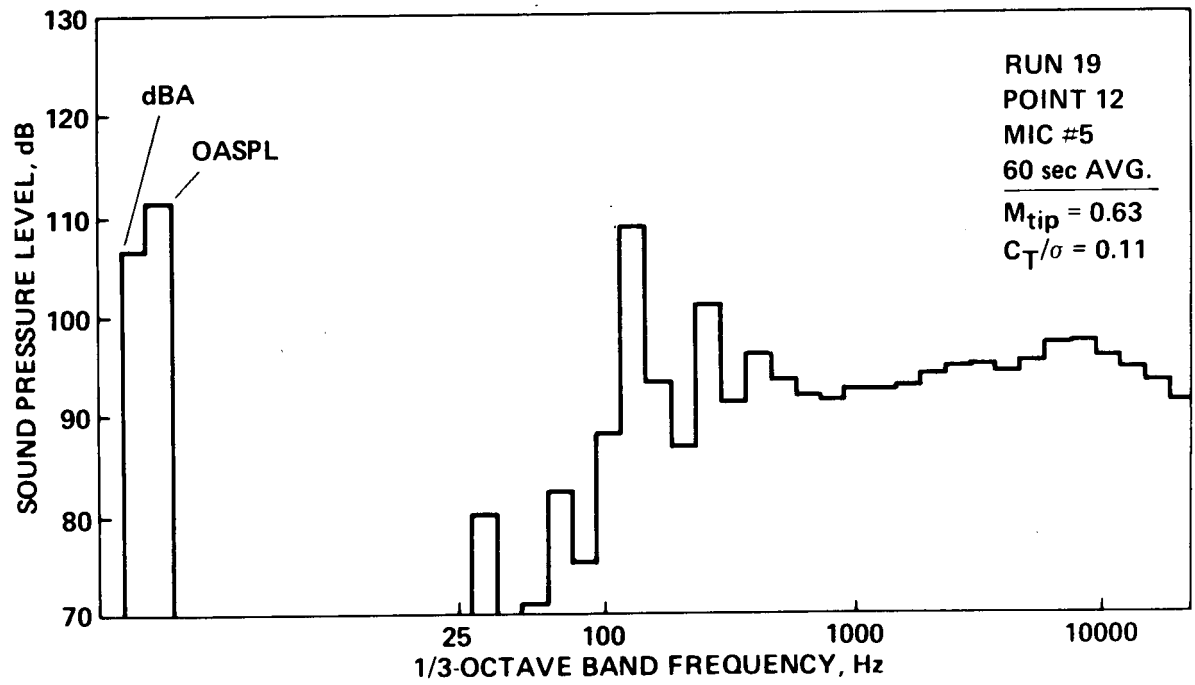

Figure A1.– Continued.

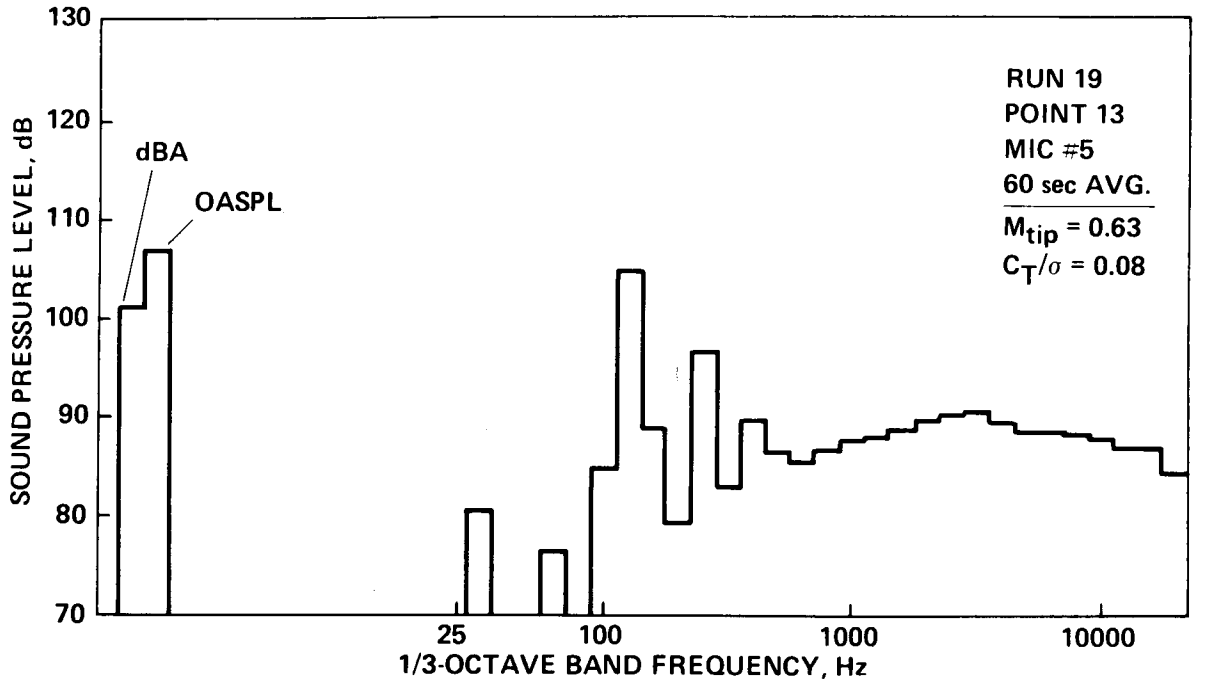

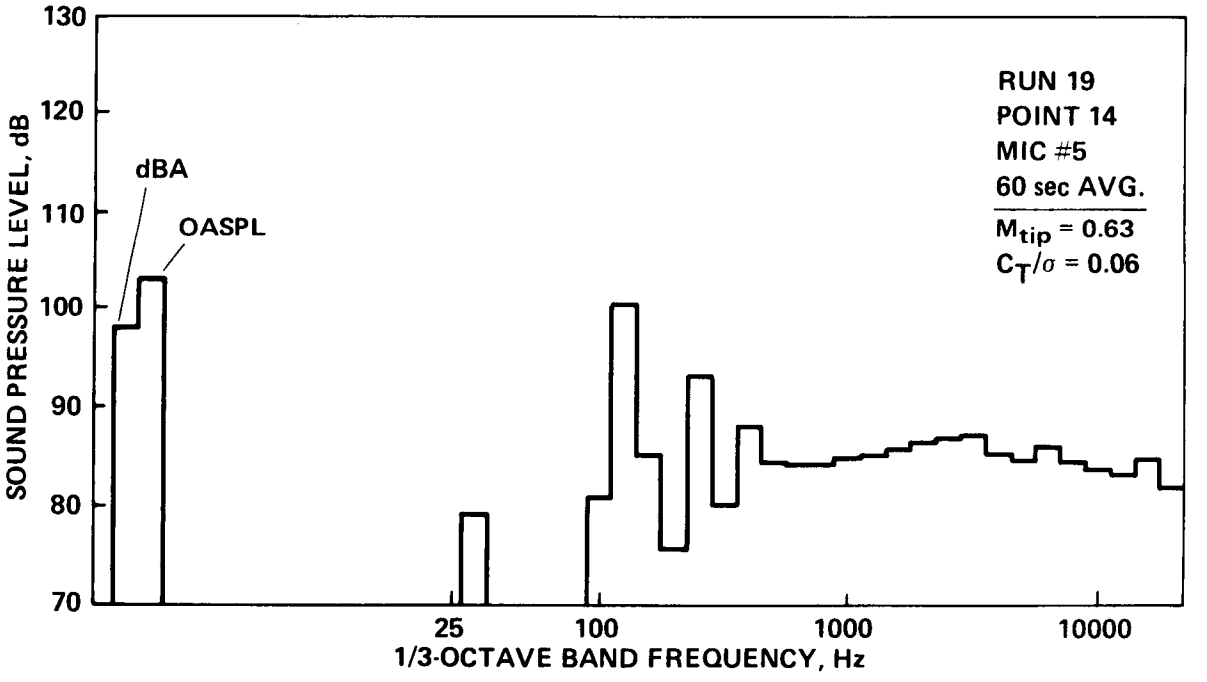

Figure A1.– Continued.

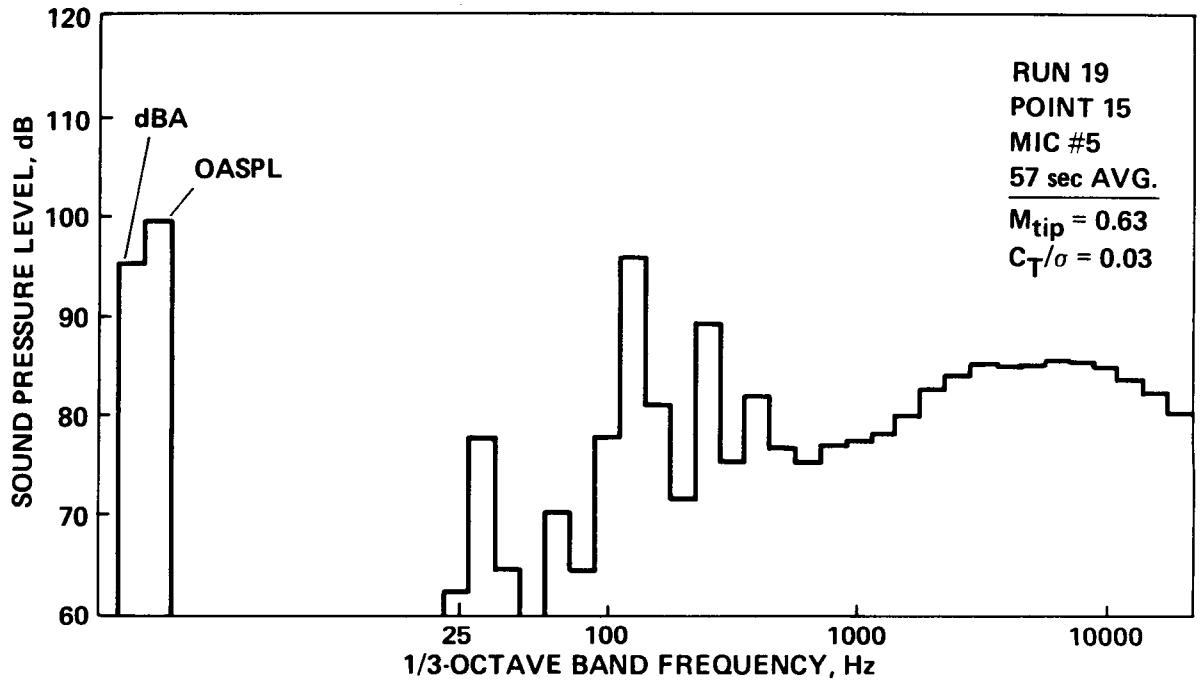

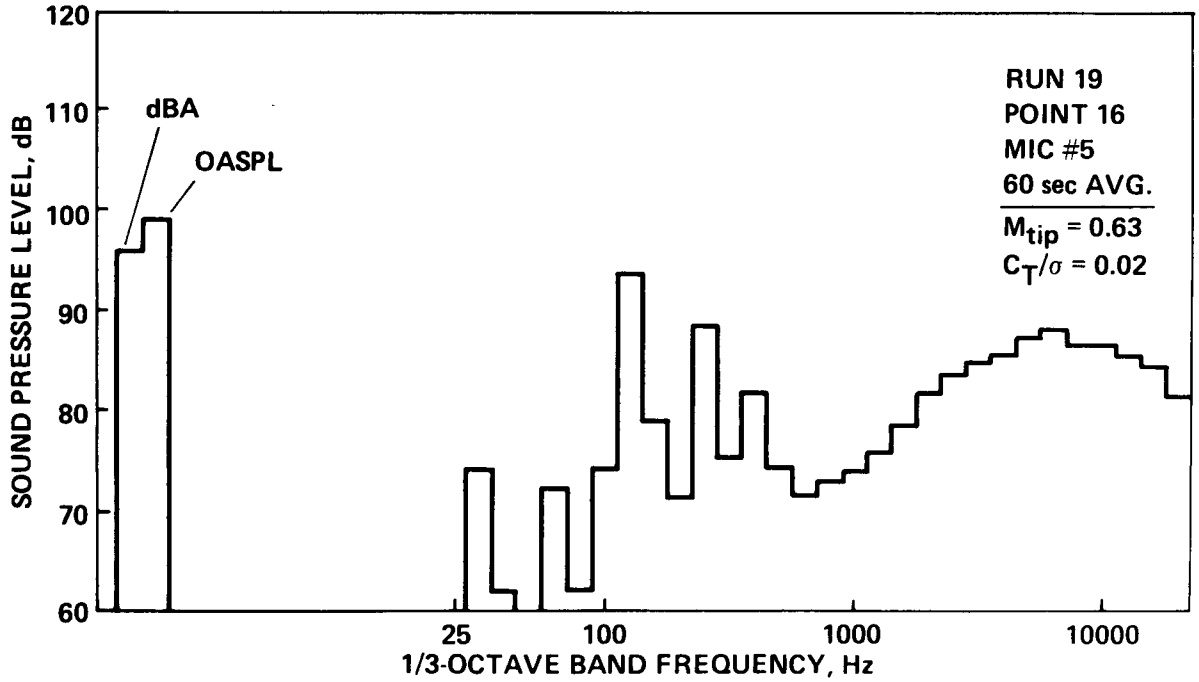

Figure A1.– Continued.

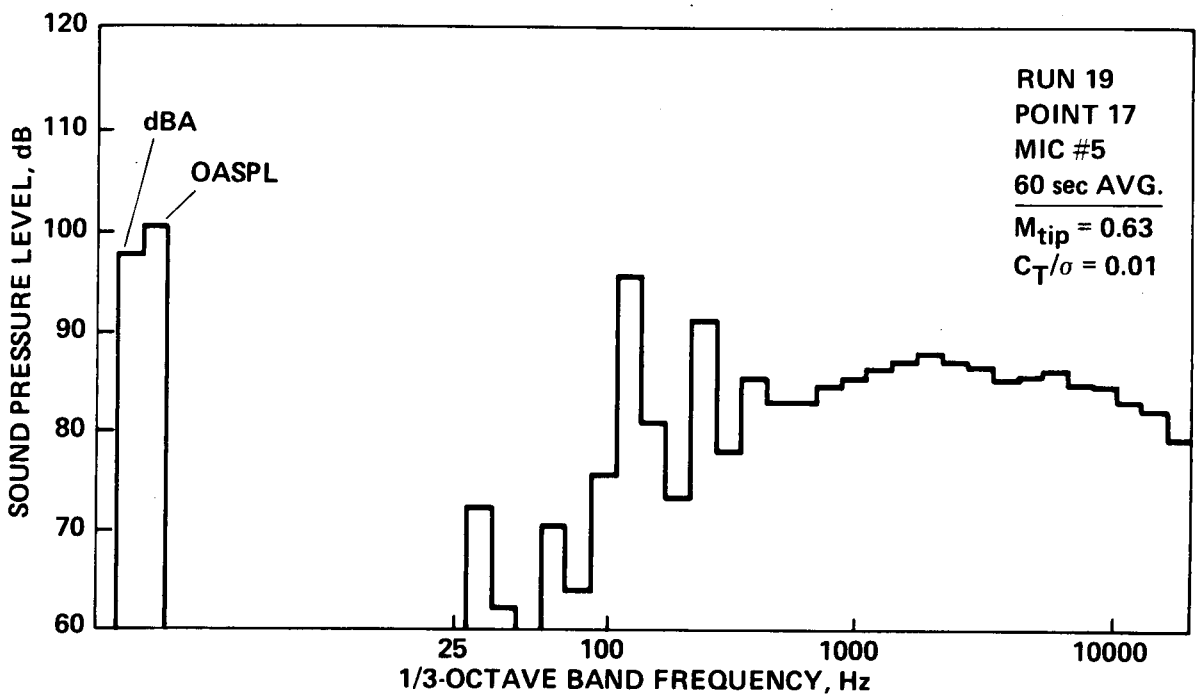

Figure A1.– Concluded.

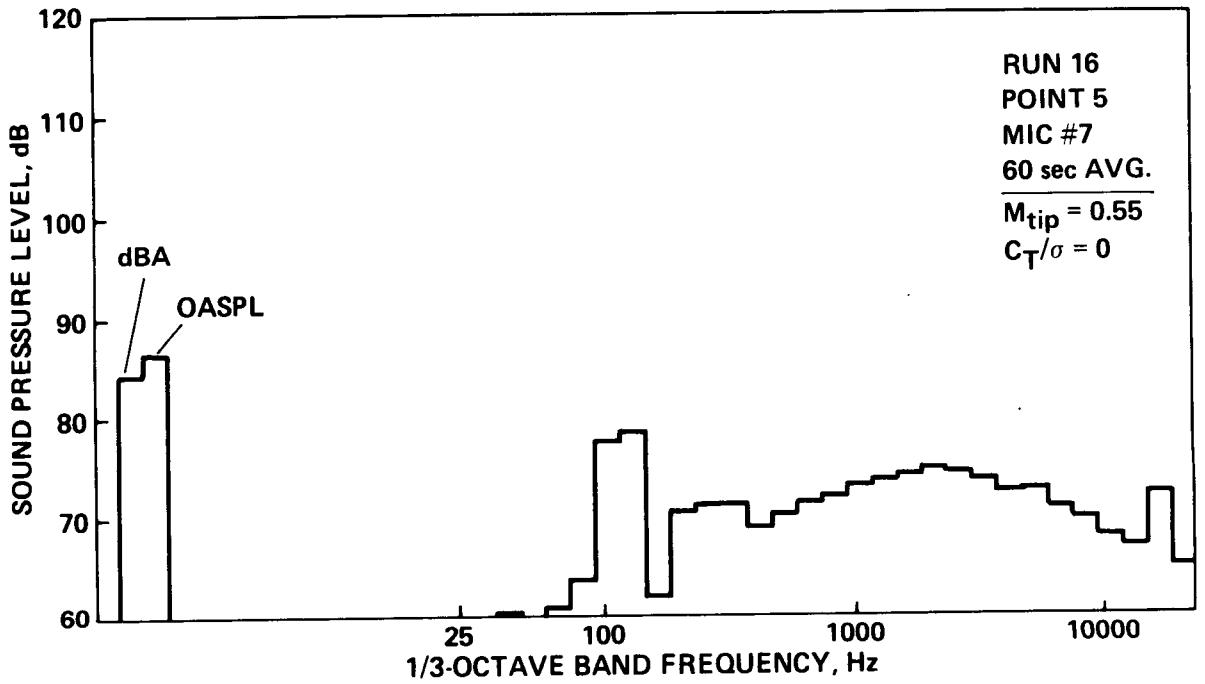

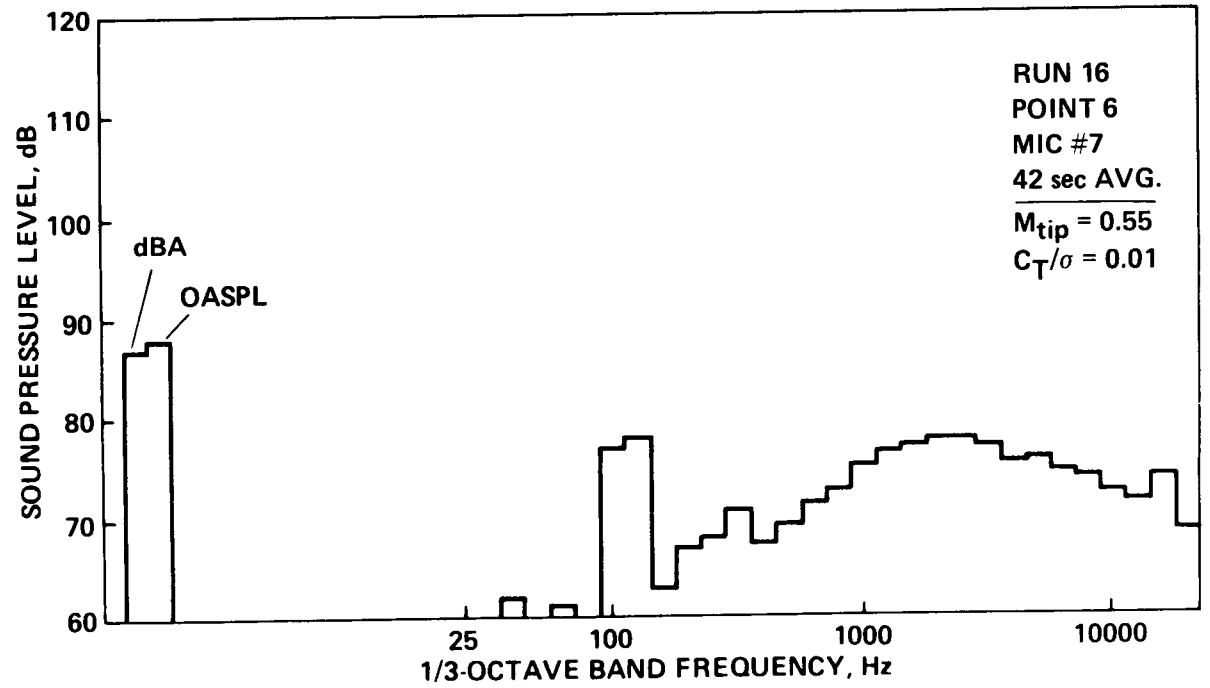

Figure A2.– 1/3-octave band acoustic spectra—Microphone No. 7: r/D = 2.0, ψ = 180°, θ = +10°.

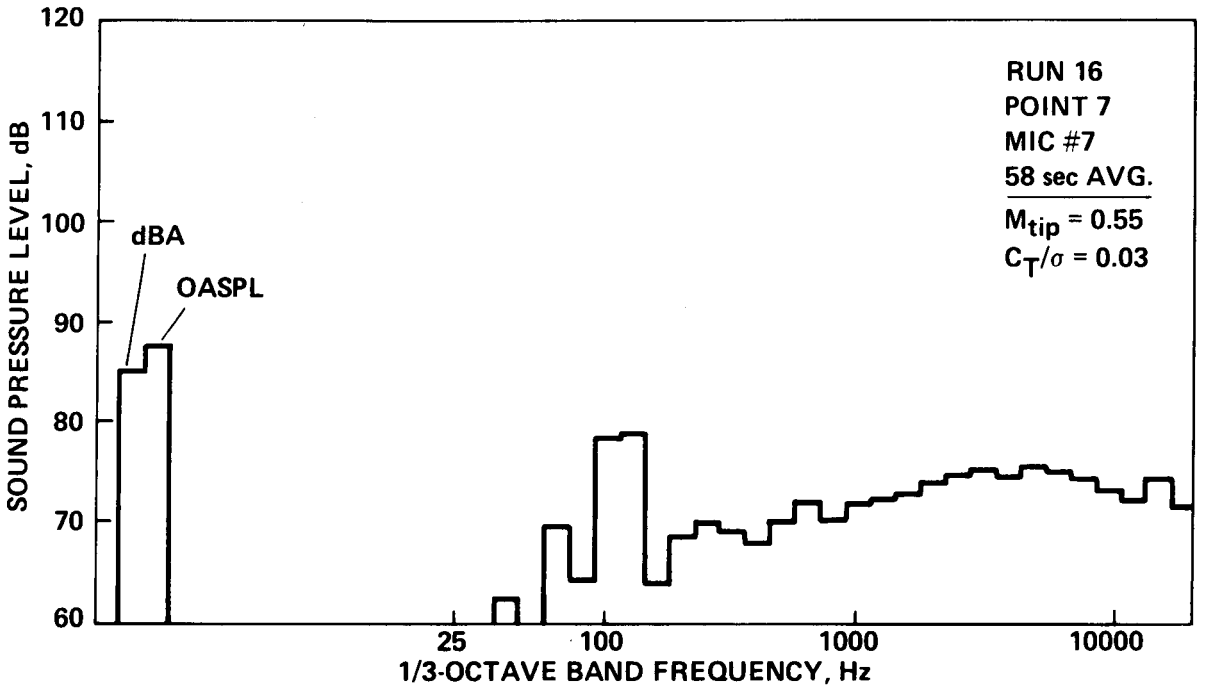

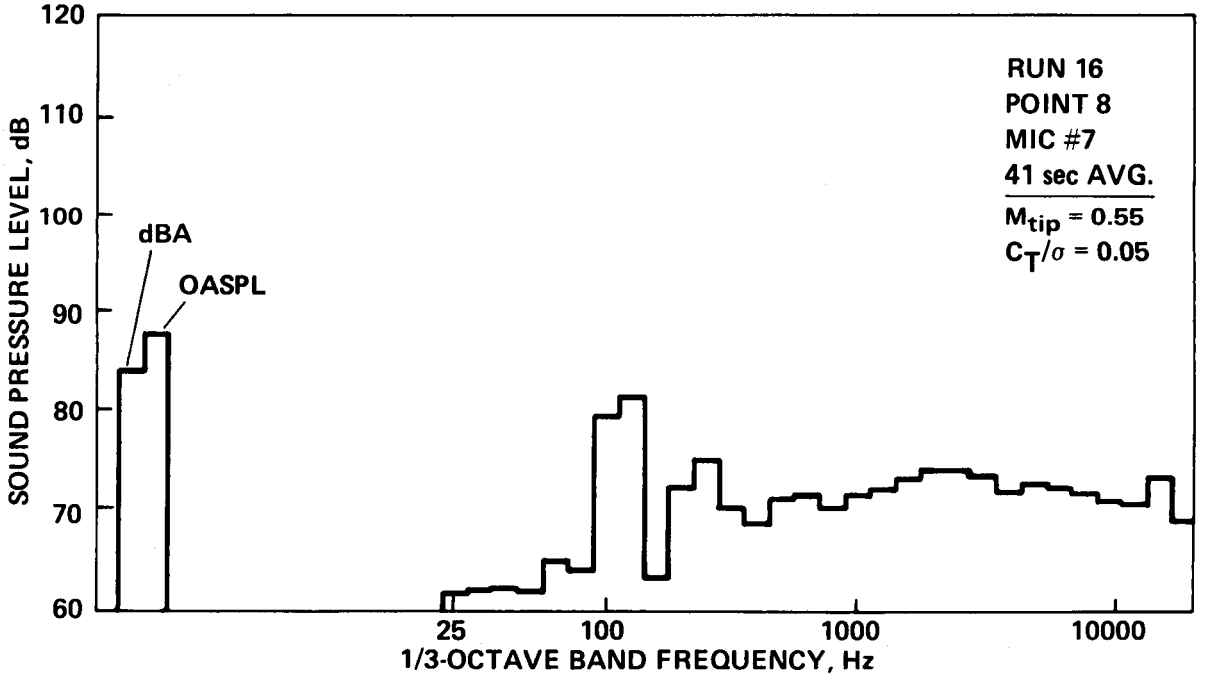

Figure A2.– Continued.

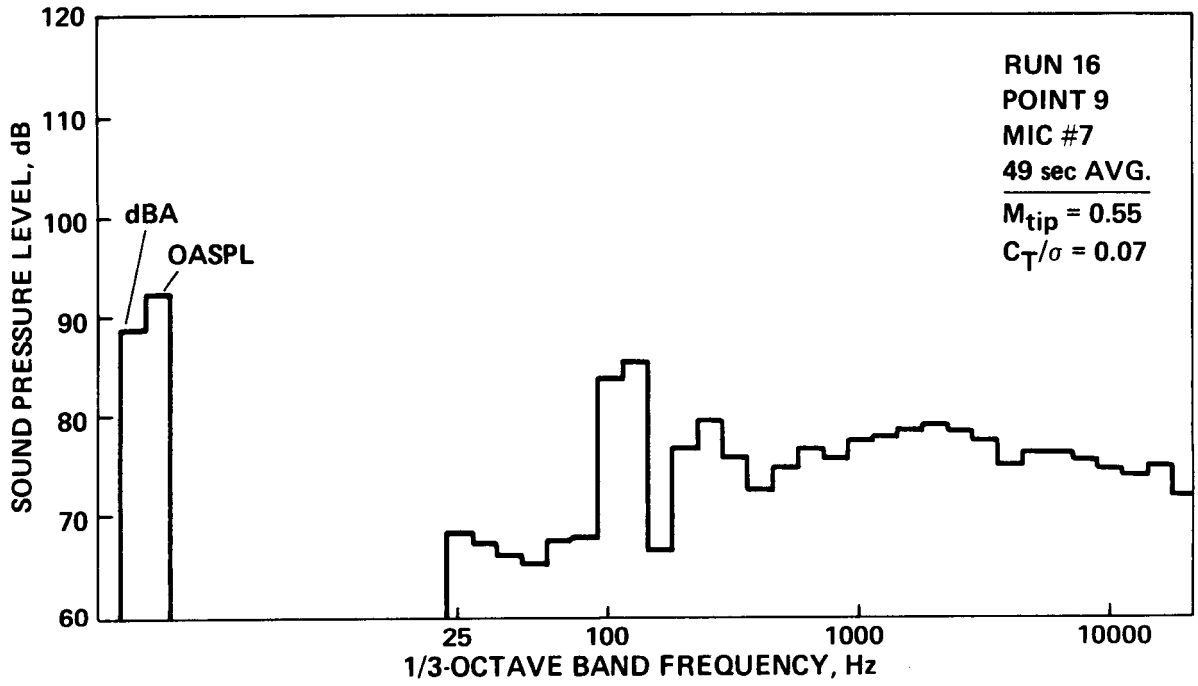

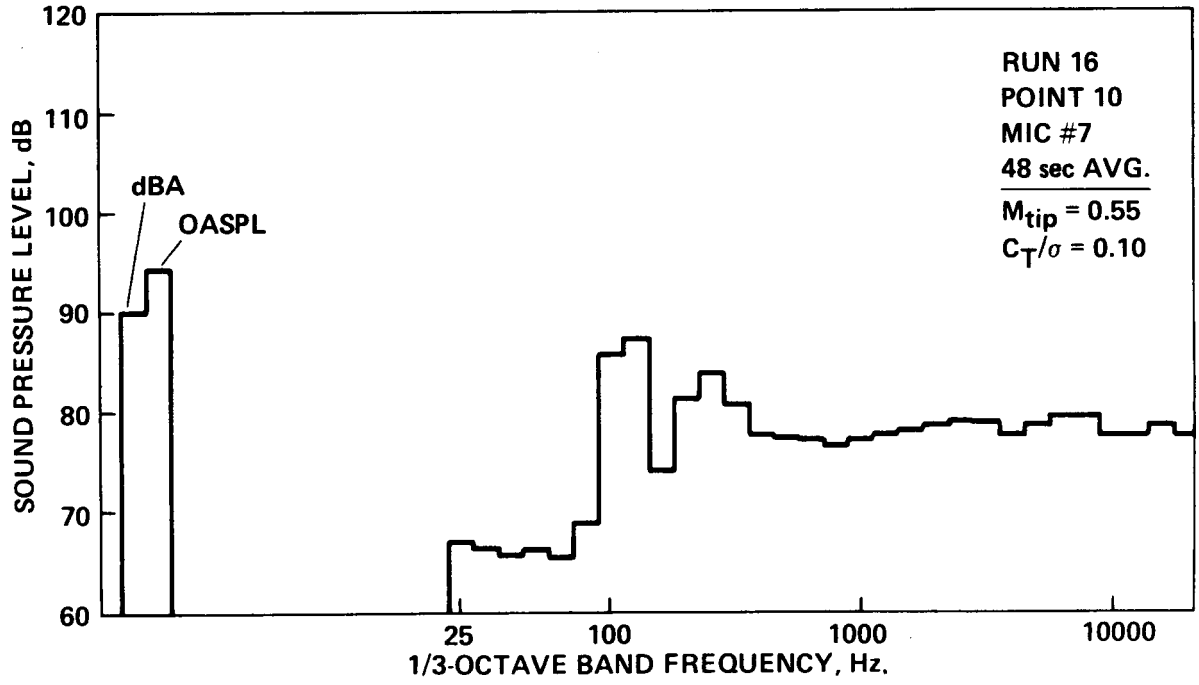

Figure A2.– Continued.

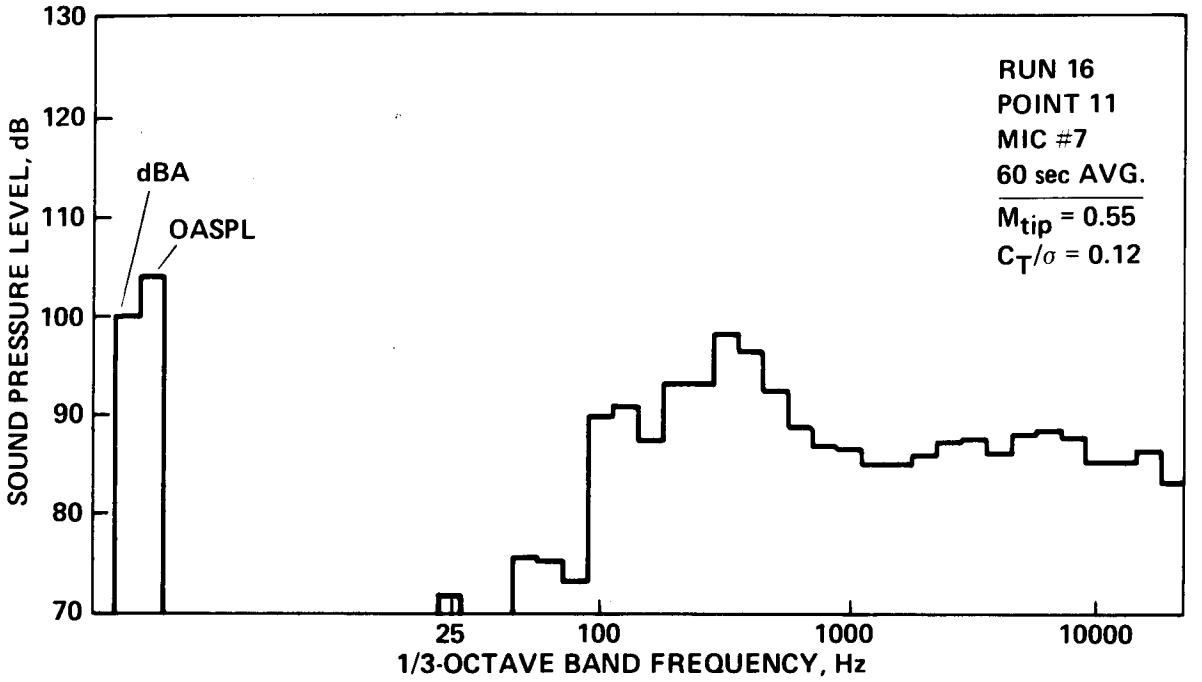

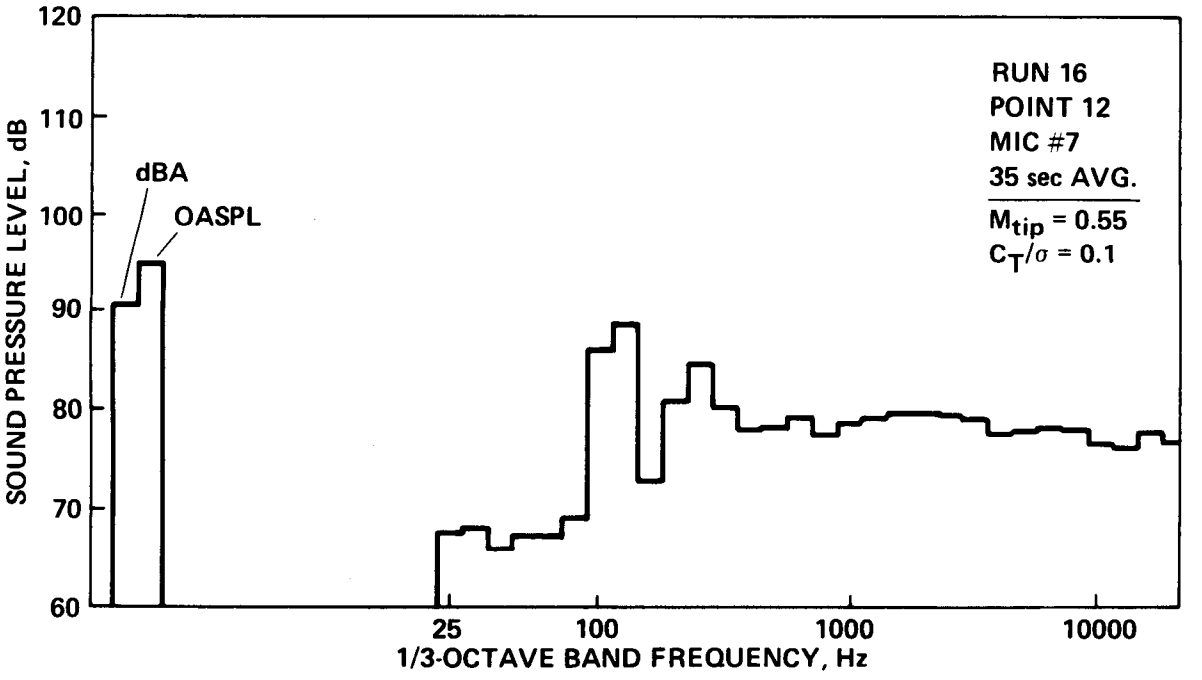

Figure A2.– Continued.

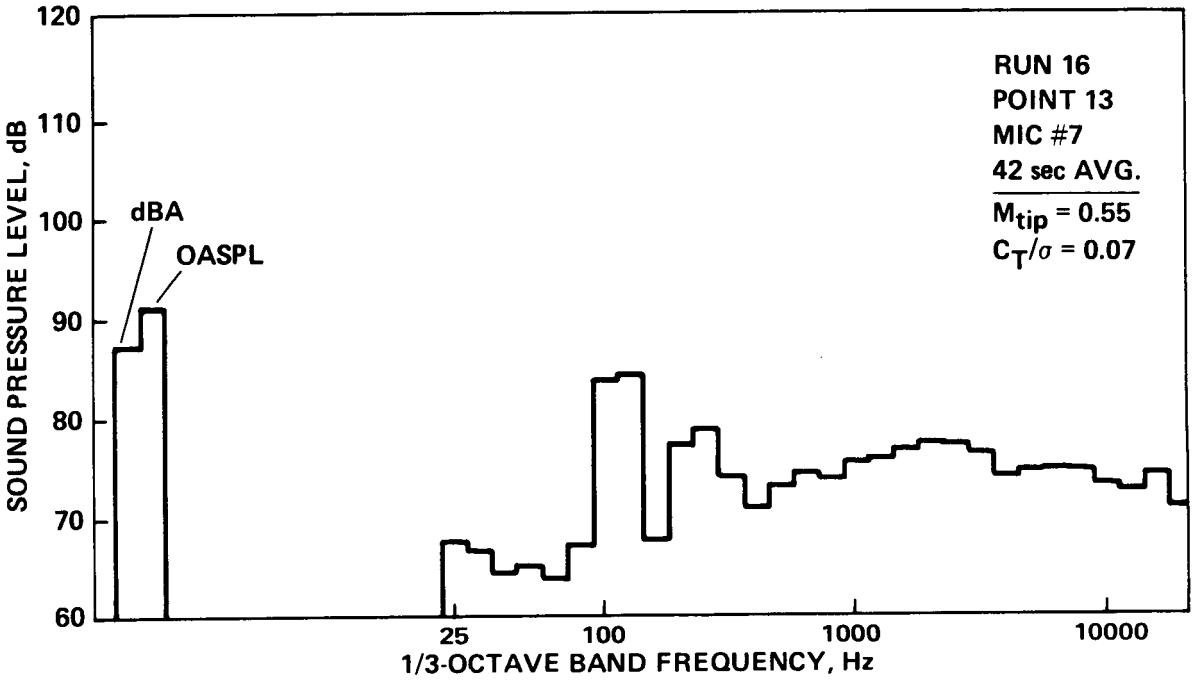

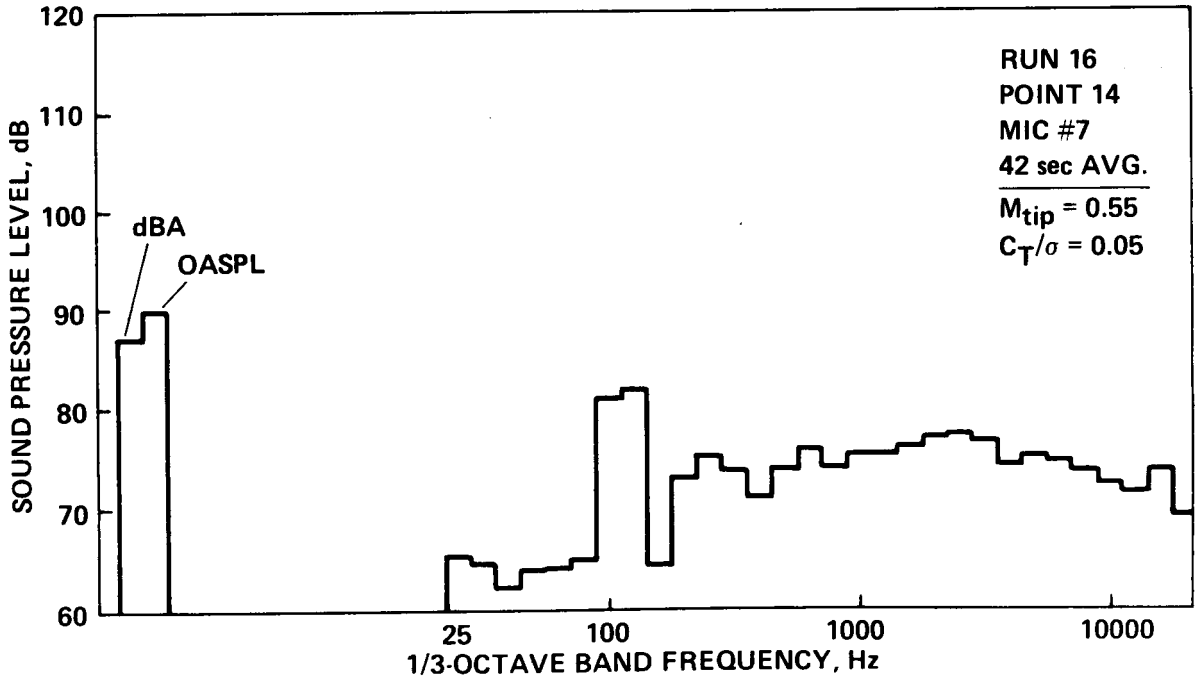

Figure A2.– Continued.

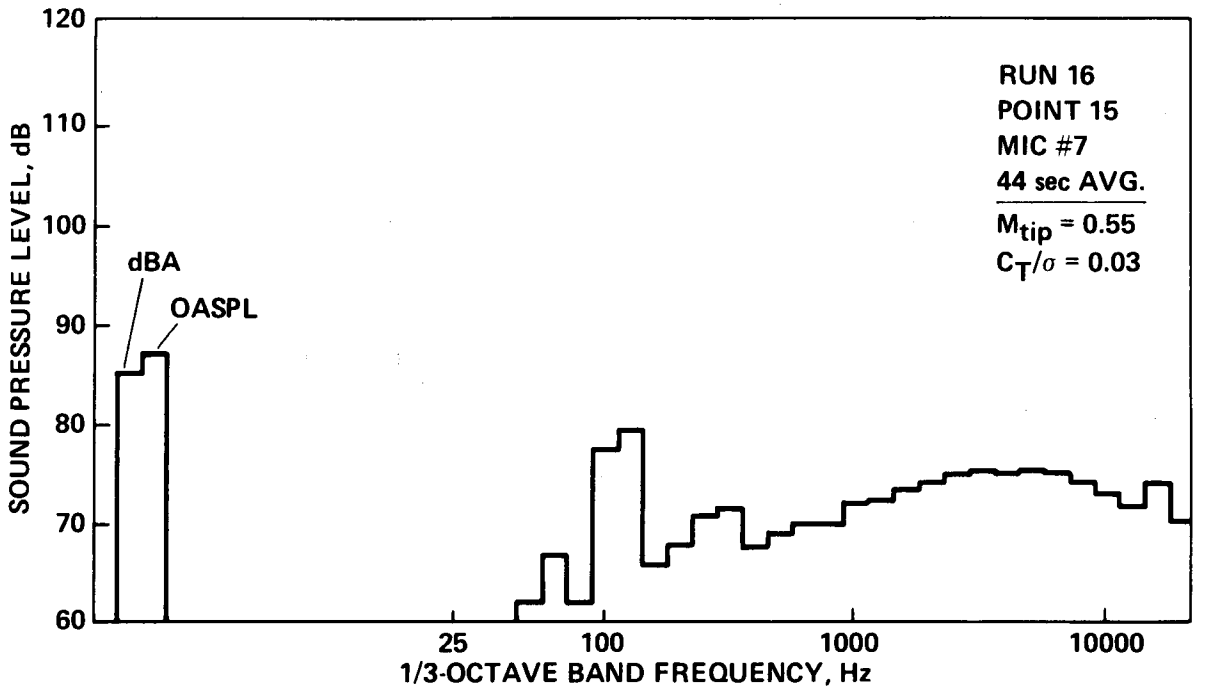

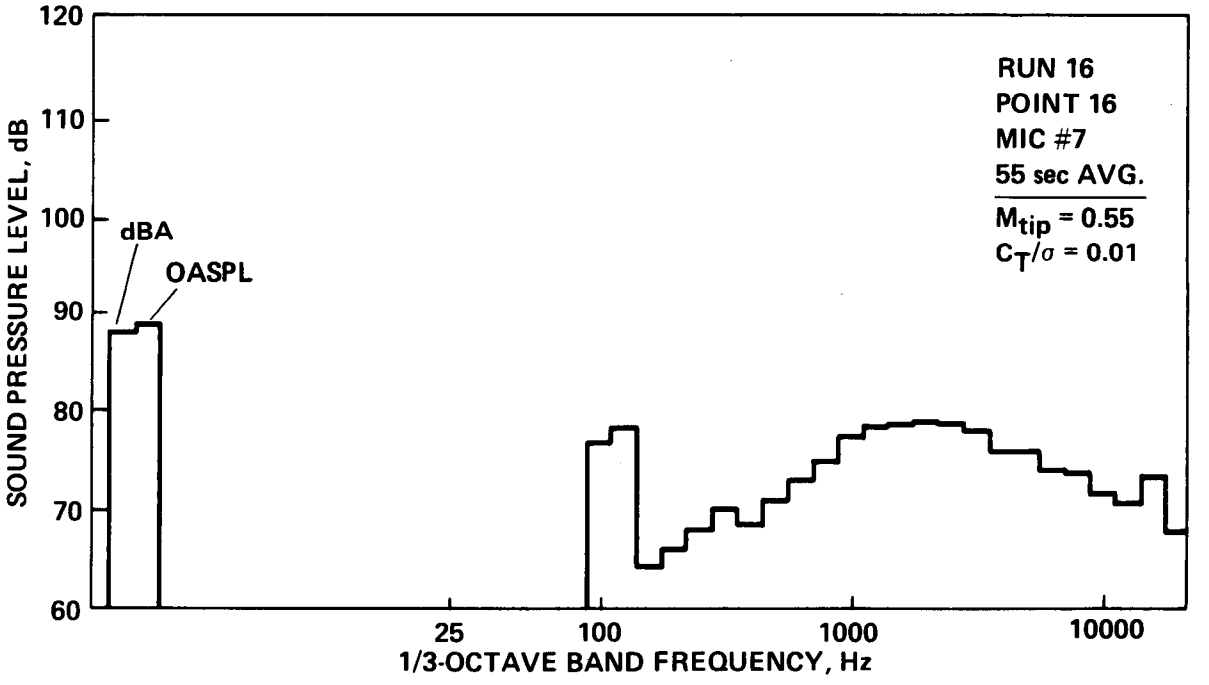

Figure A2.– Continued.

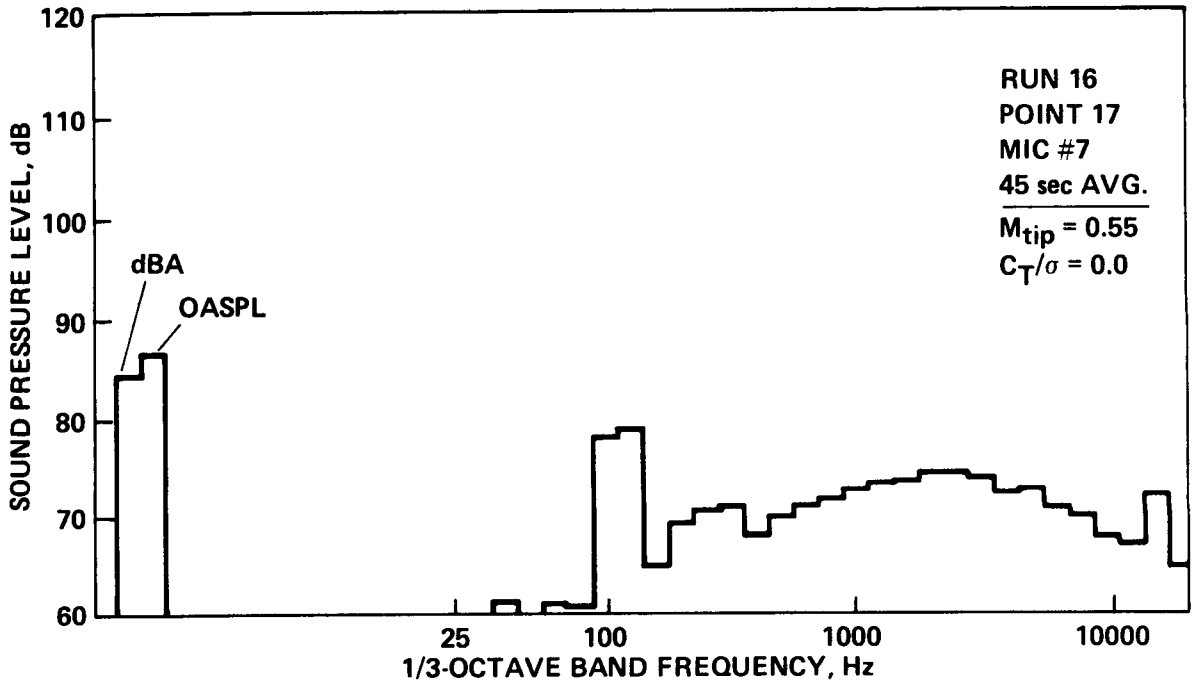

Figure A2.– Continued.

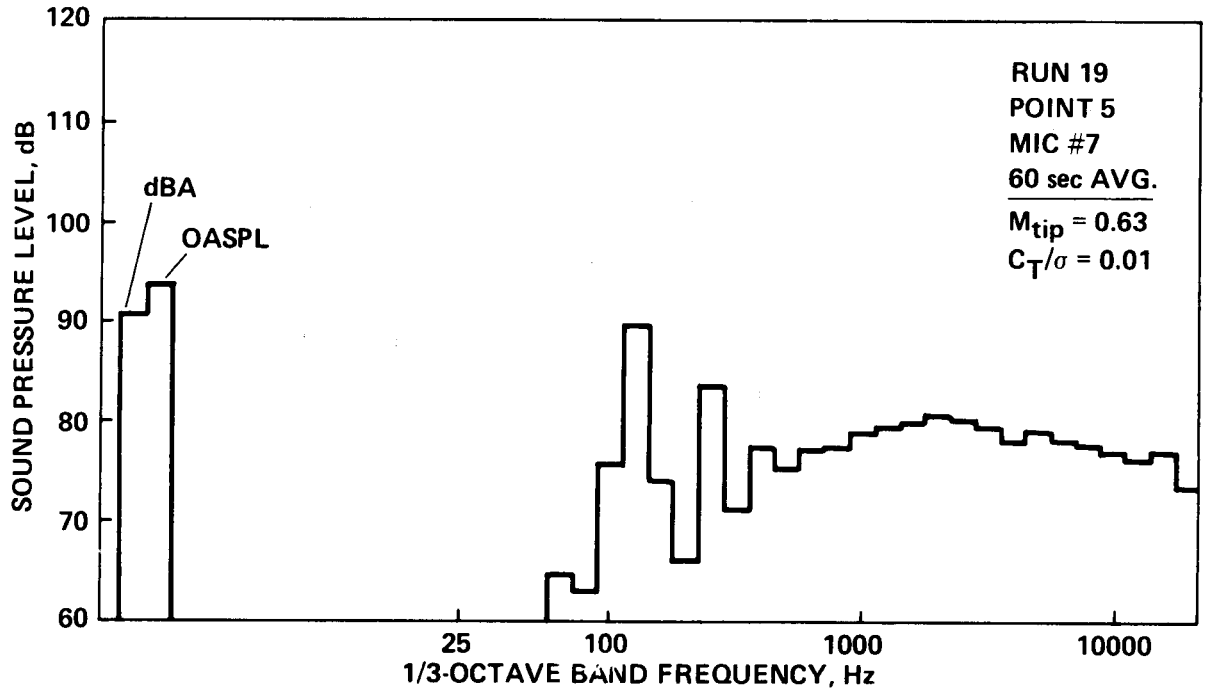

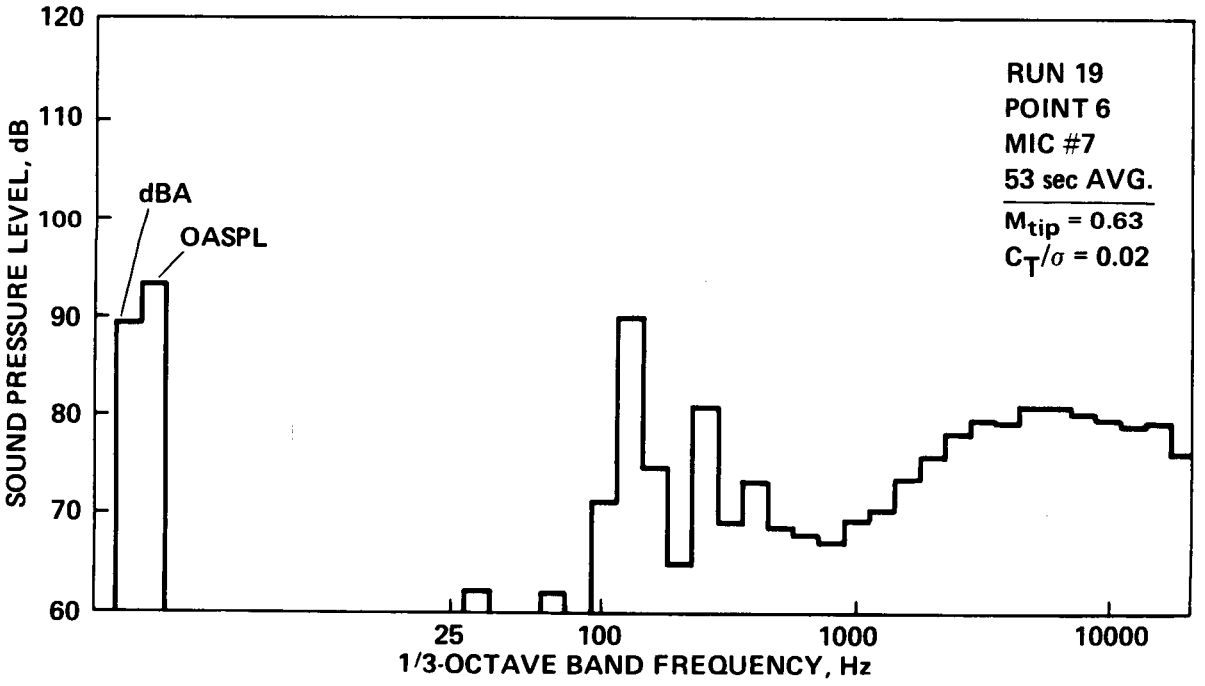

Figure A2.– Continued.

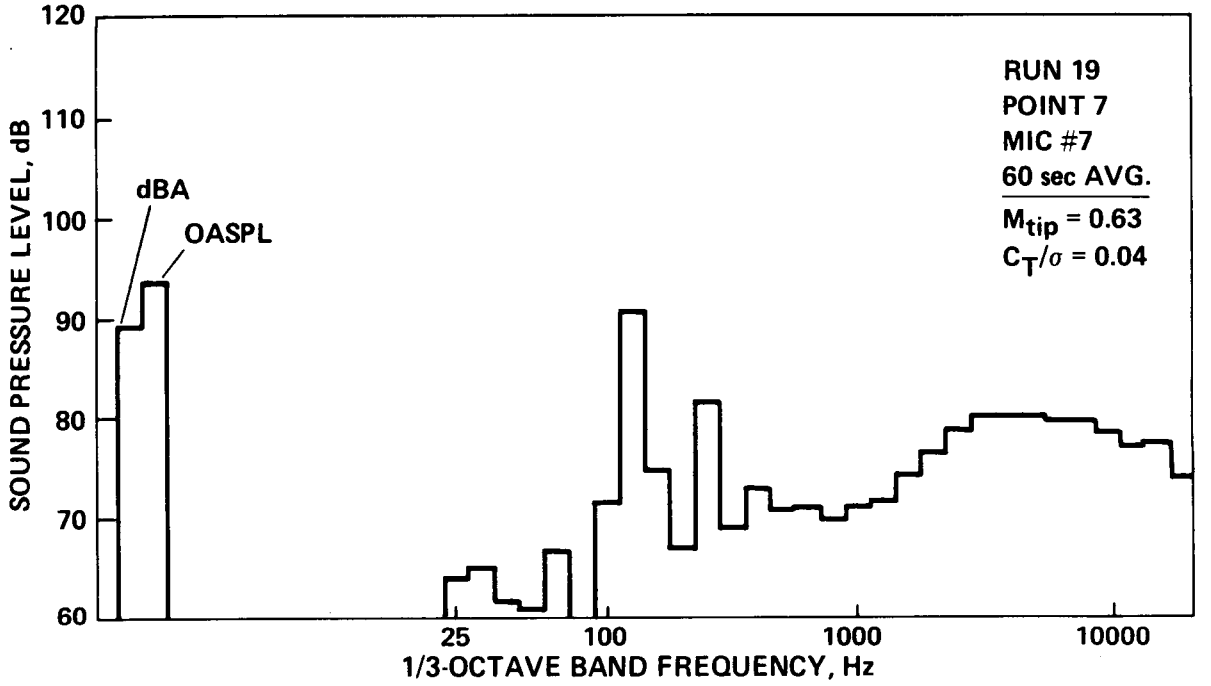

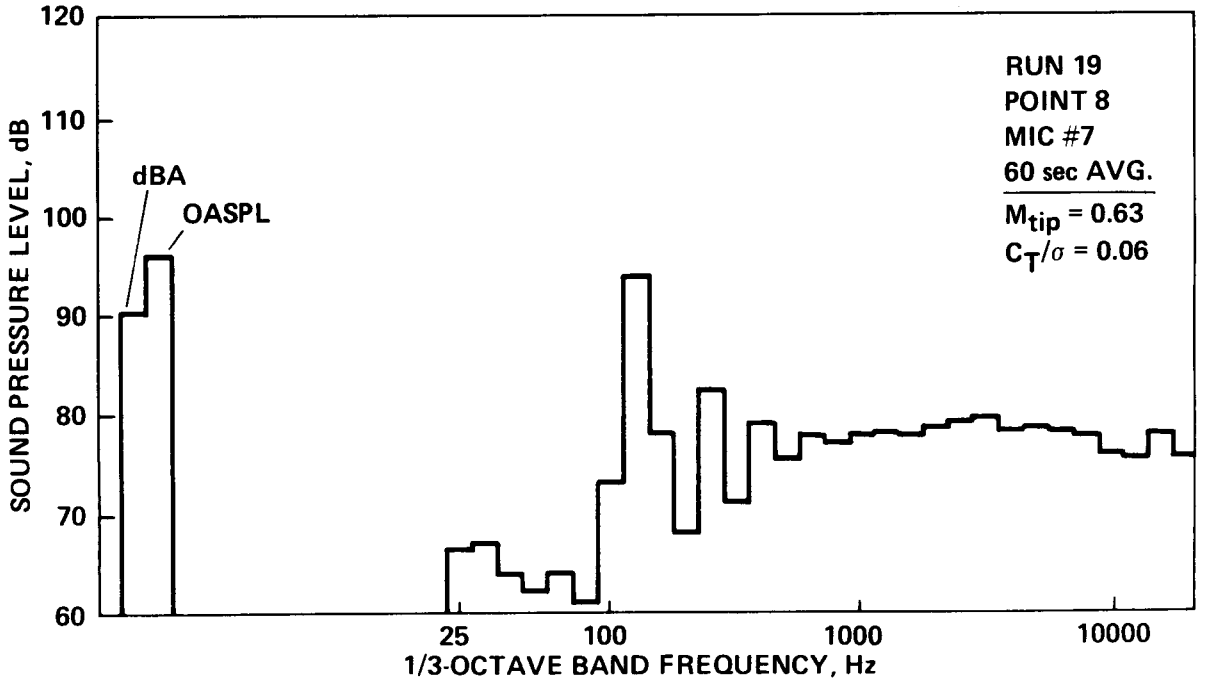

Figure A2.– Continued.

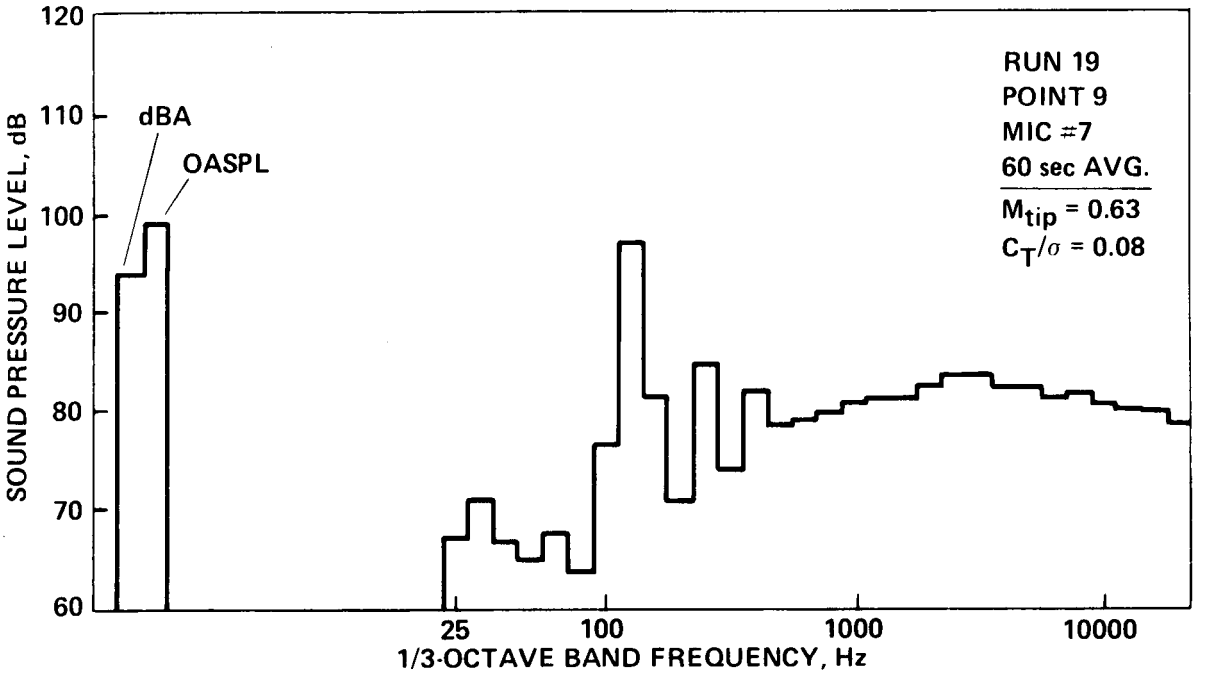

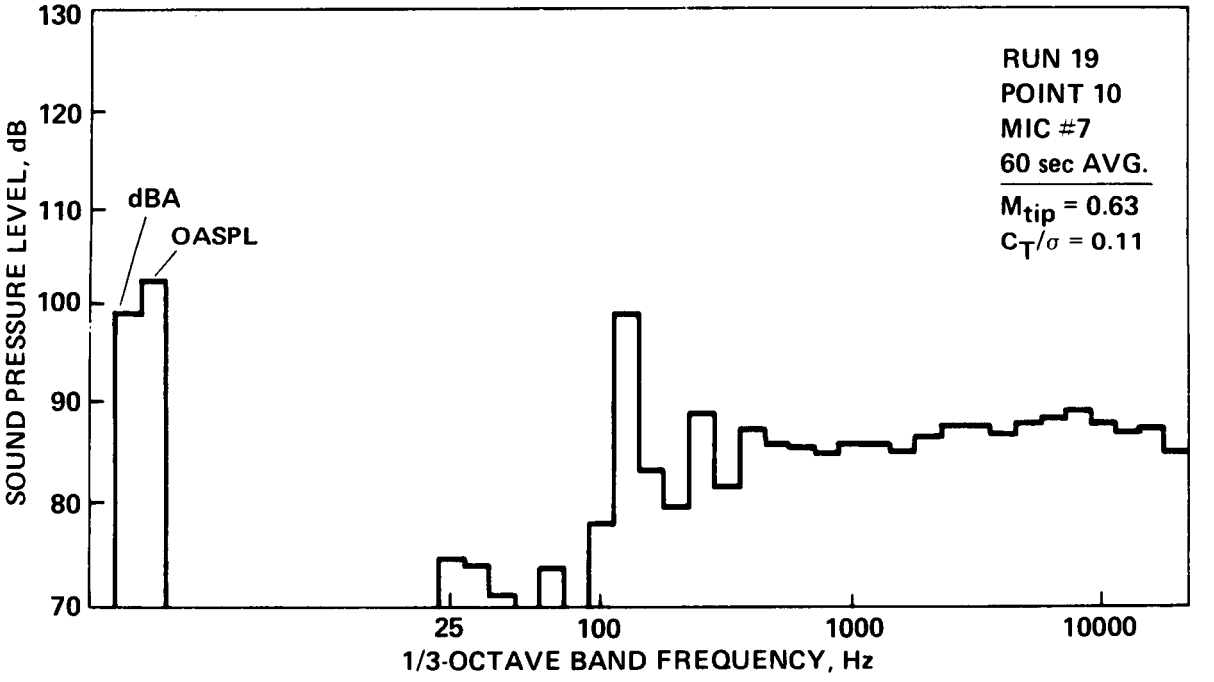

Figure A2.– Continued.

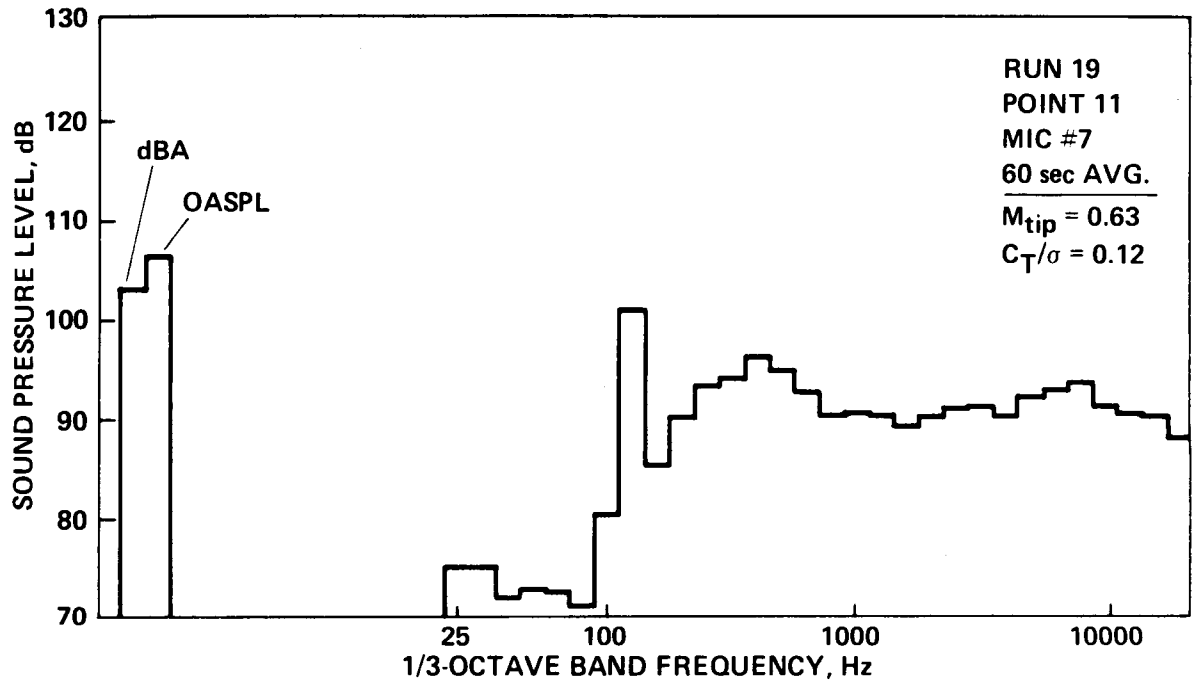

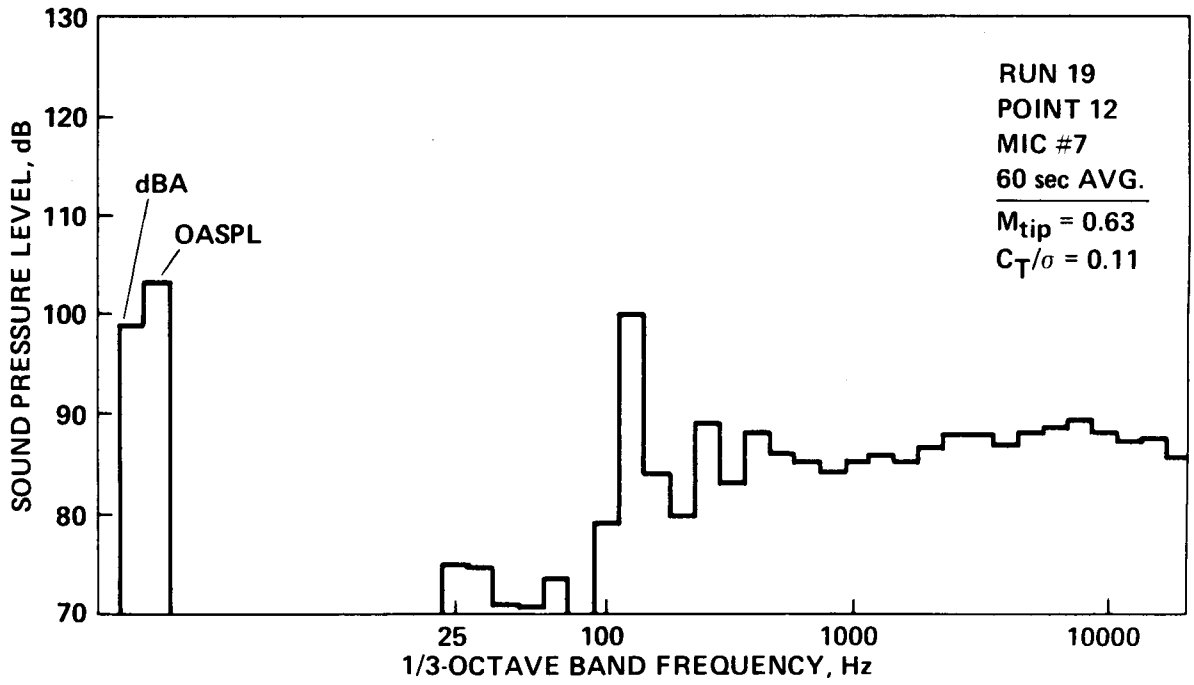

Figure A2.– Continued.

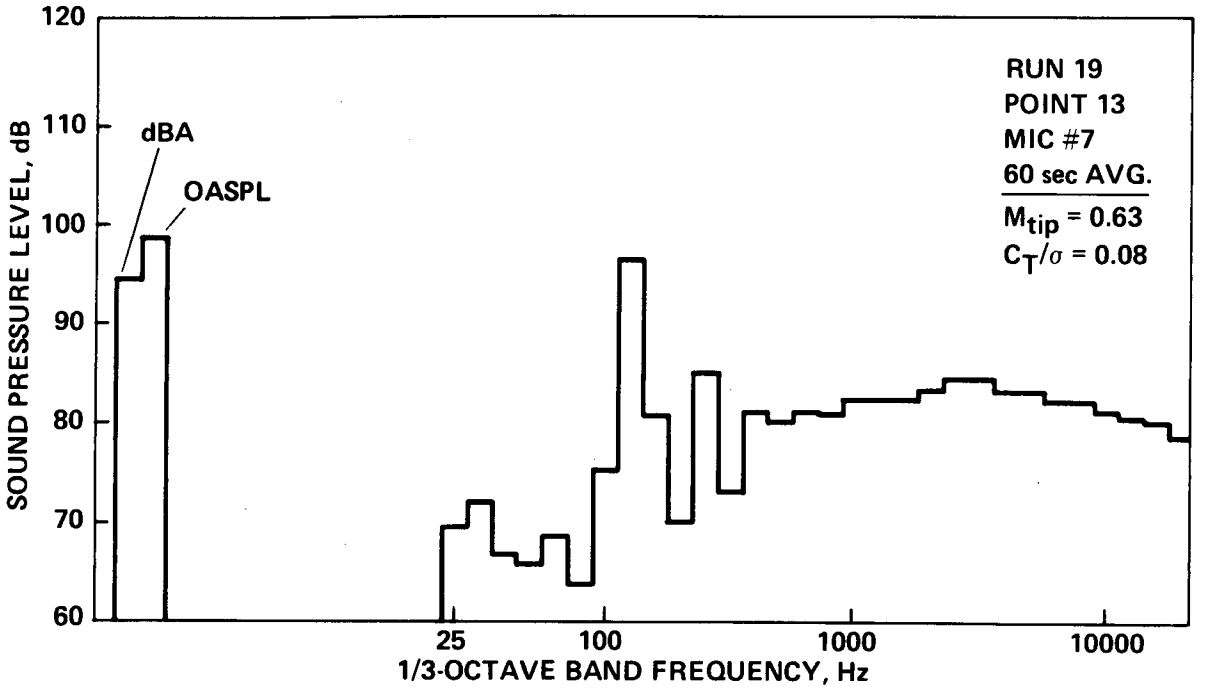

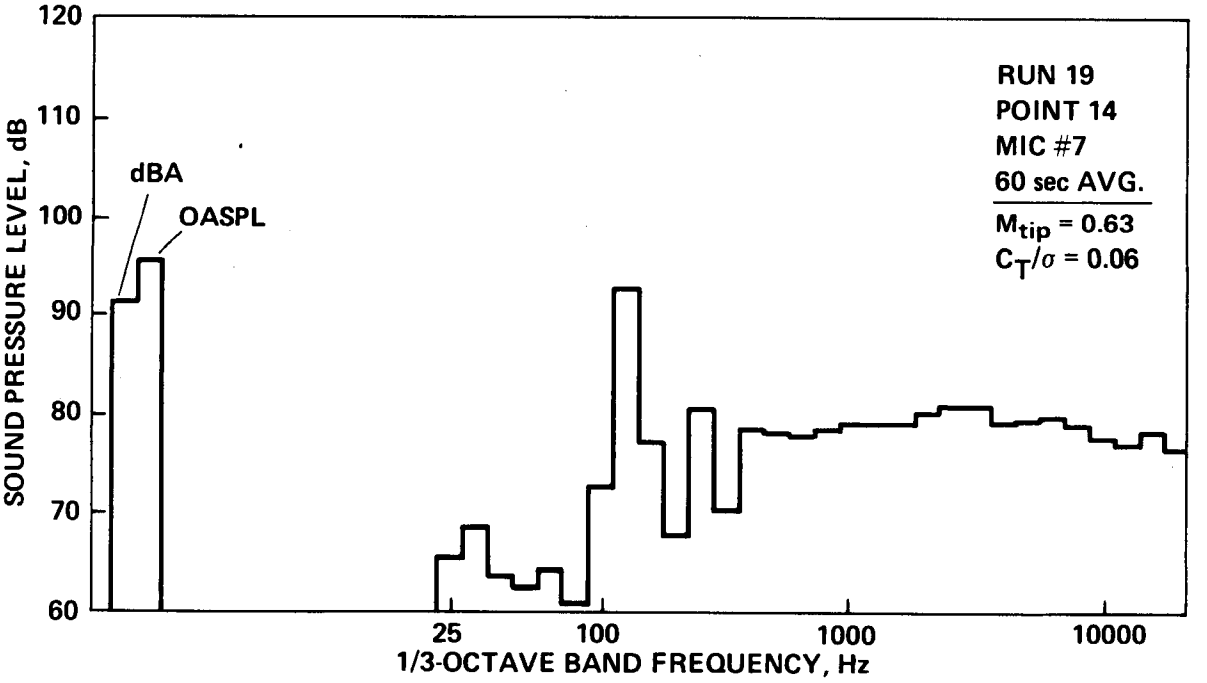

Figure A2.– Continued.

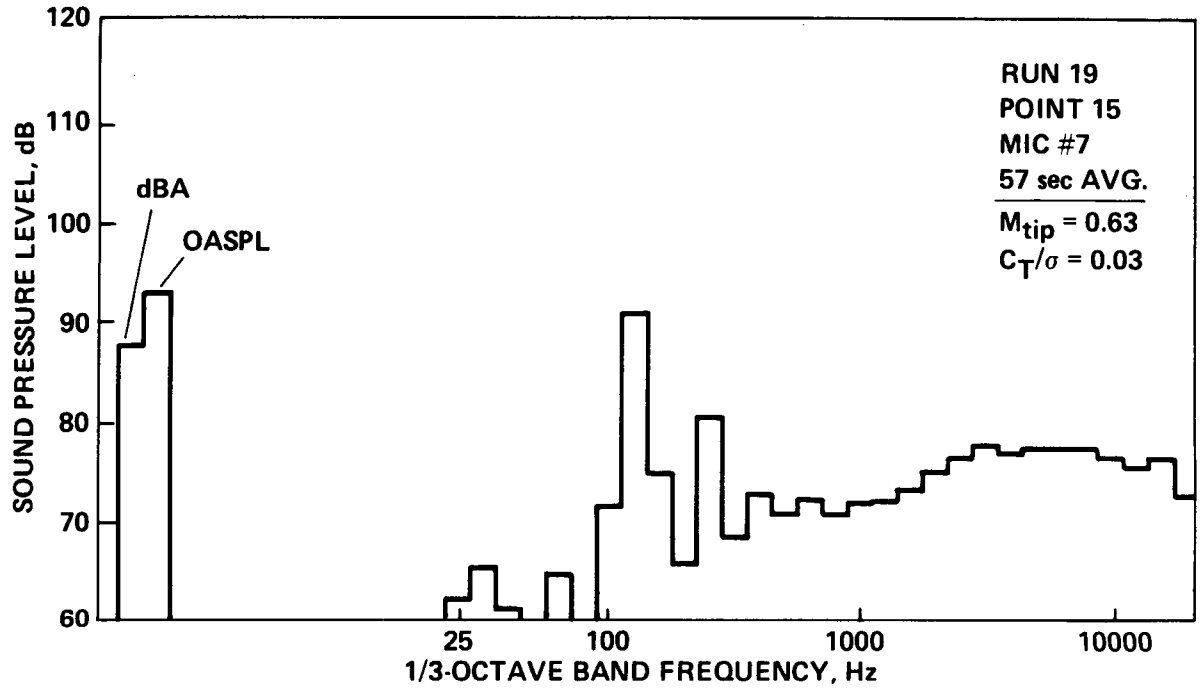

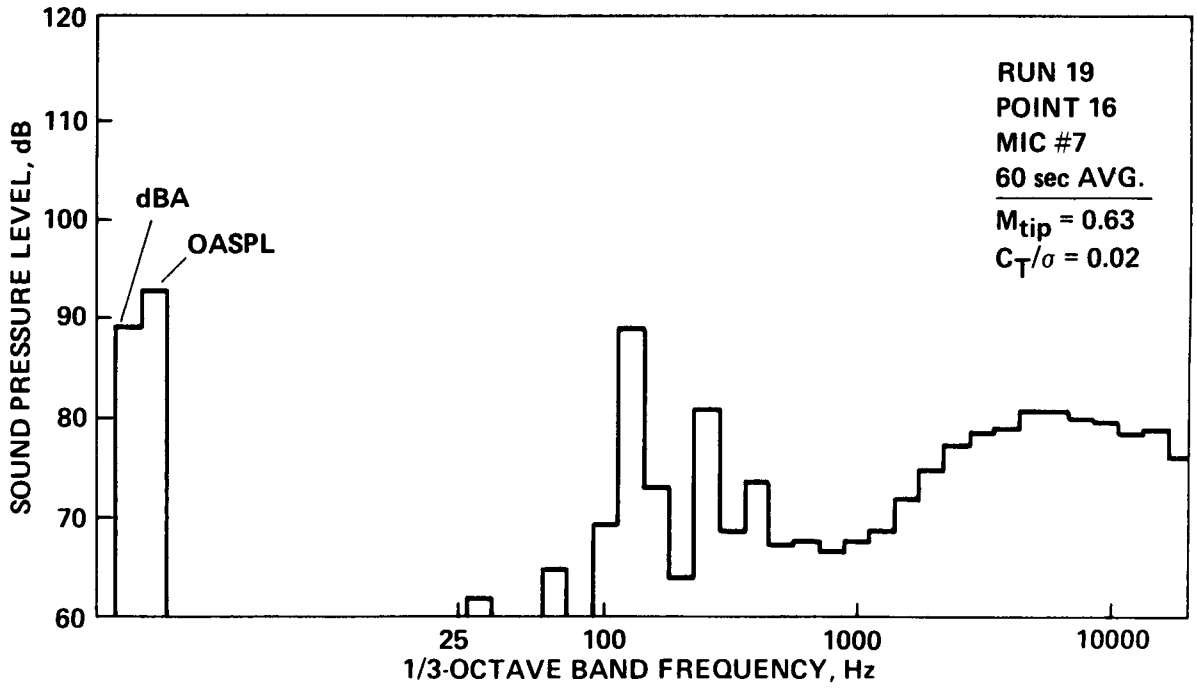

Figure A2.– Continued.

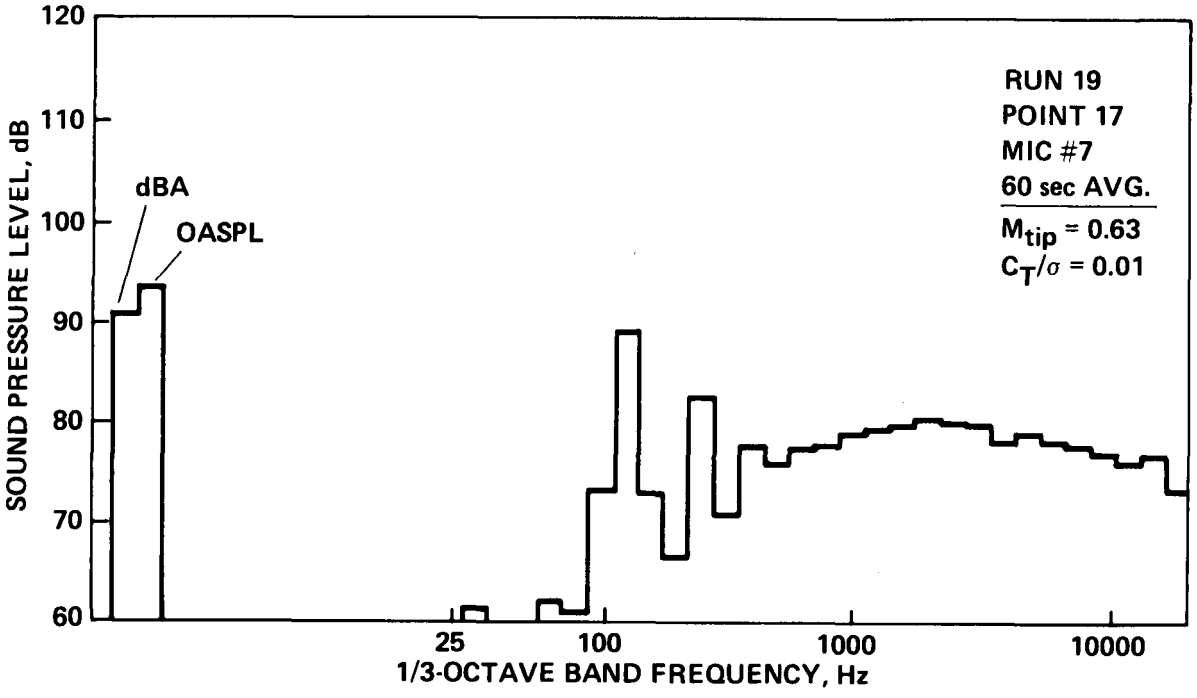

Figure A2.– Concluded.

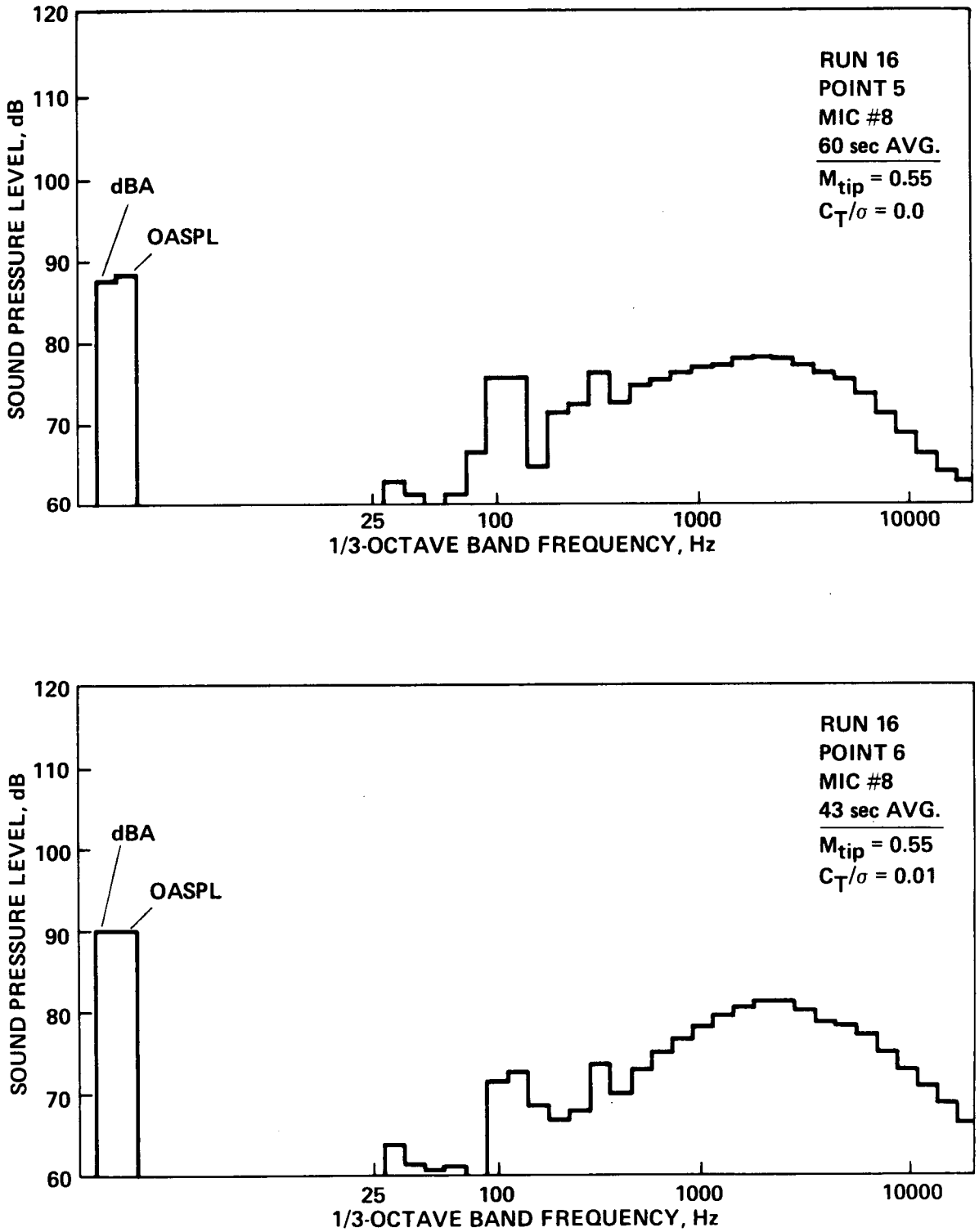

Figure A3.– 1/3-octave band acoustic spectra—Microphone No. 8: r/D = 2.0, ψ = 180°, θ = +30°.

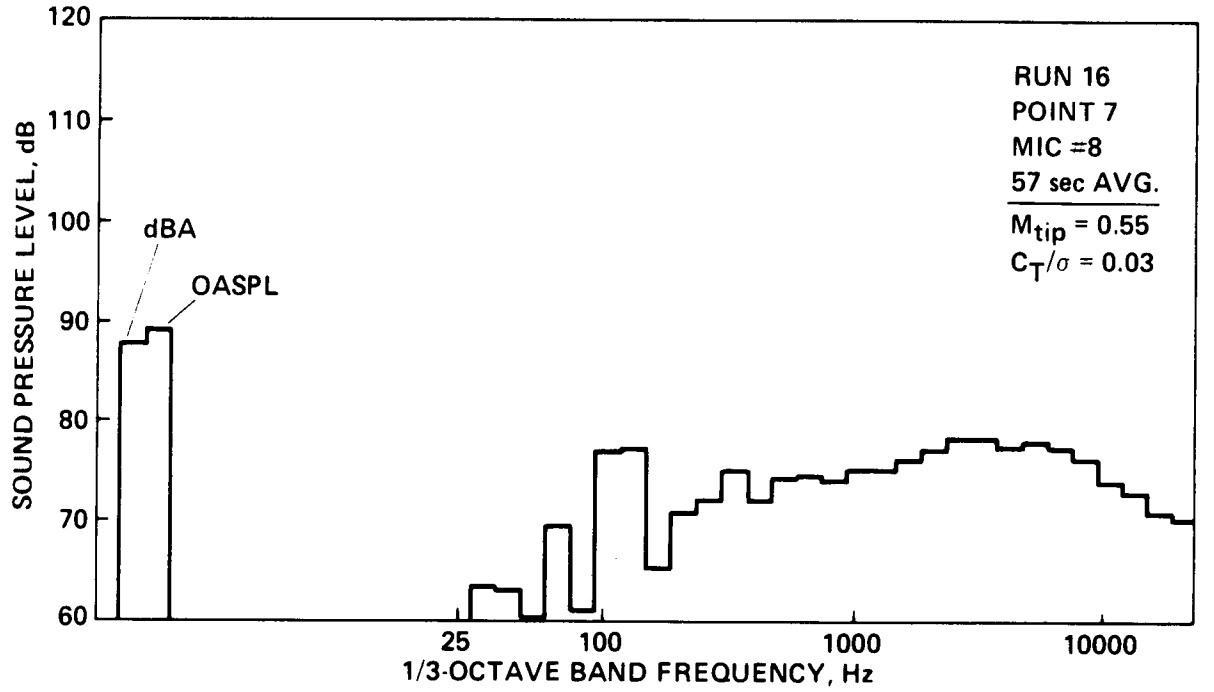

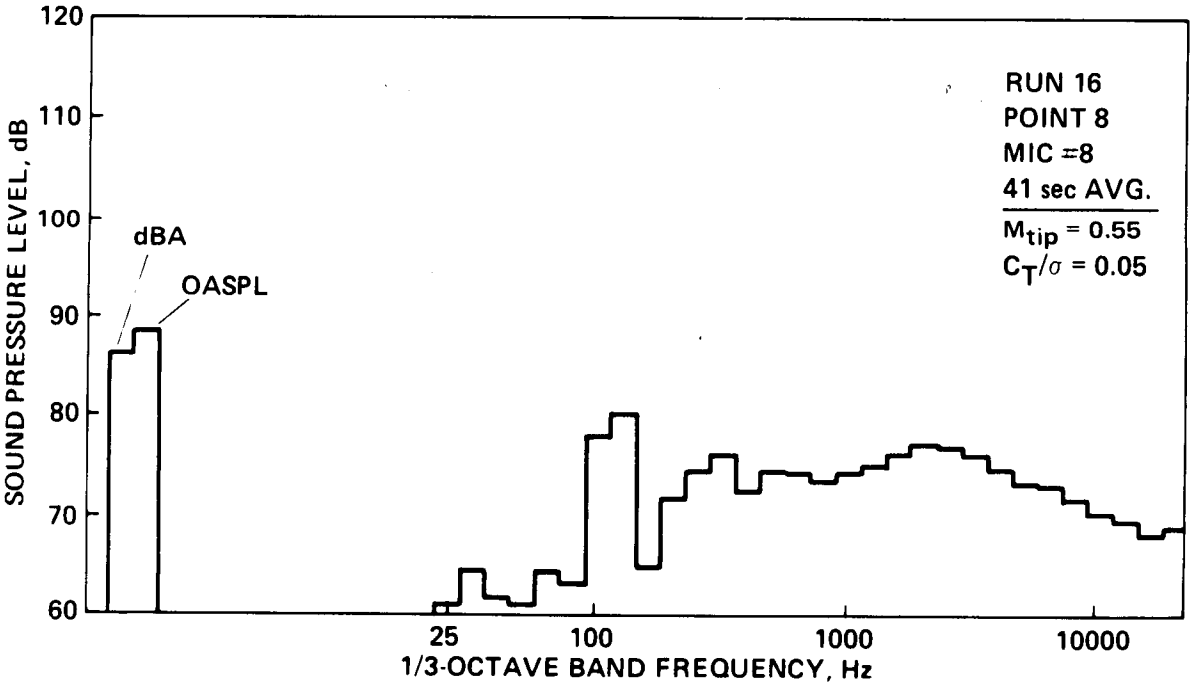

Figure A3.– Continued.

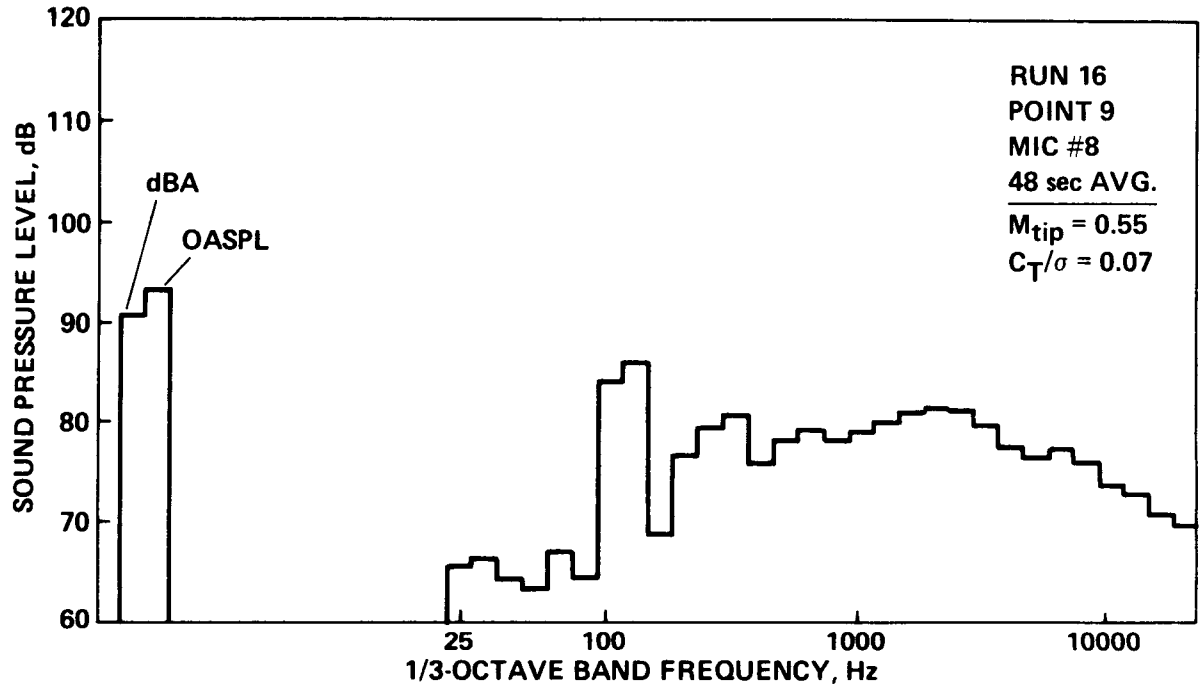

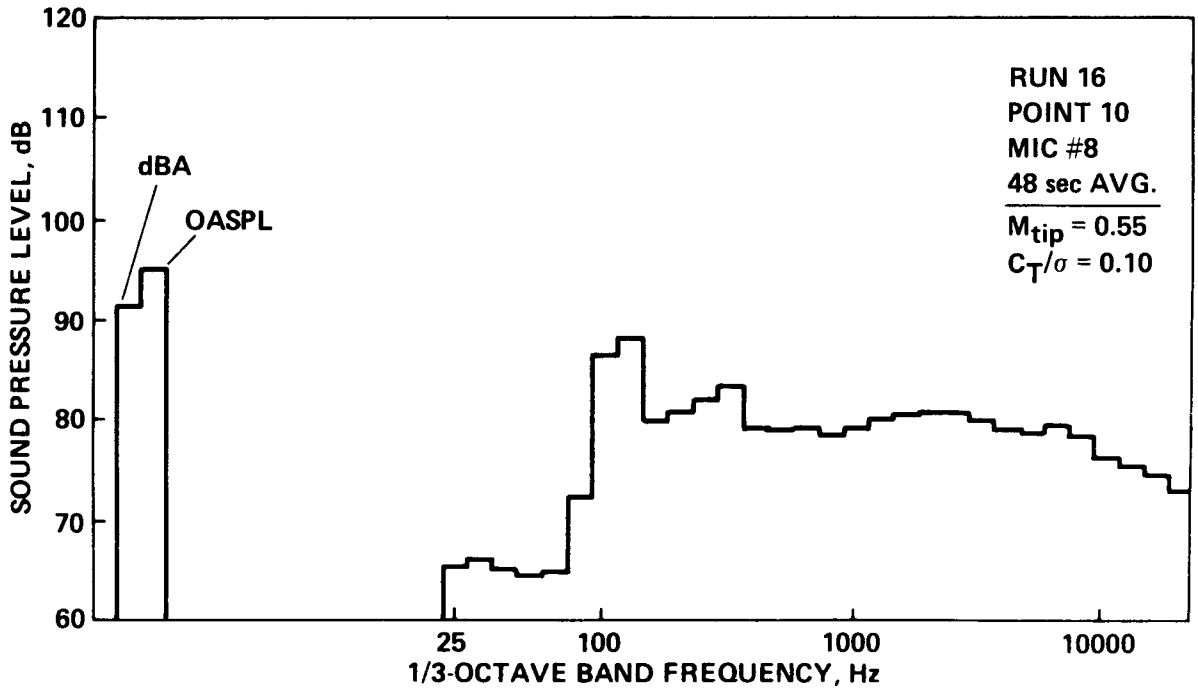

Figure A3.– Continued.

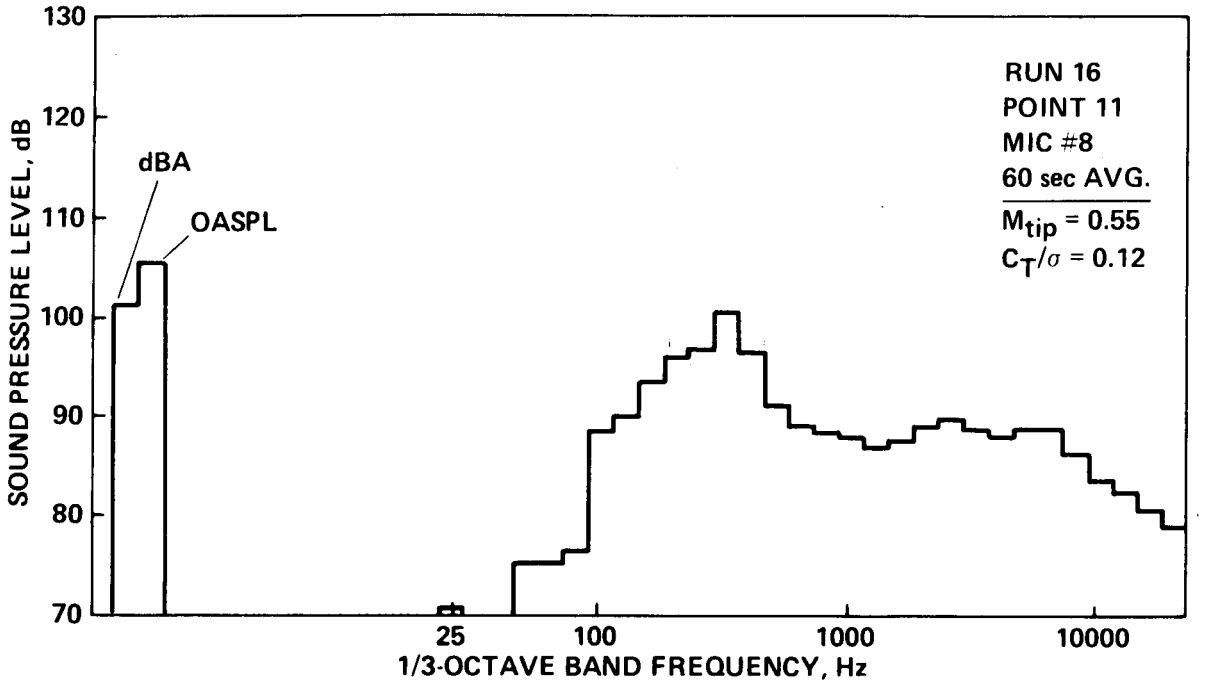

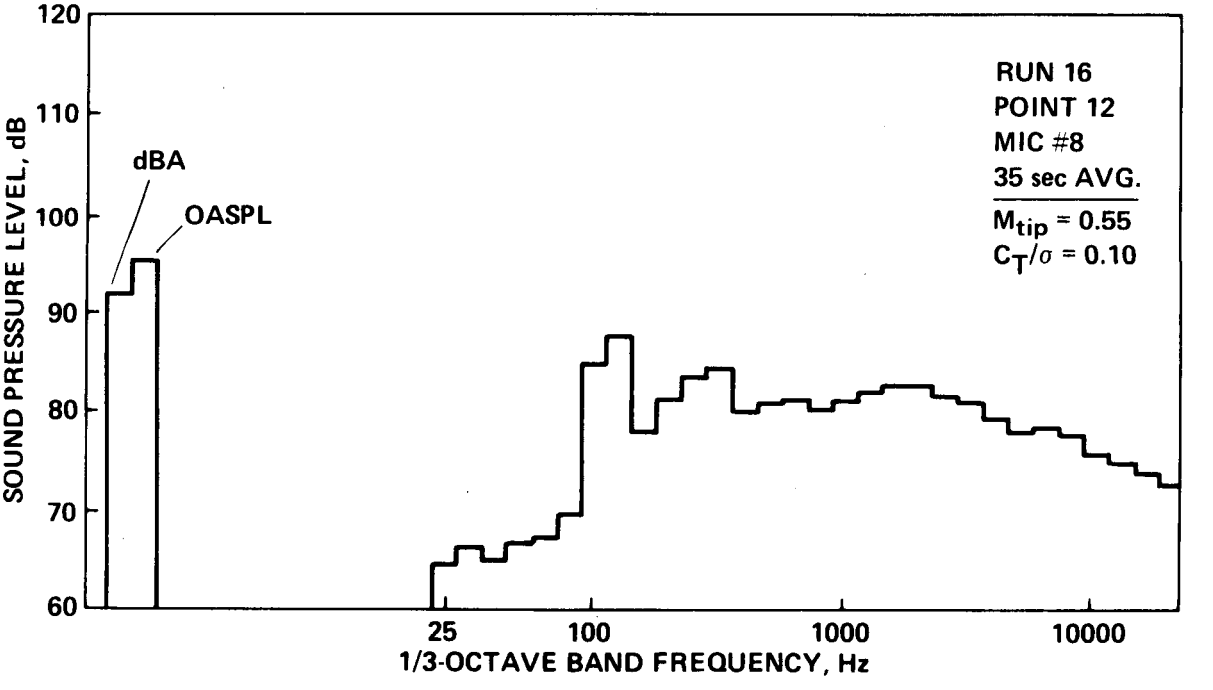

Figure A3.– Continued.

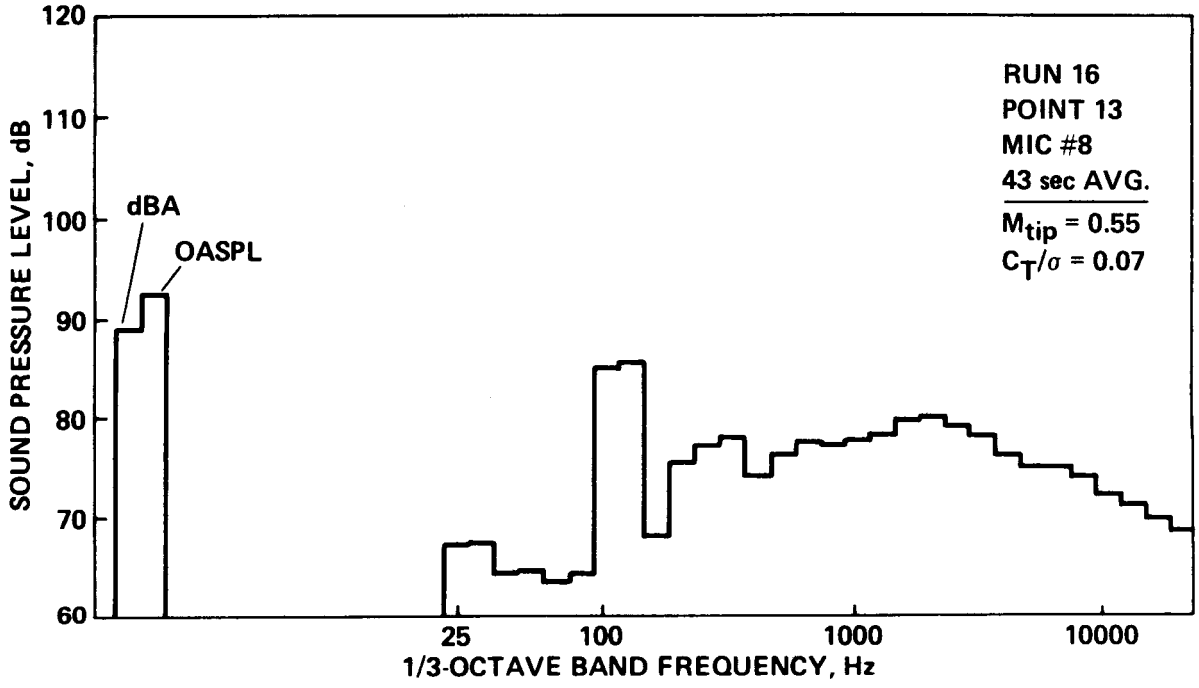

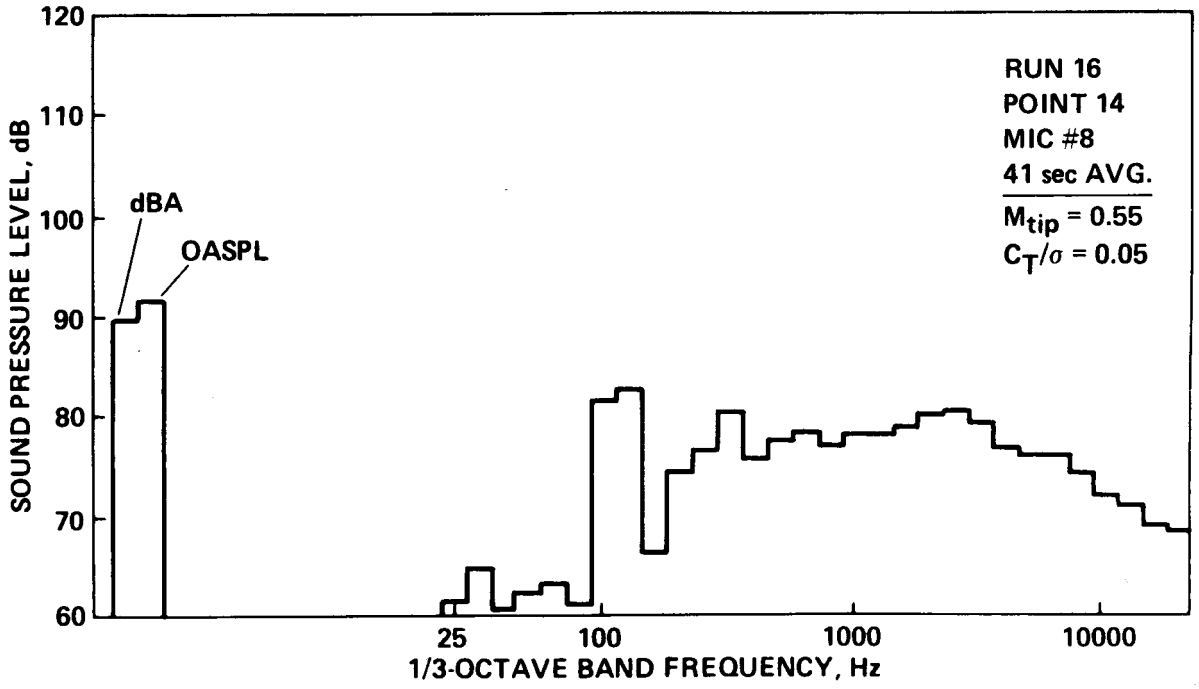

Figure A3.– Continued.

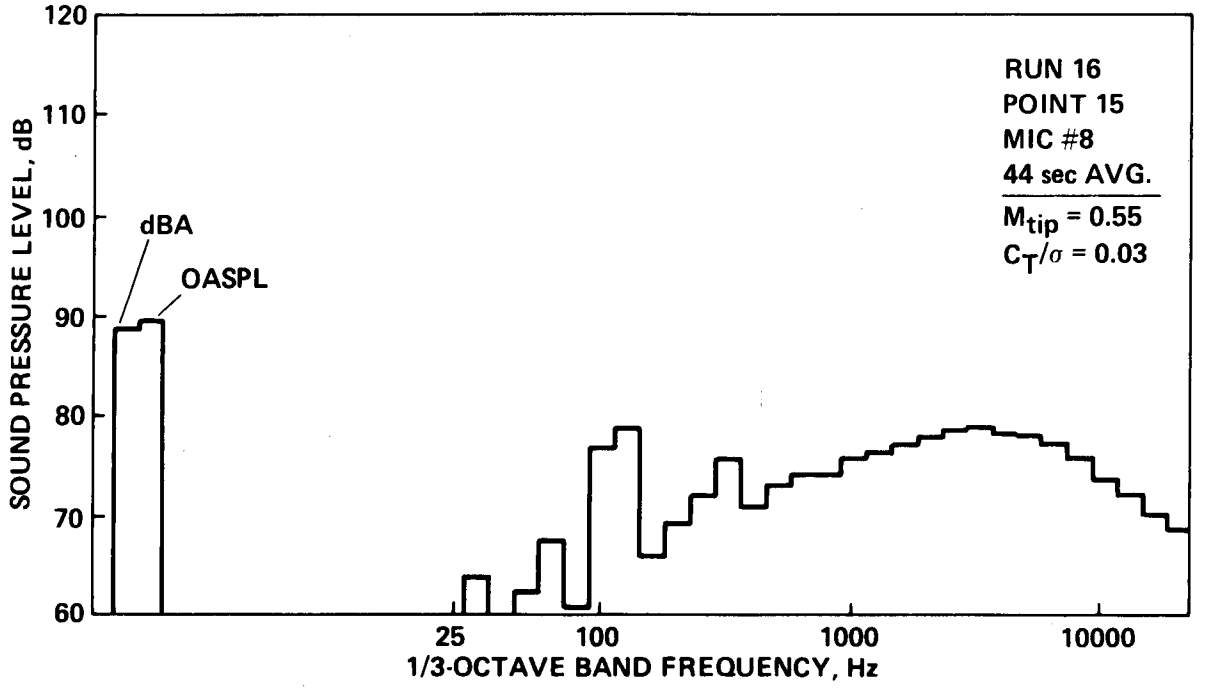

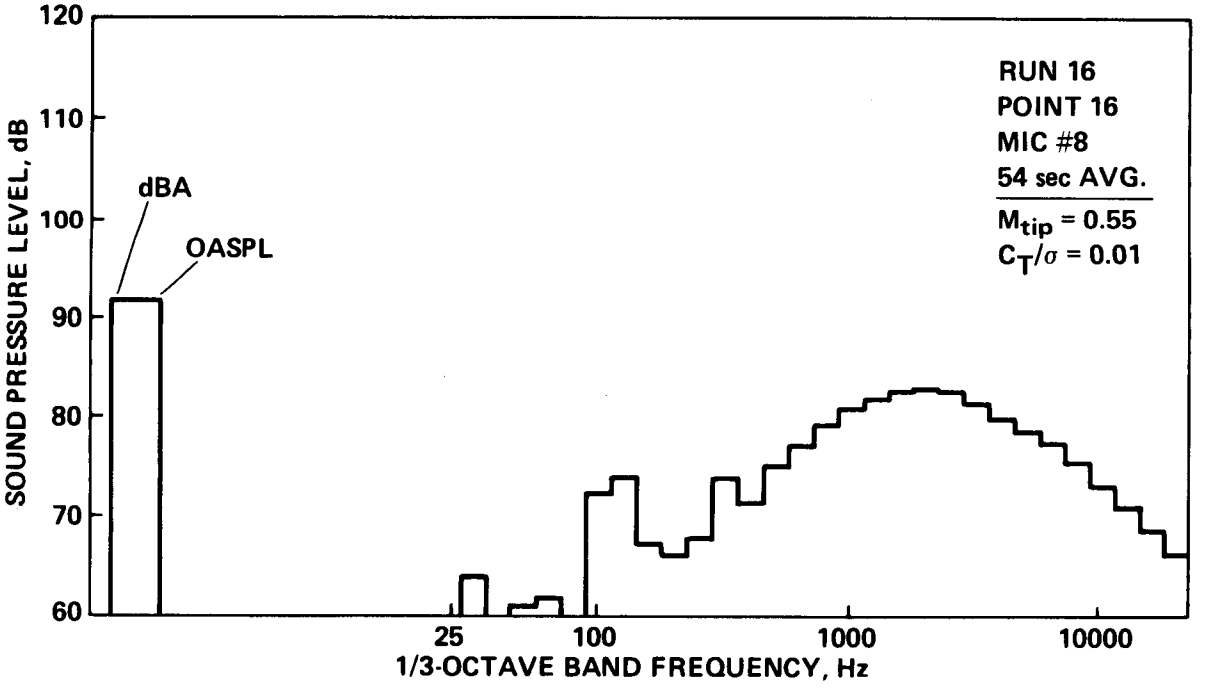

Figure A3.– Continued.

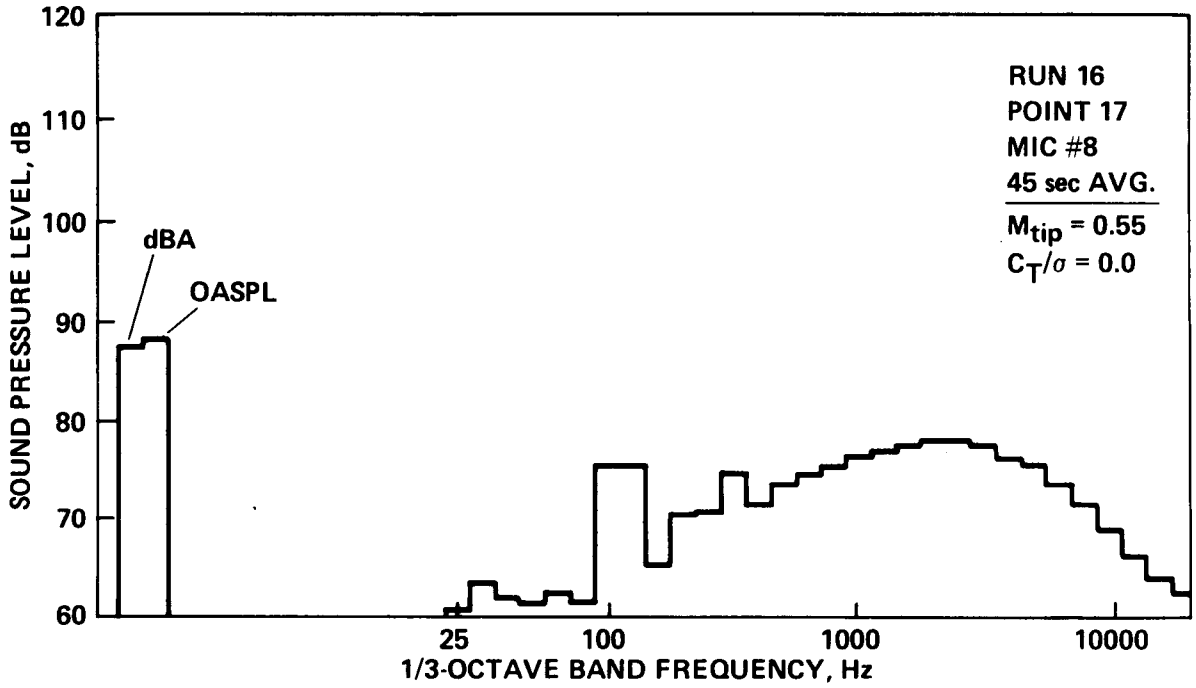

Figure A3.– Continued.

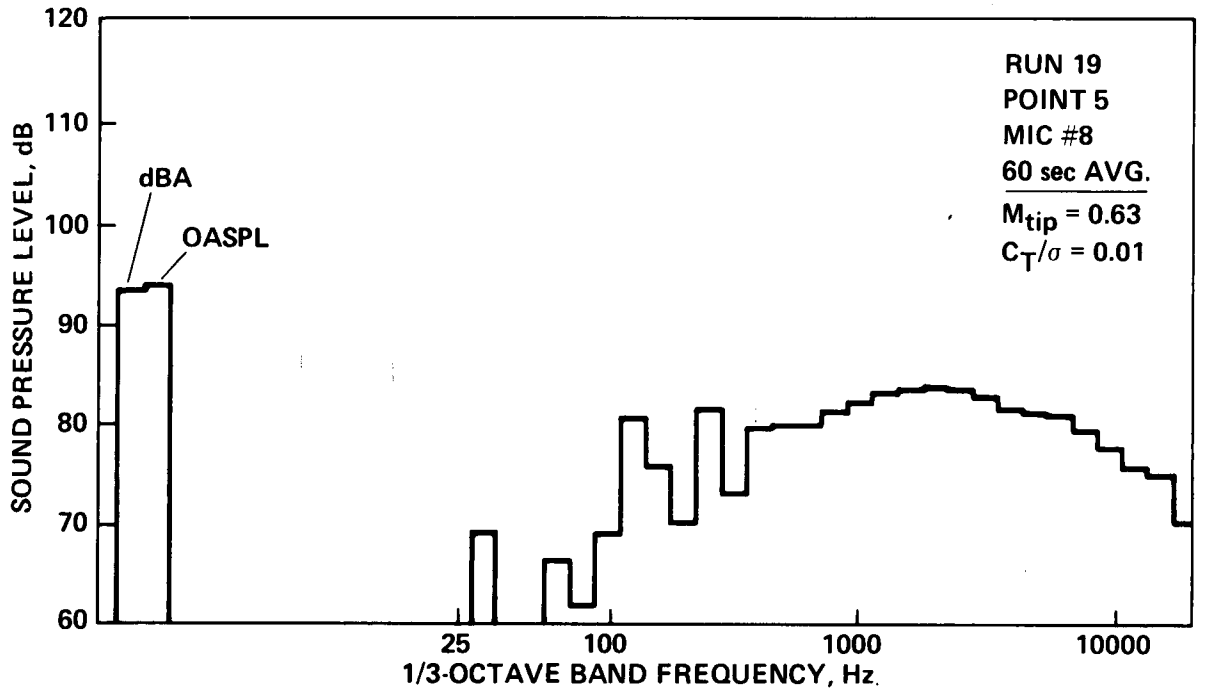

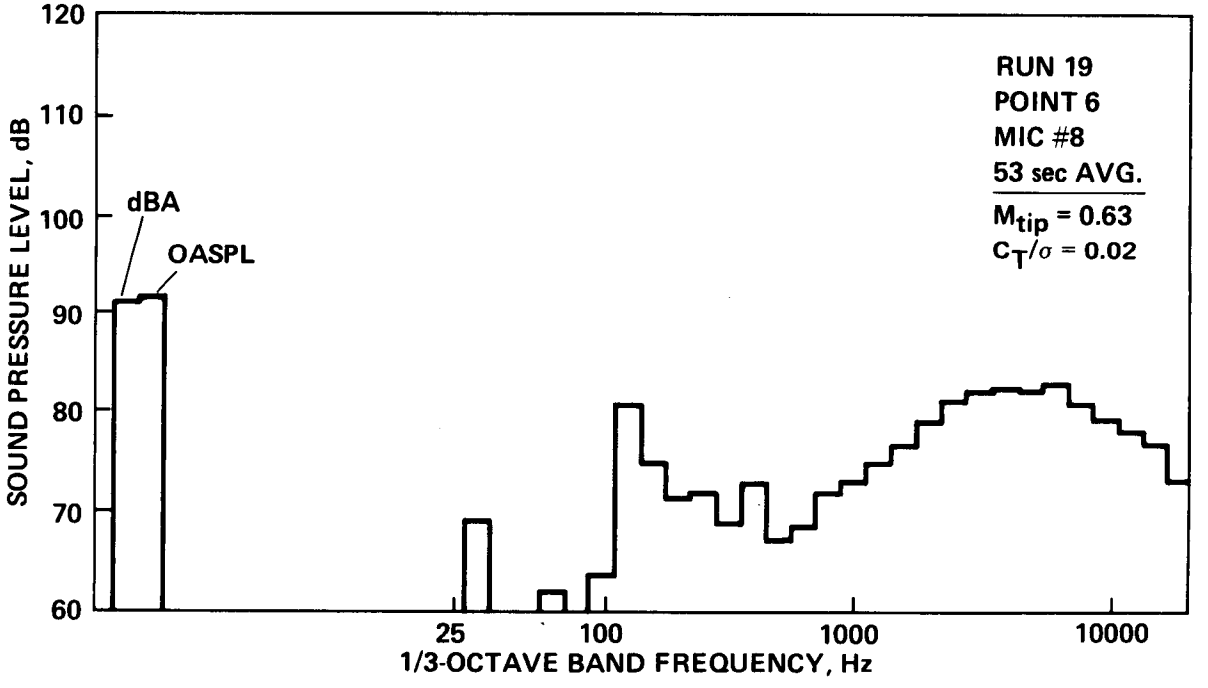

Figure A3.– Continued.

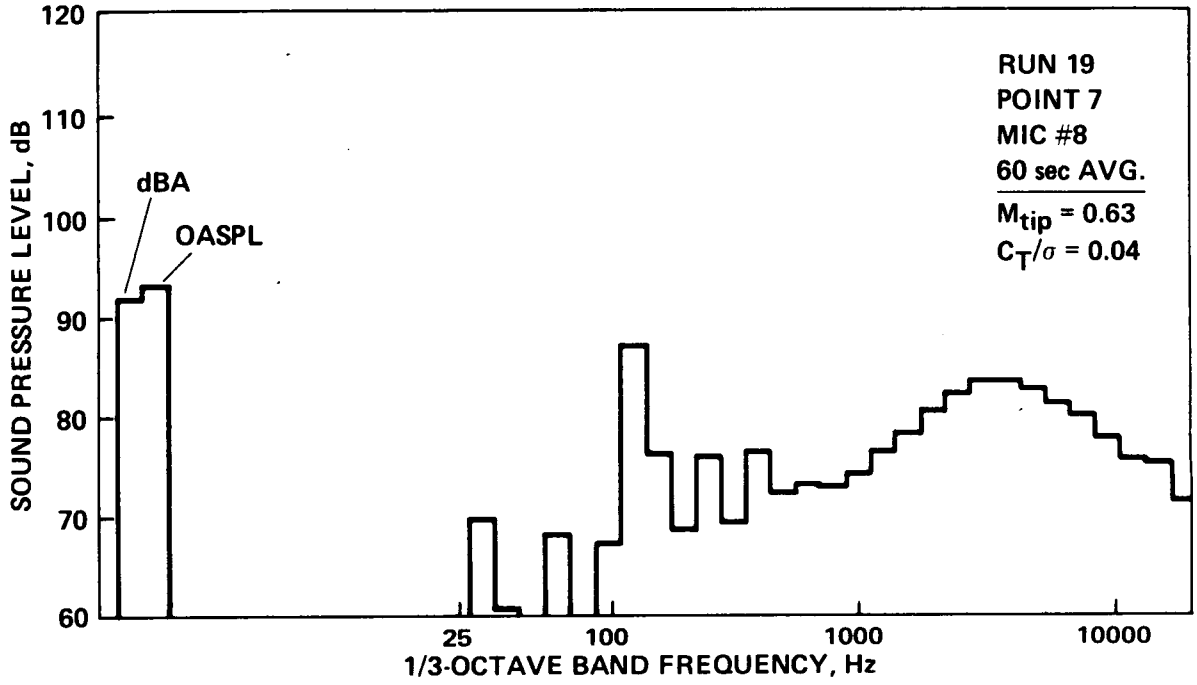

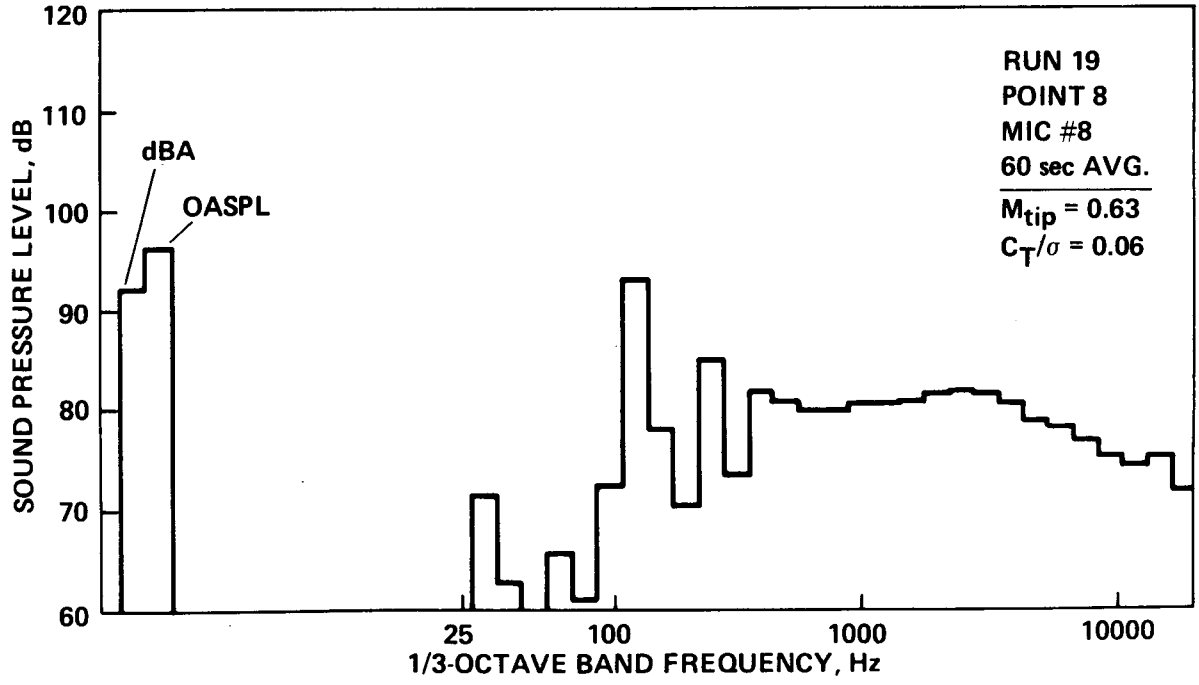

Figure A3.– Continued.

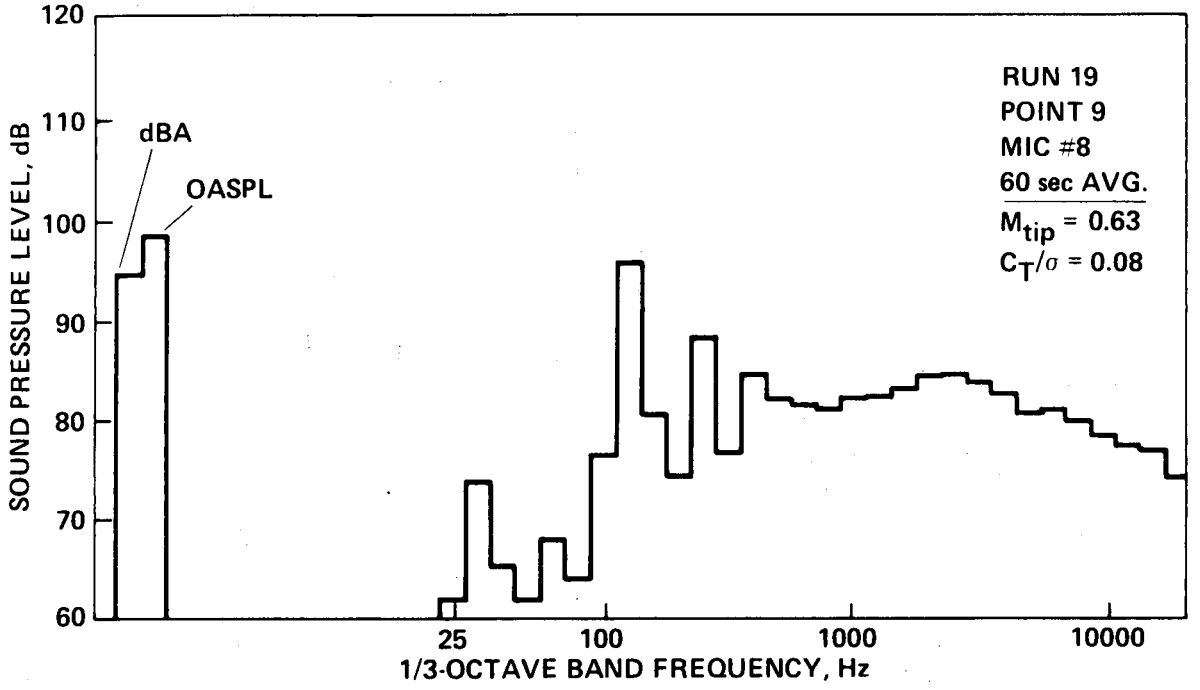

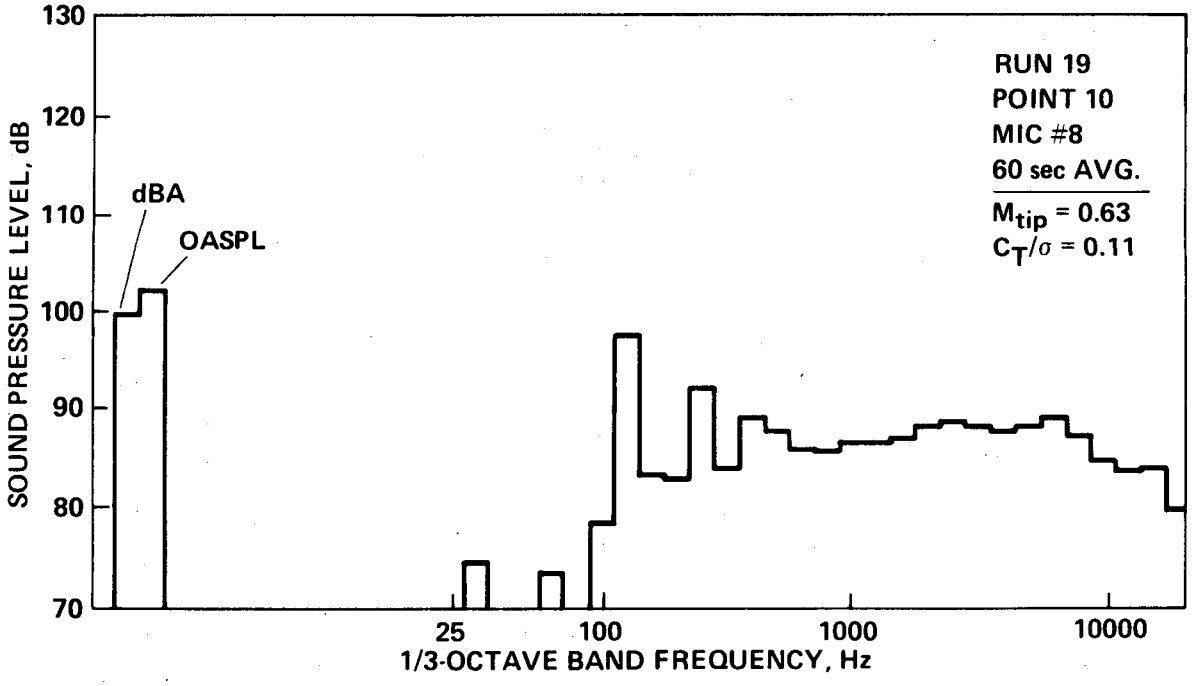

Figure A3.– Continued.

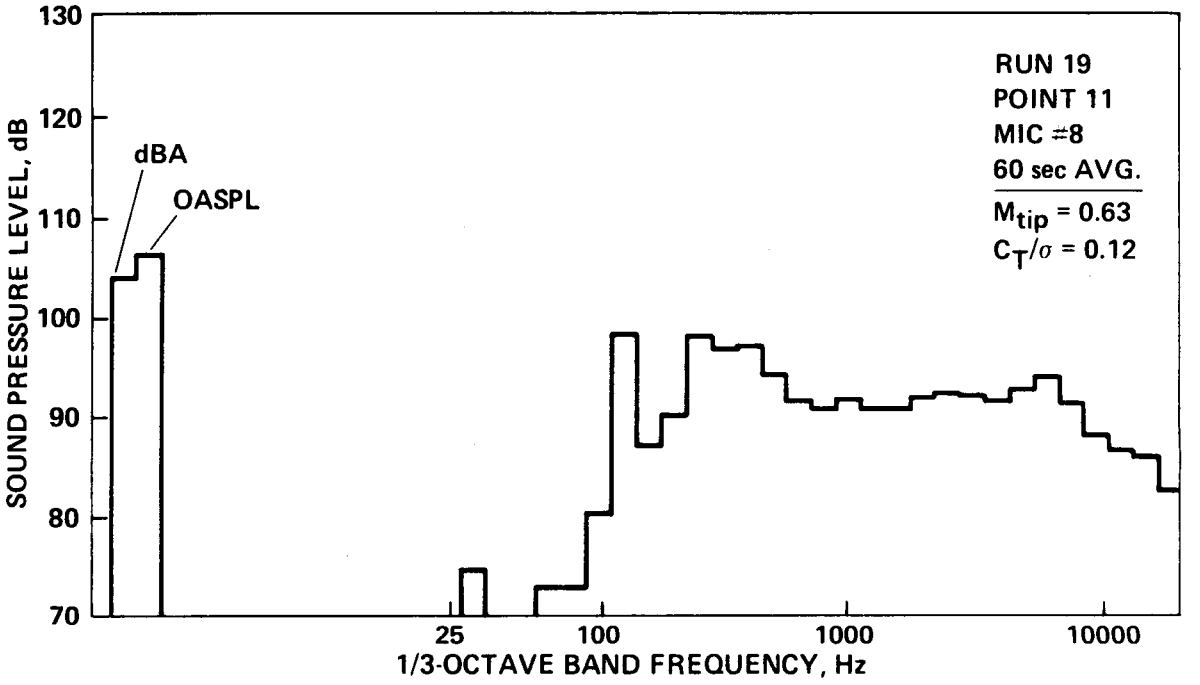

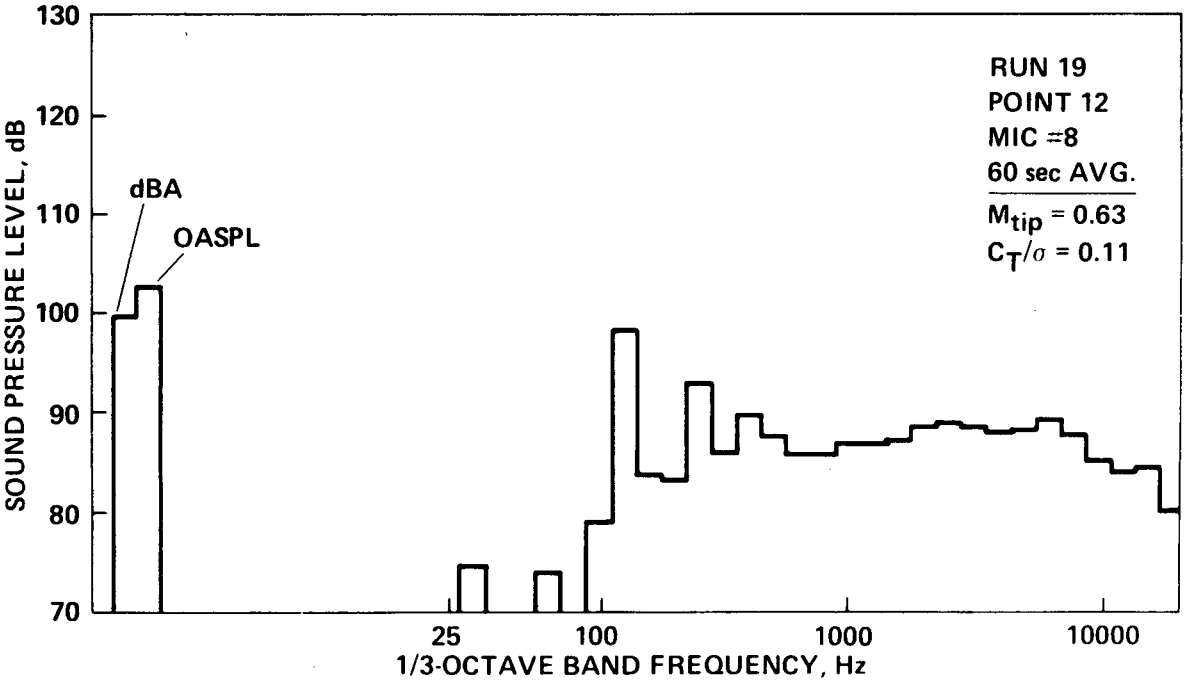

Figure A3.– Continued.

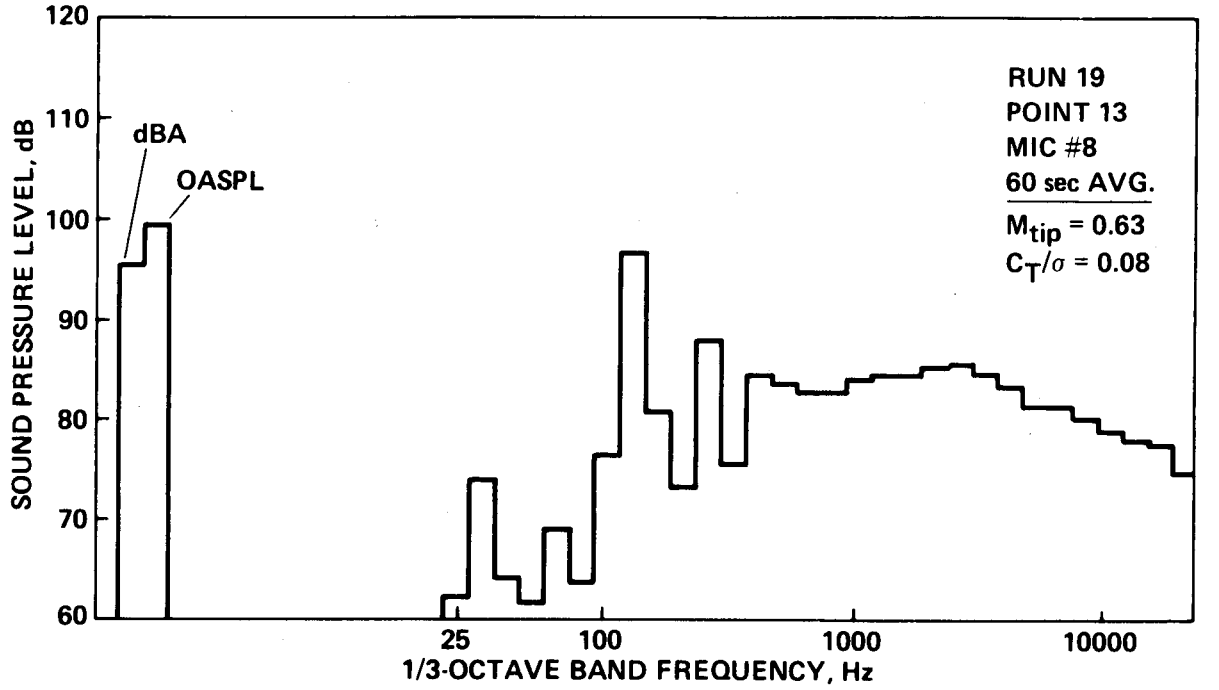

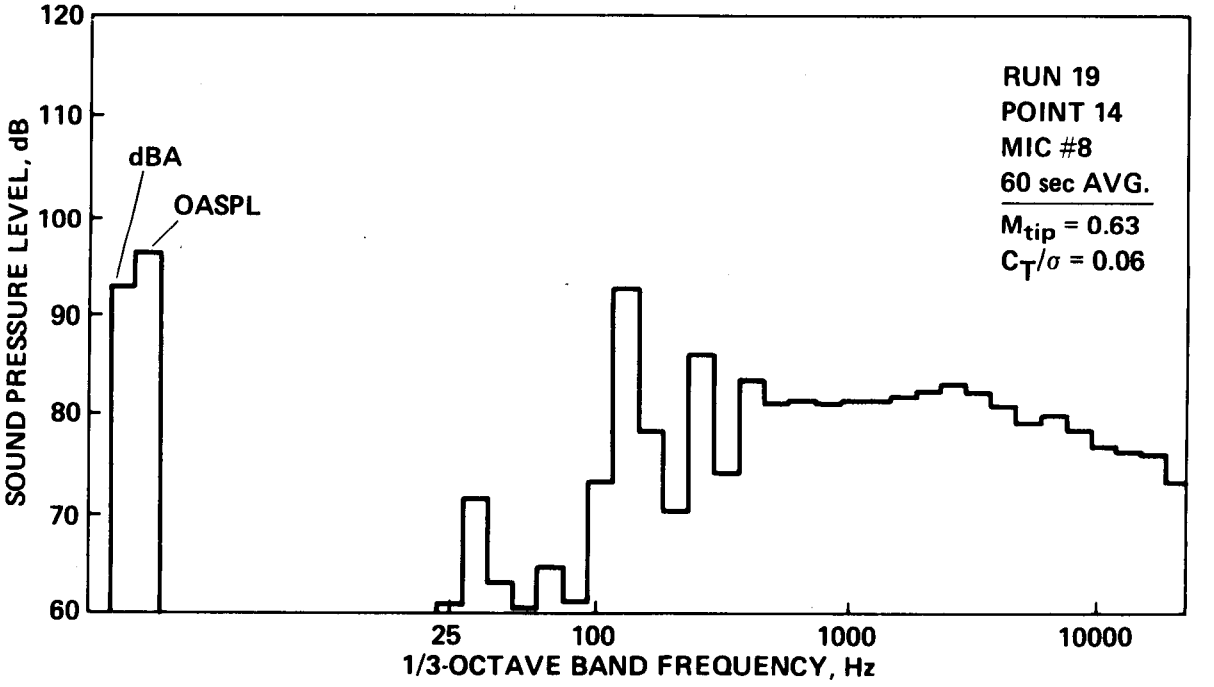

Figure A3.– Continued.

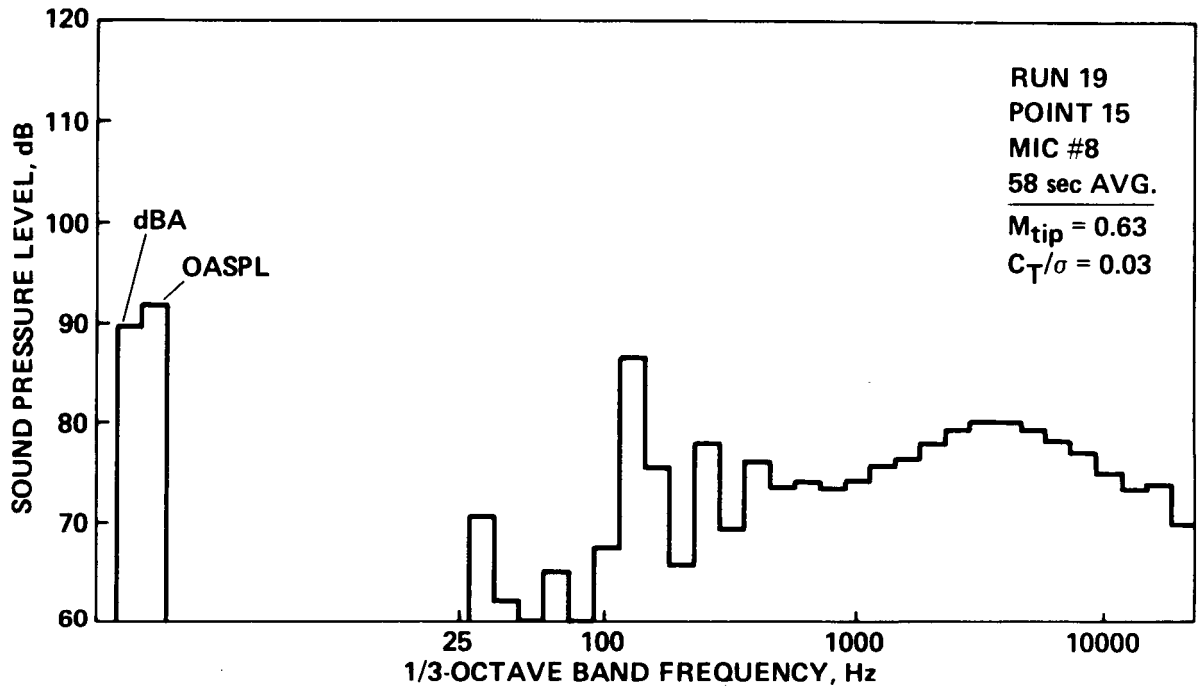

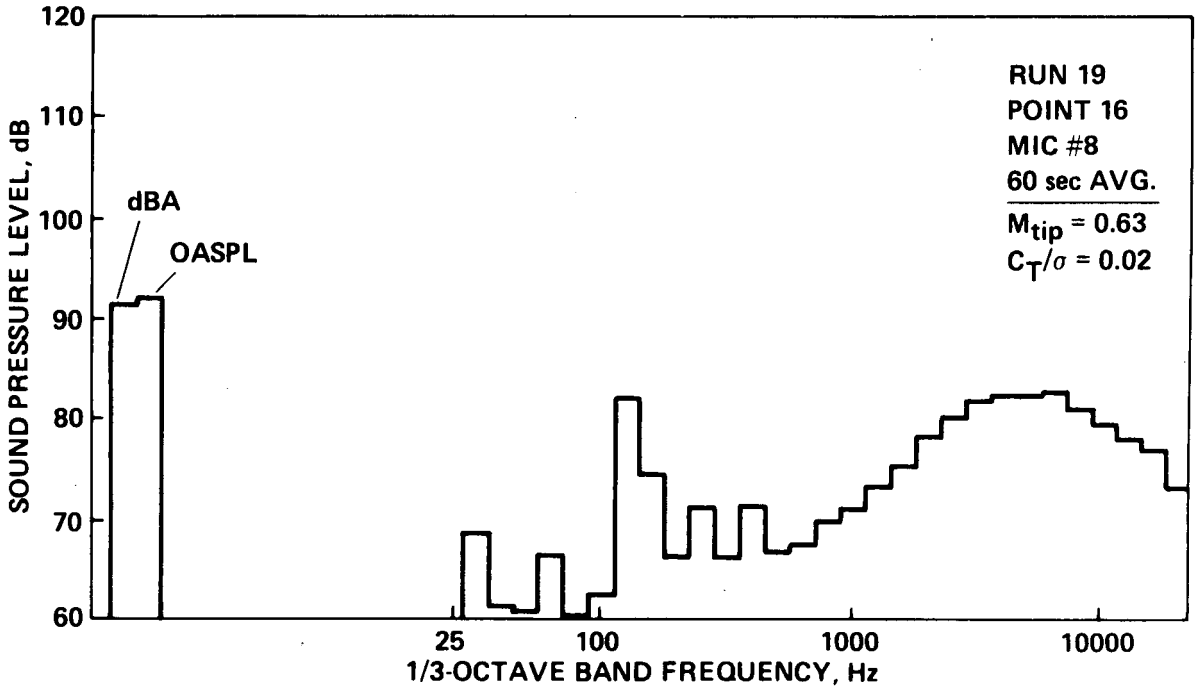

Figure A3.– Continued.

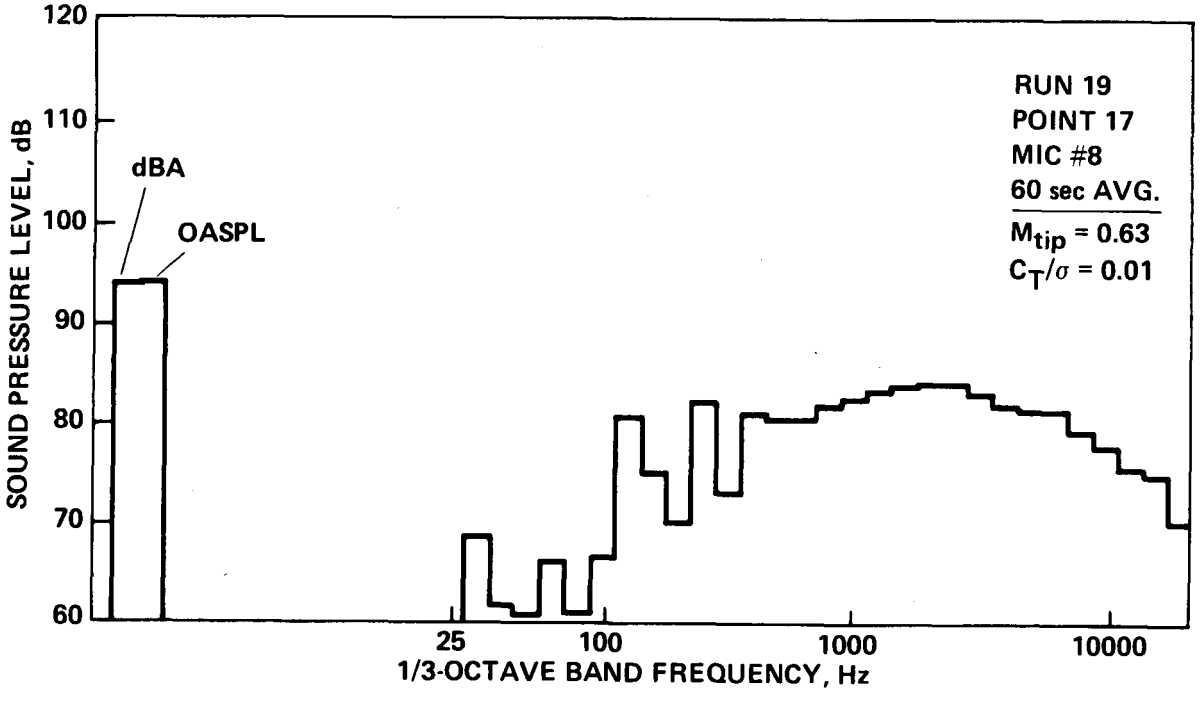

Figure A3.– Concluded.

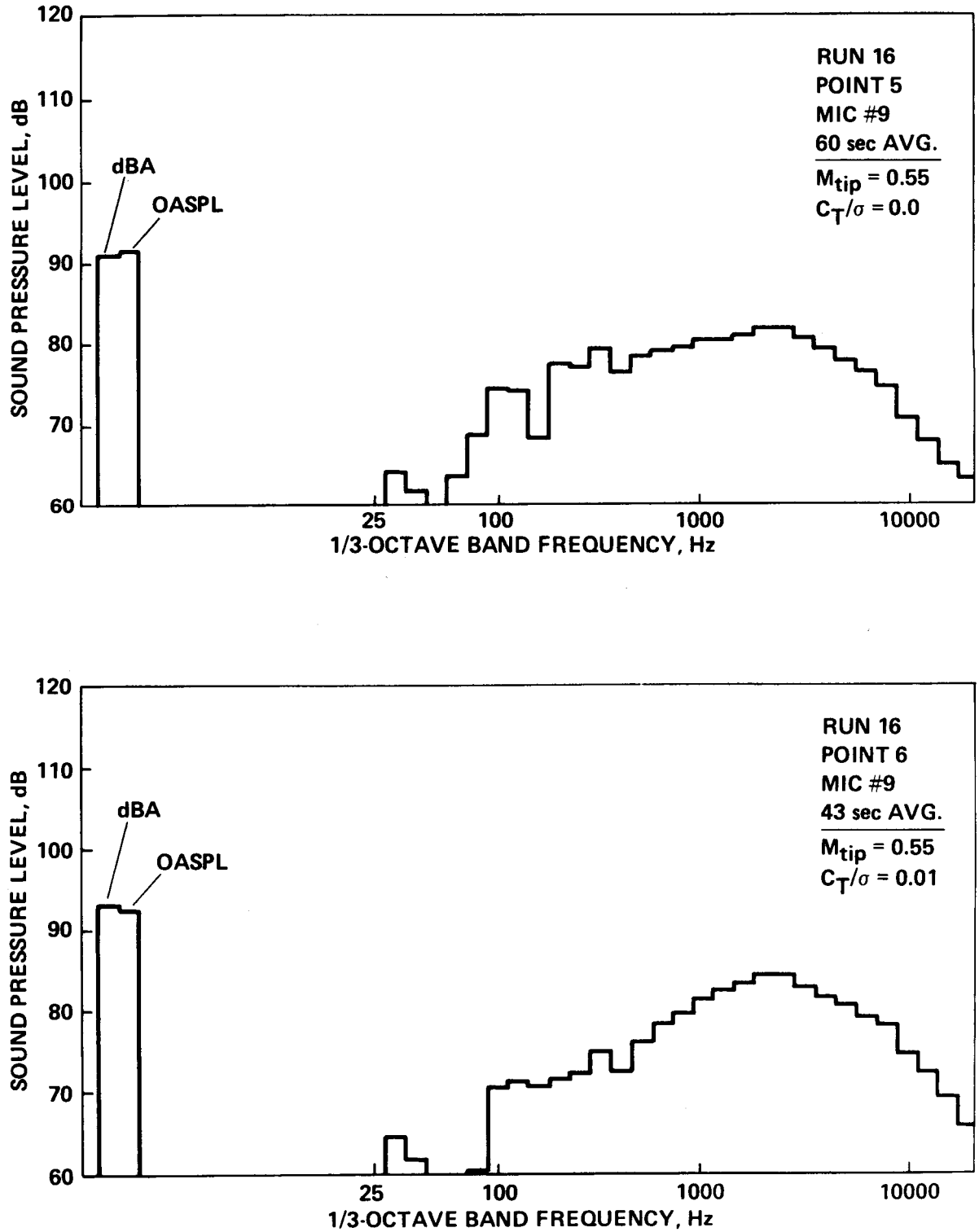

Figure A4.– 1/3-octave band acoustic spectra—Microphone No. 9: r/D = 2.0, ψ = 180°, θ = +45°.

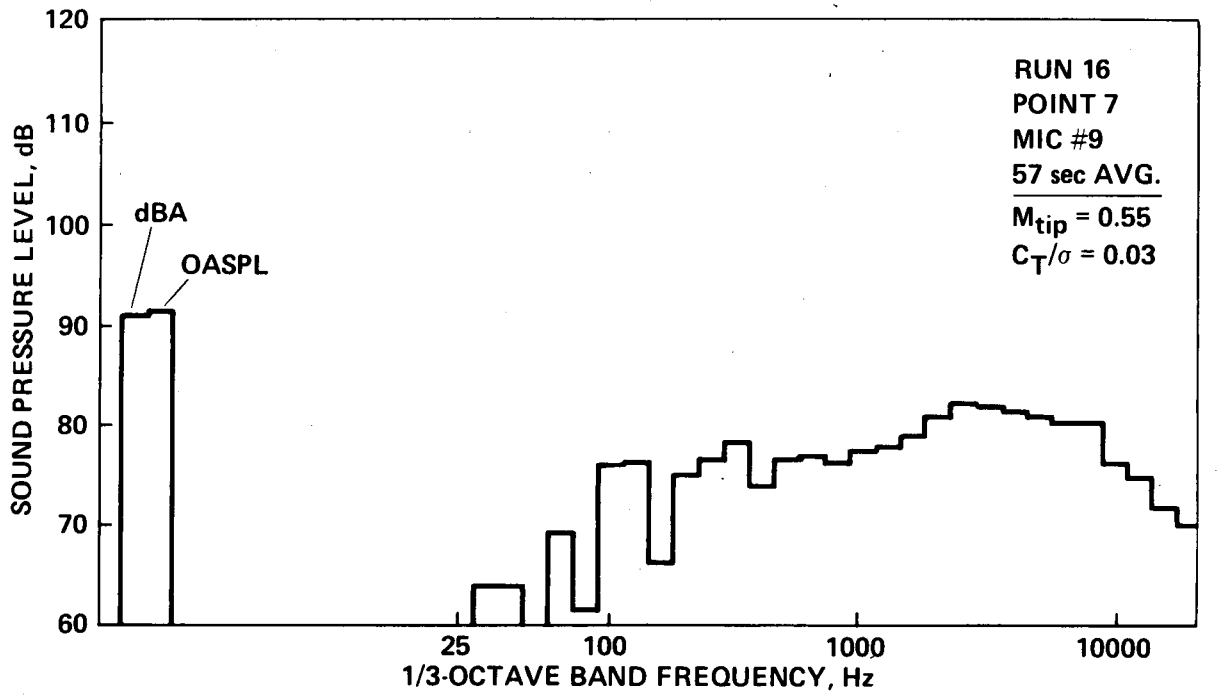

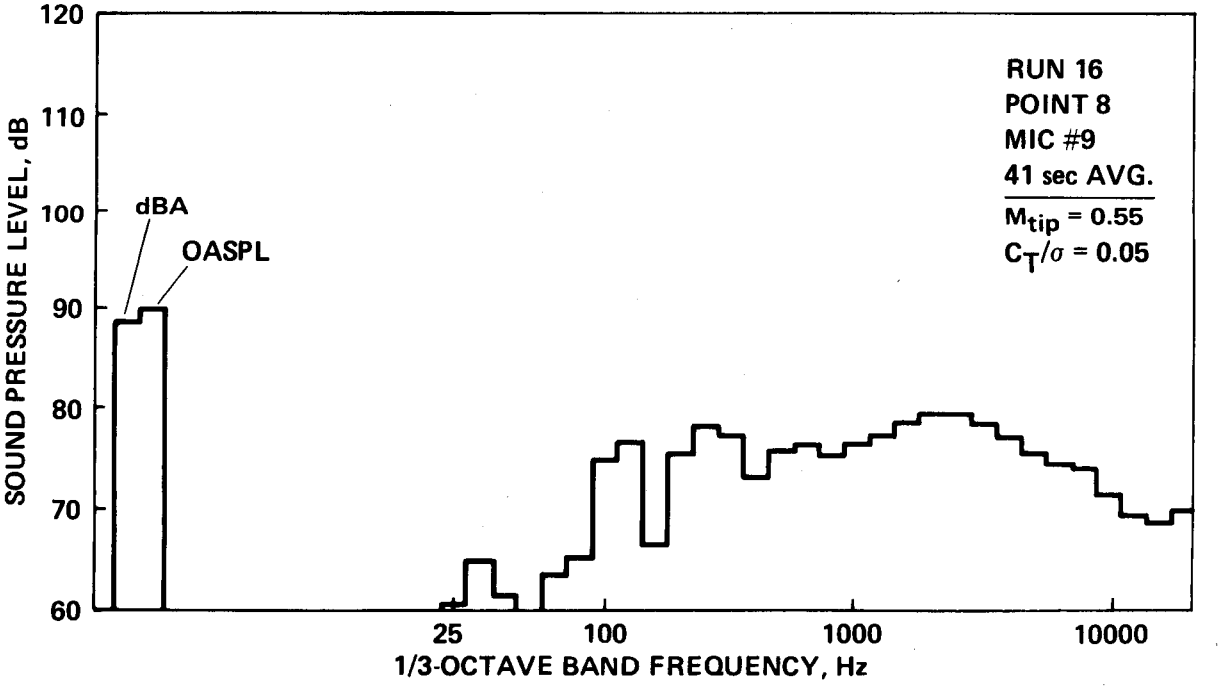

Figure A4.– Continued.

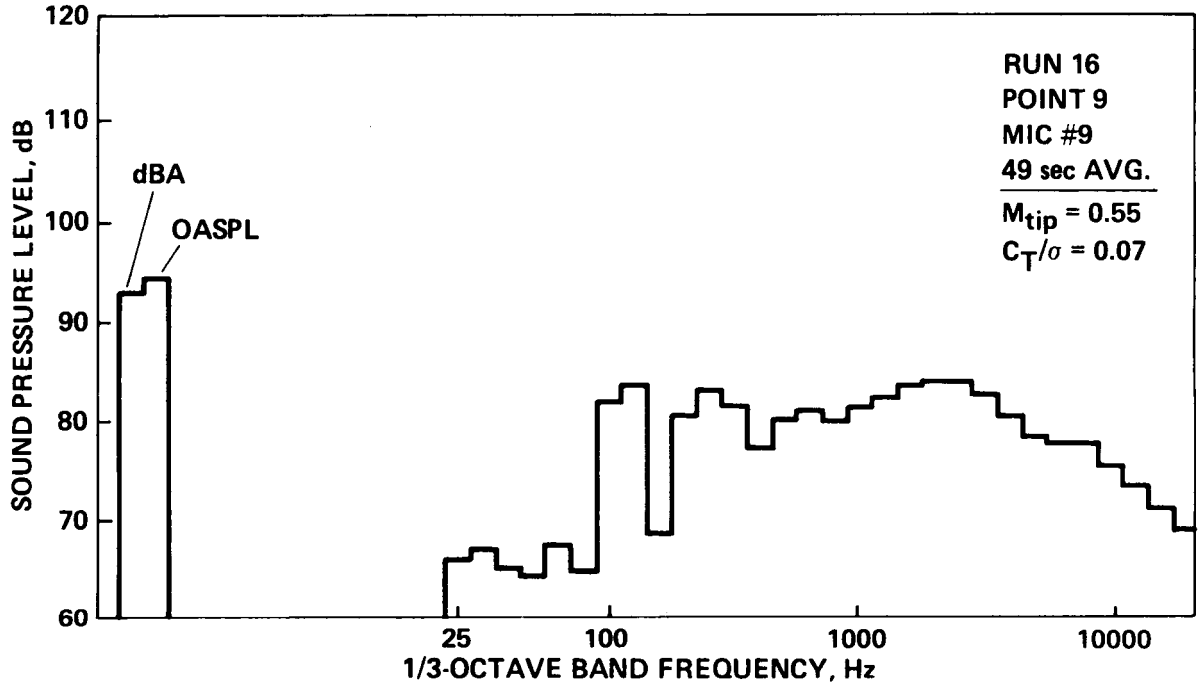

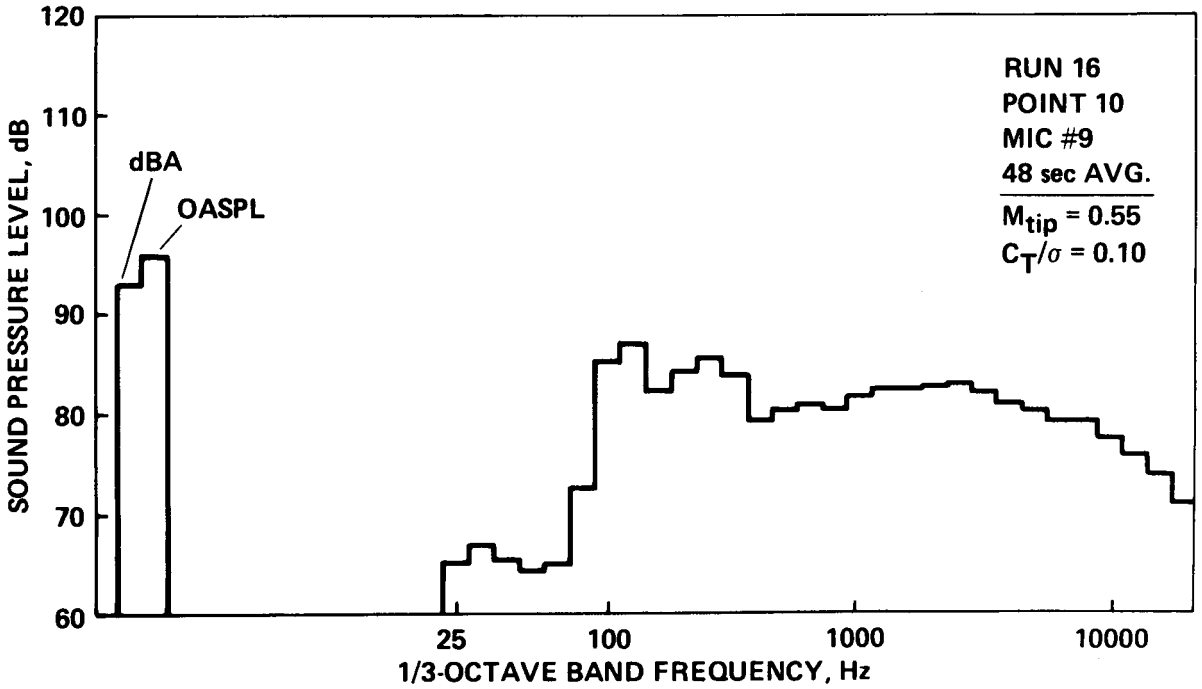

Figure A4.– Continued.

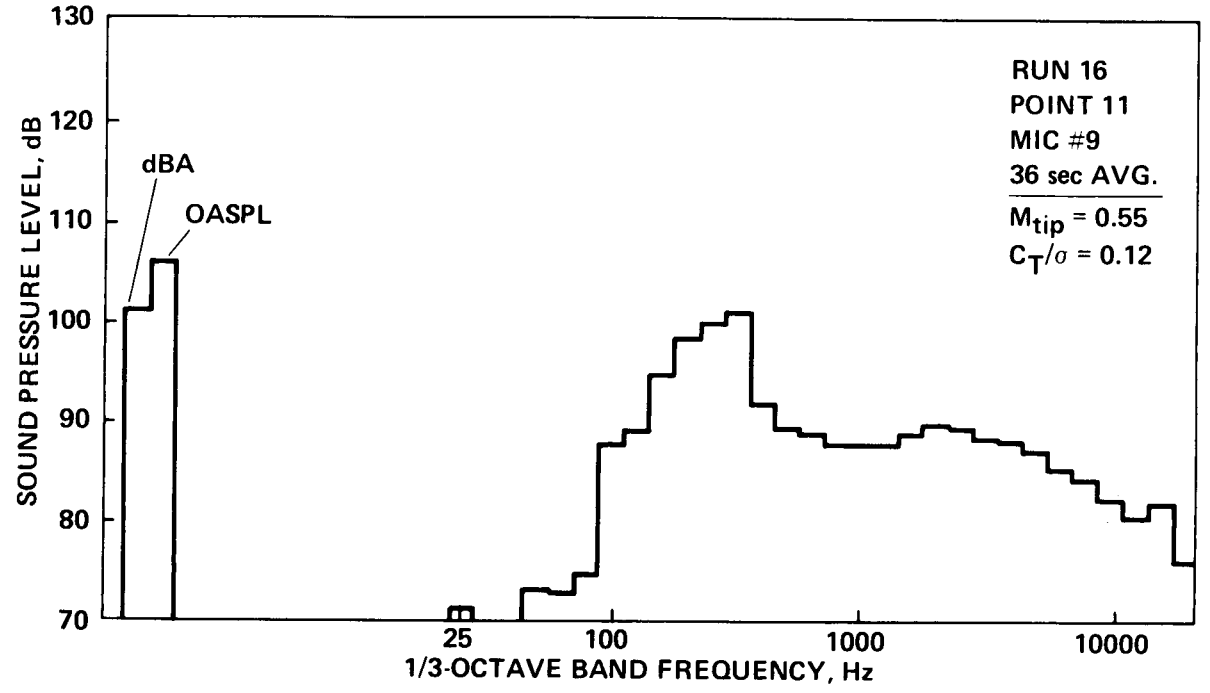

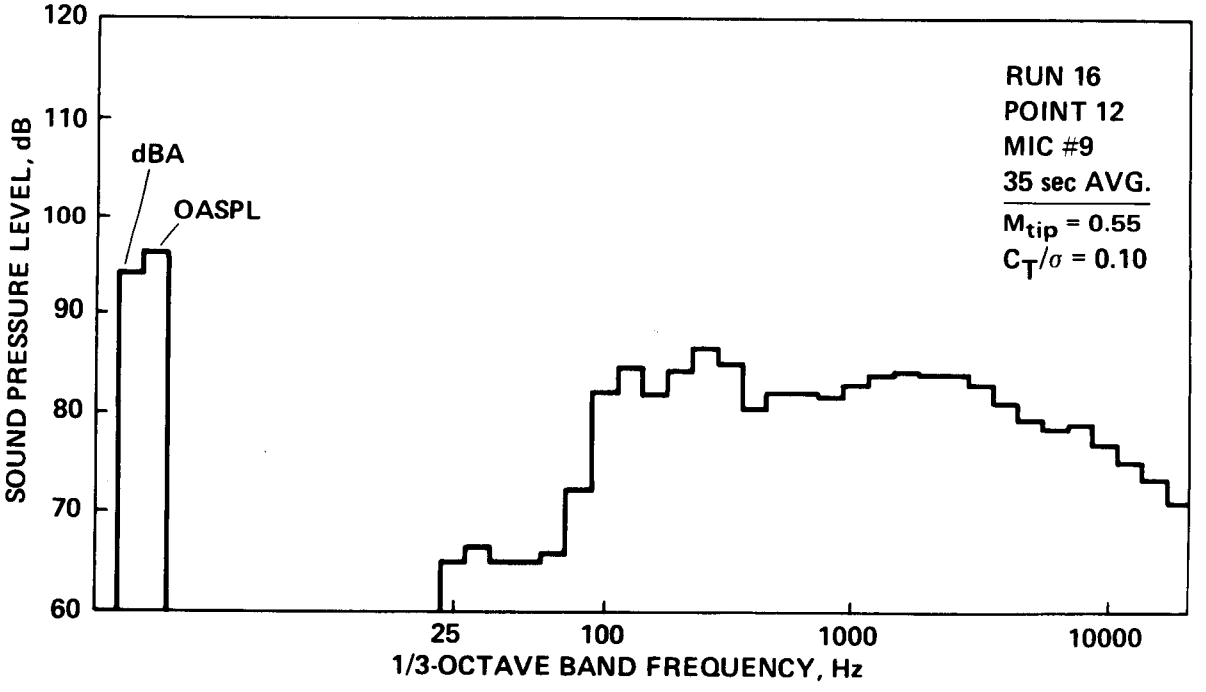

Figure A4.– Continued.

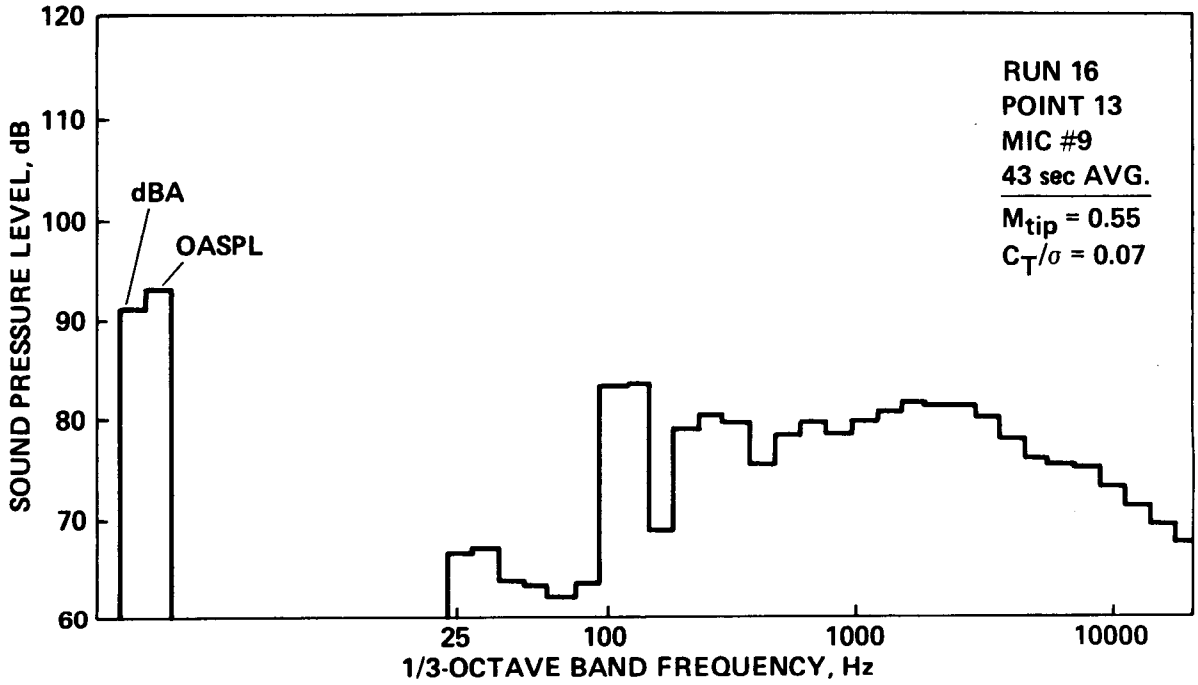

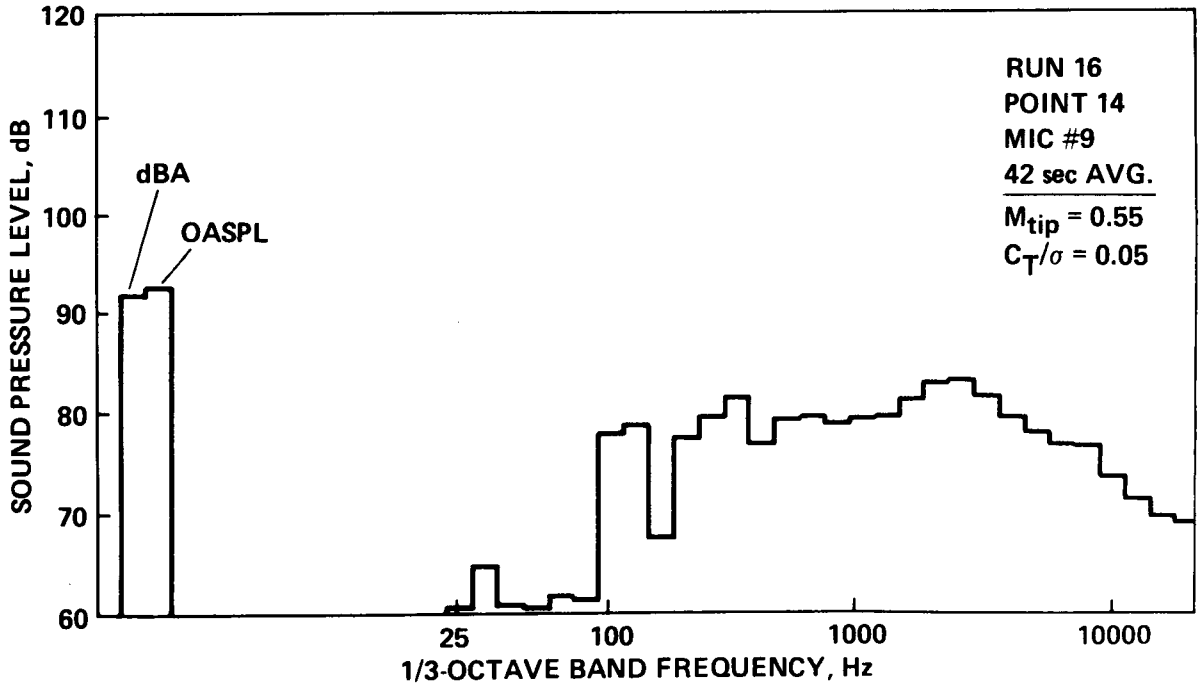

Figure A4.– Continued.

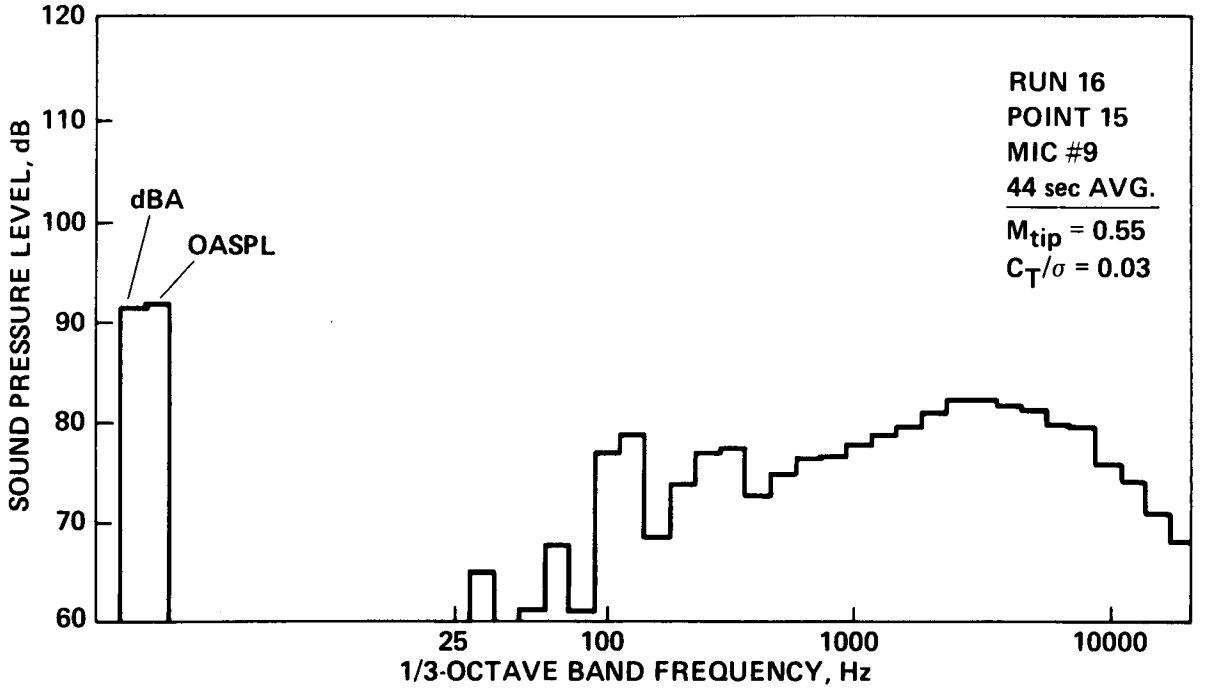

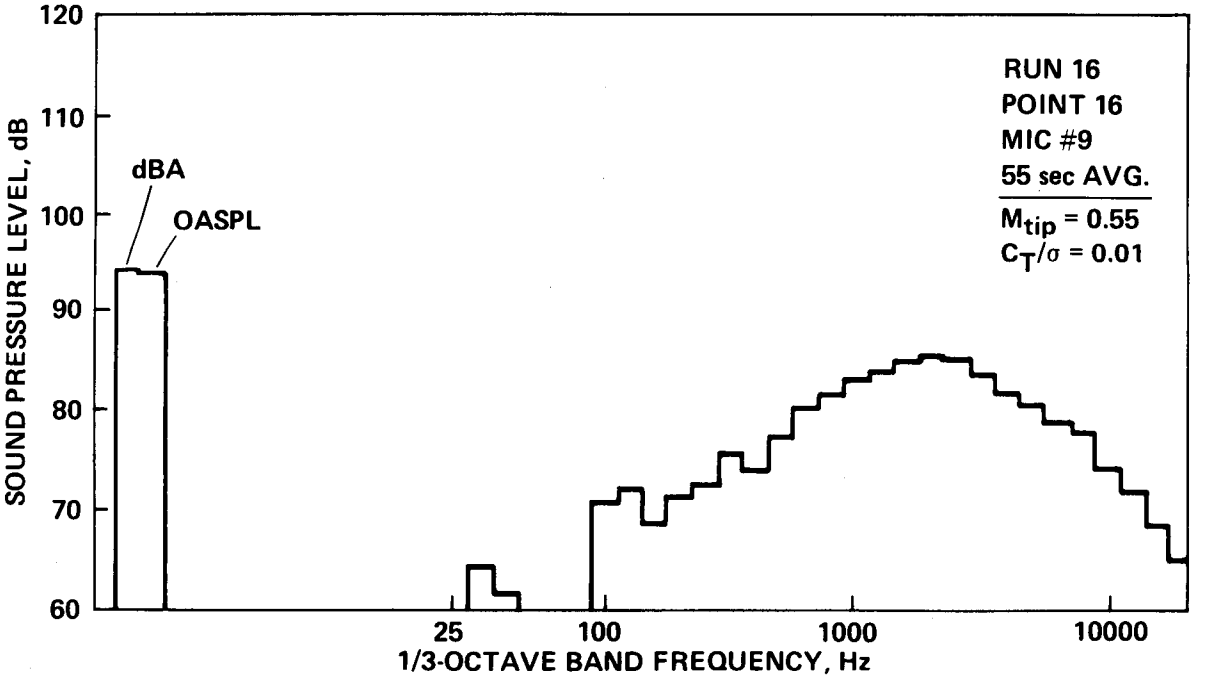

Figure A4.– Continued.

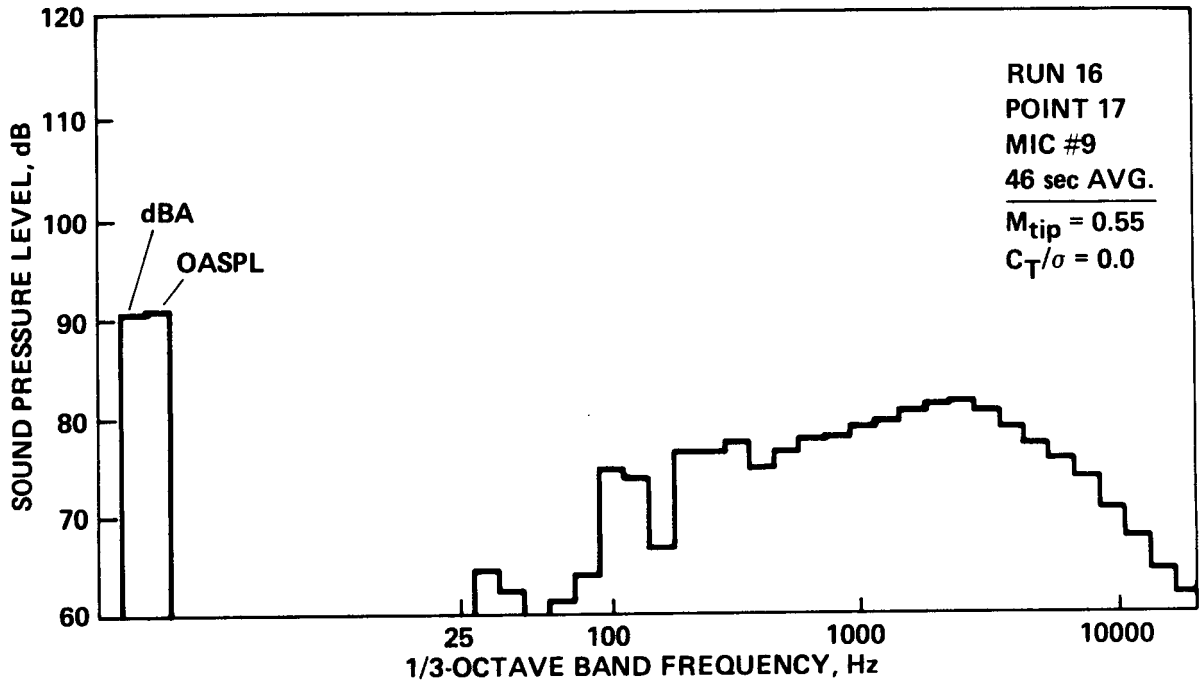

Figure A4.– Continued.

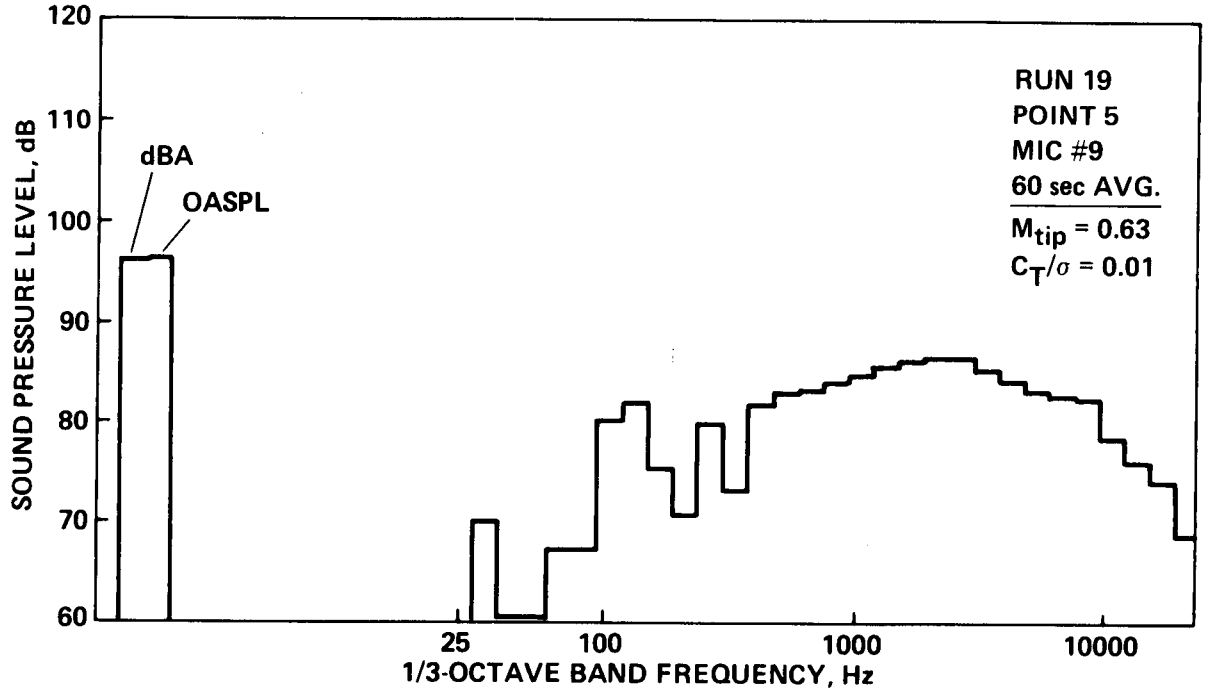

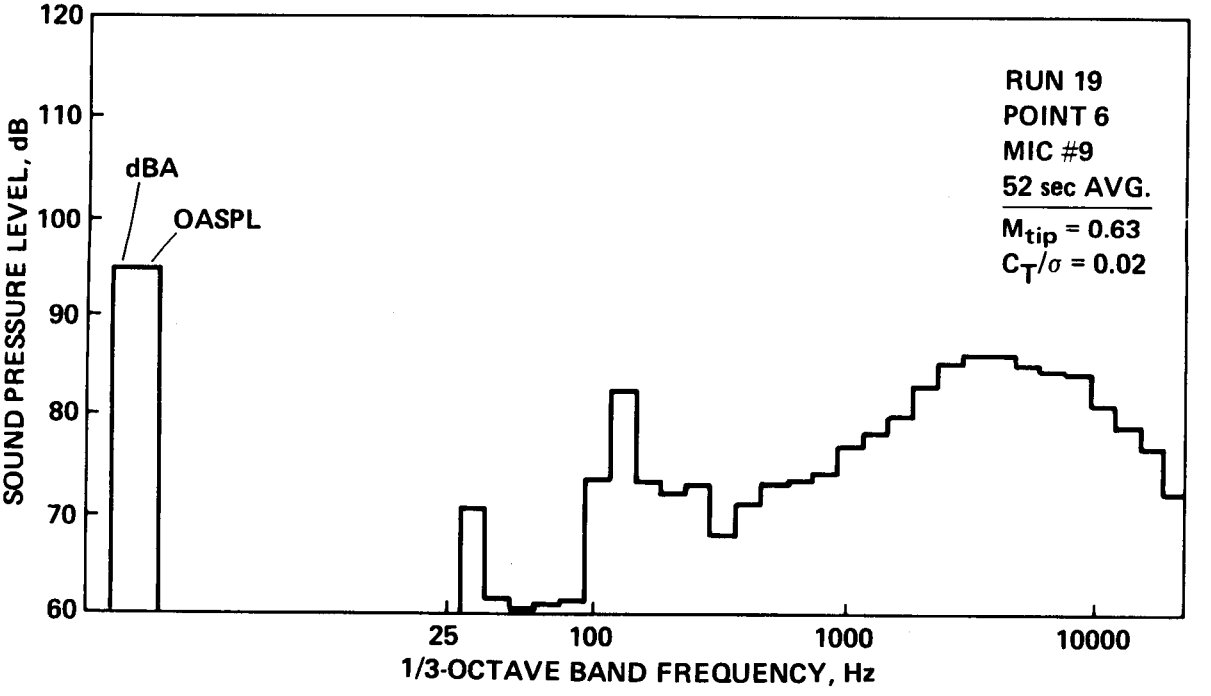

Figure A4.– Continued.

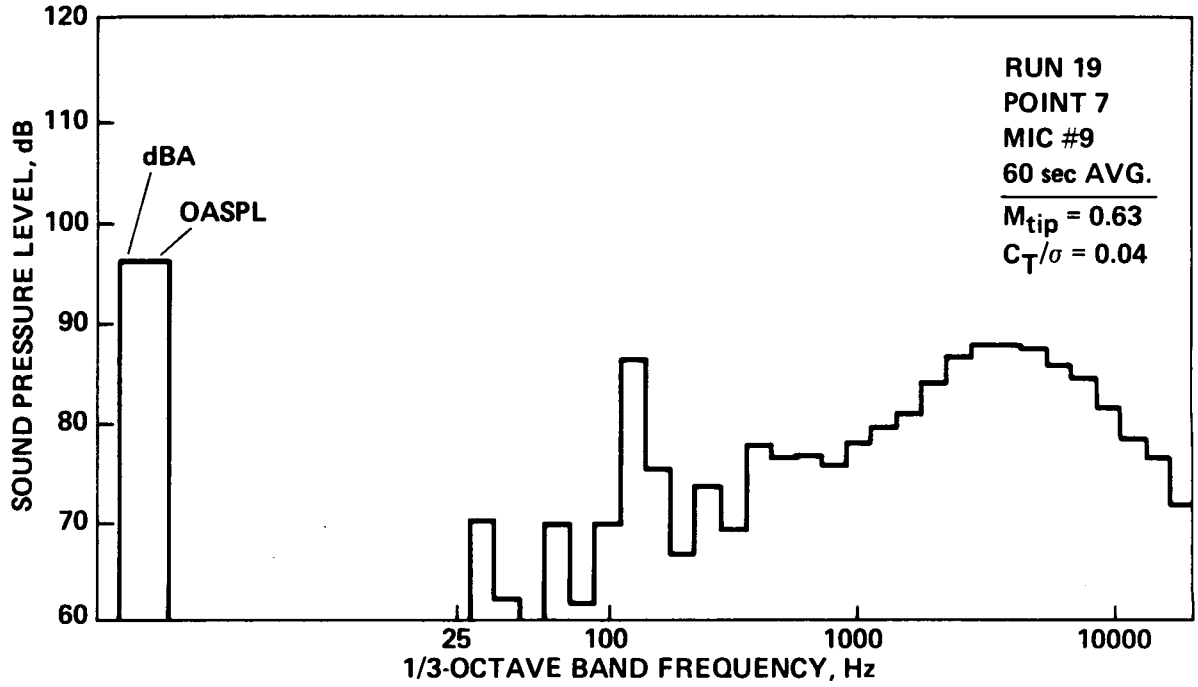

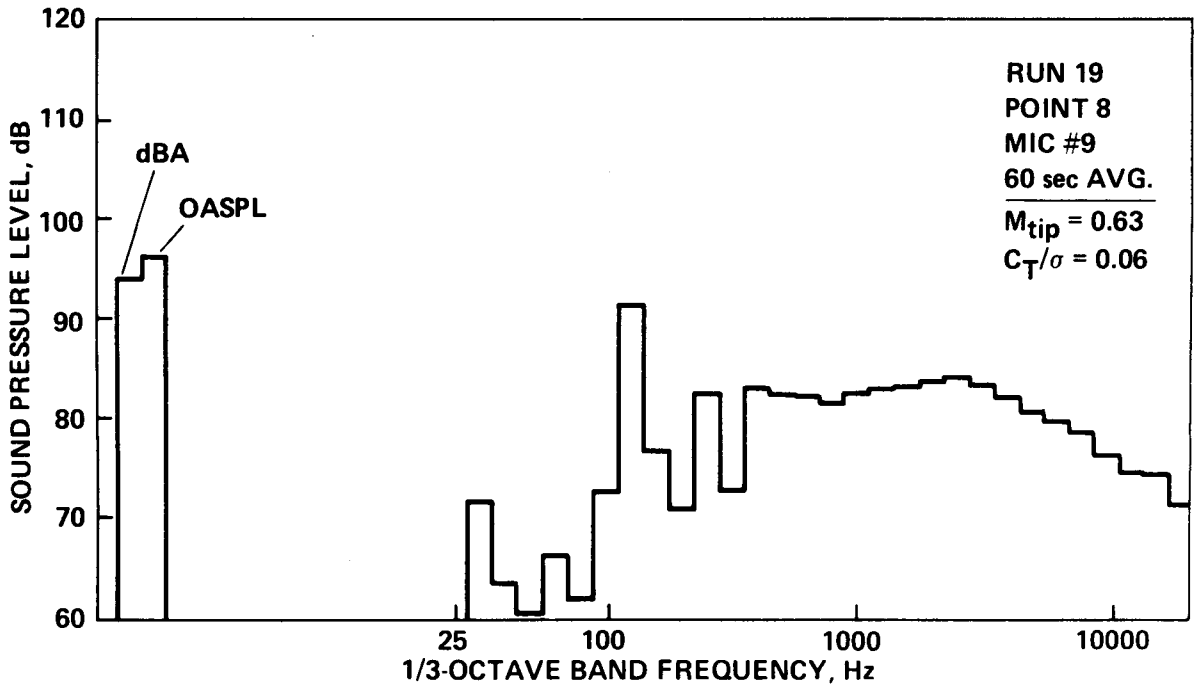

Figure A4.– Continued.

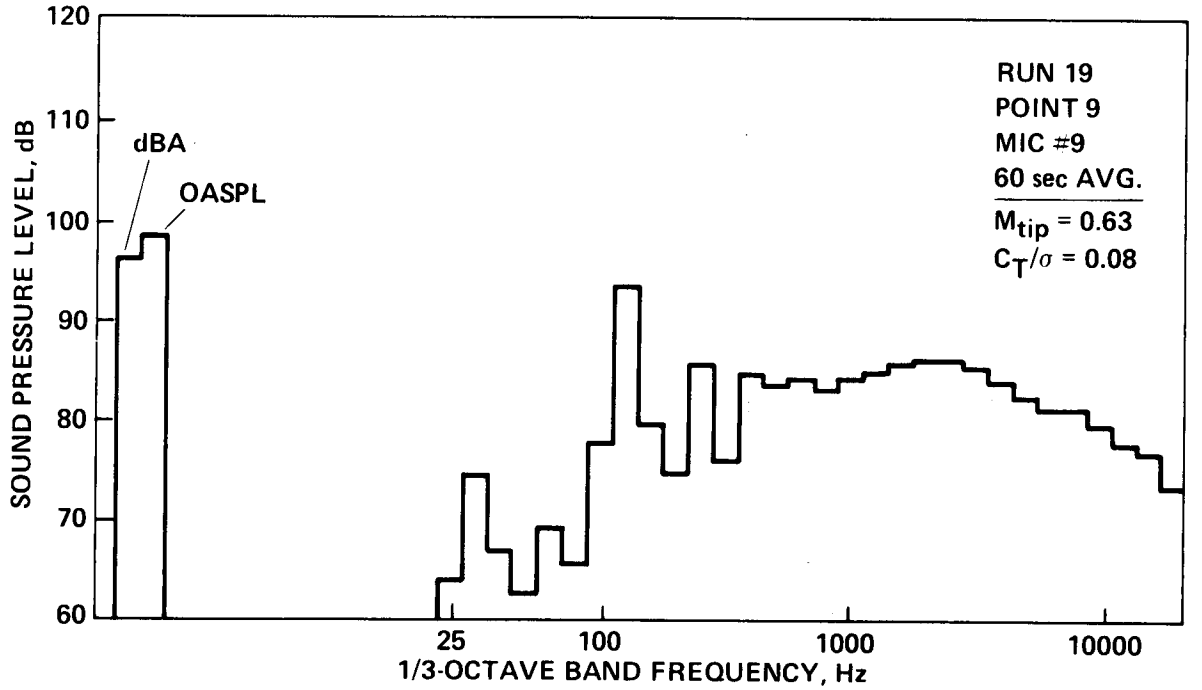

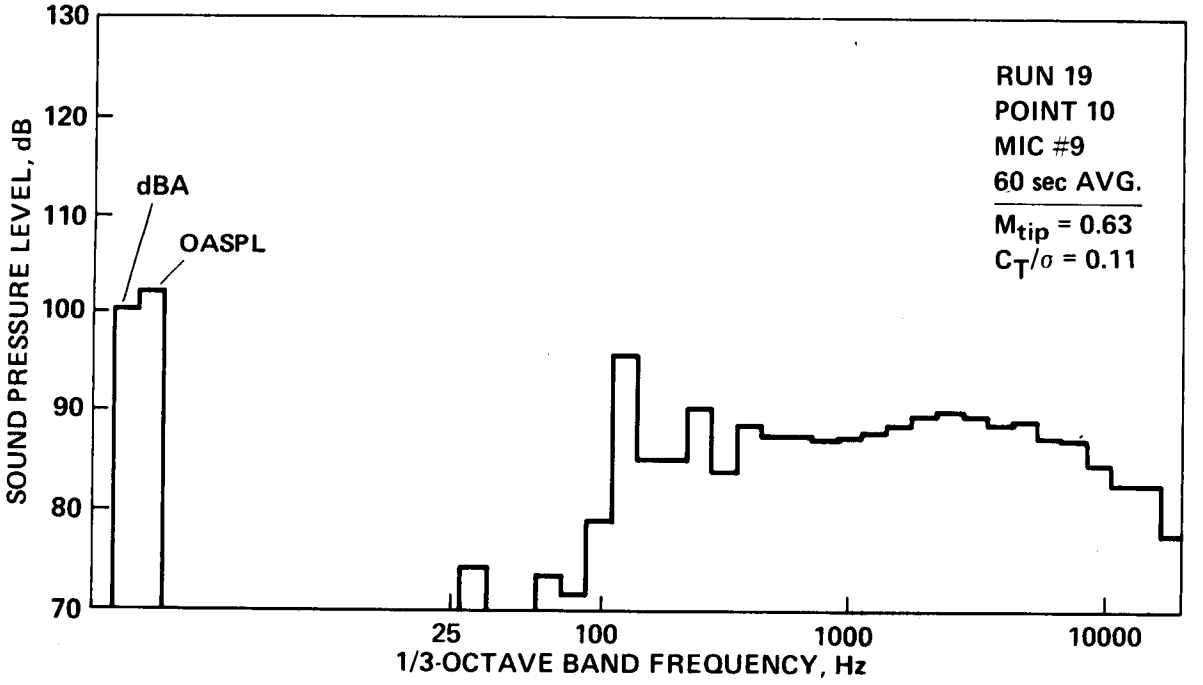

Figure A4.– Continued.

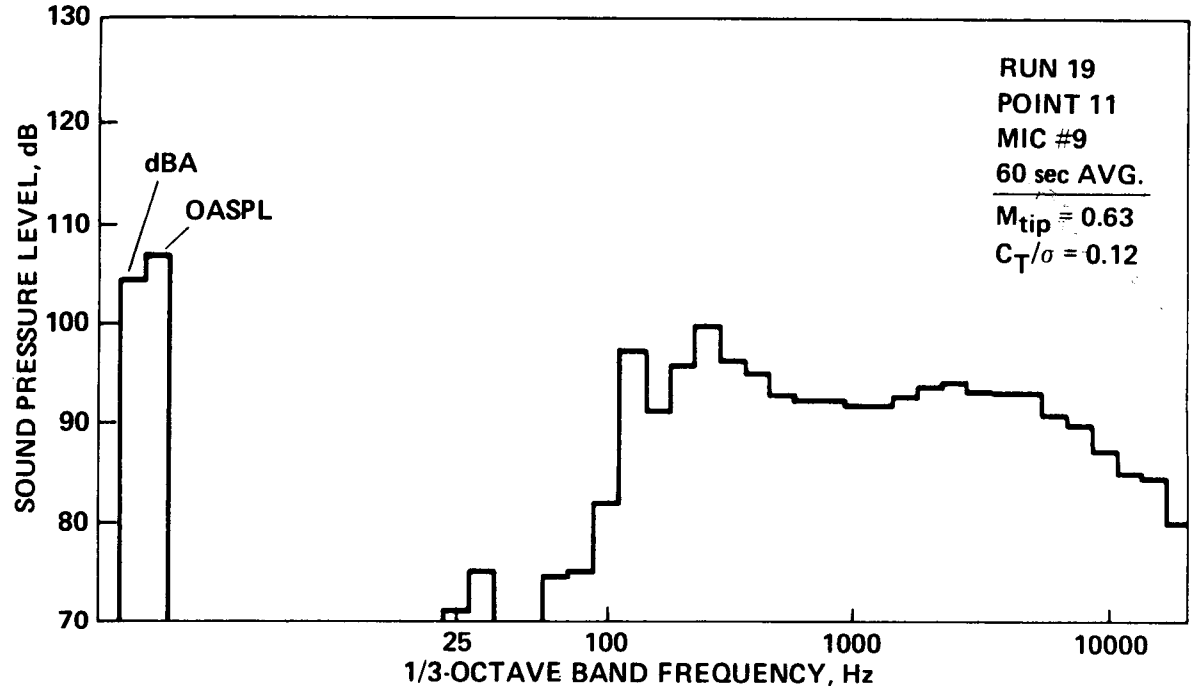

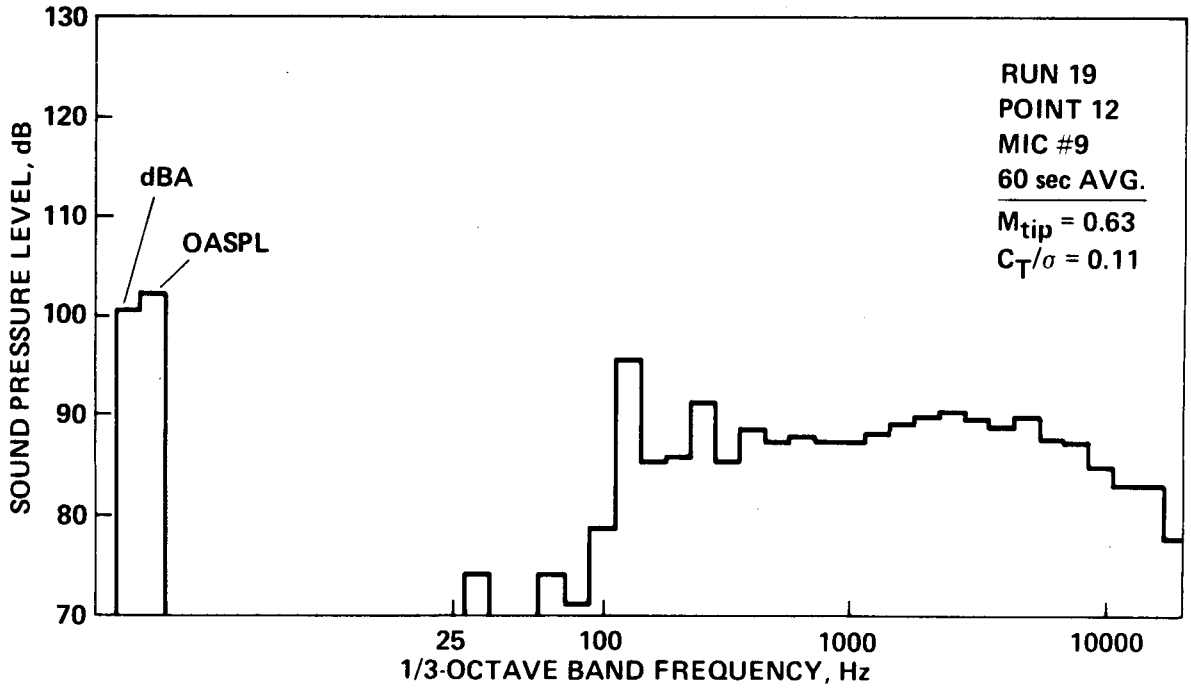

Figure A4.– Continued.

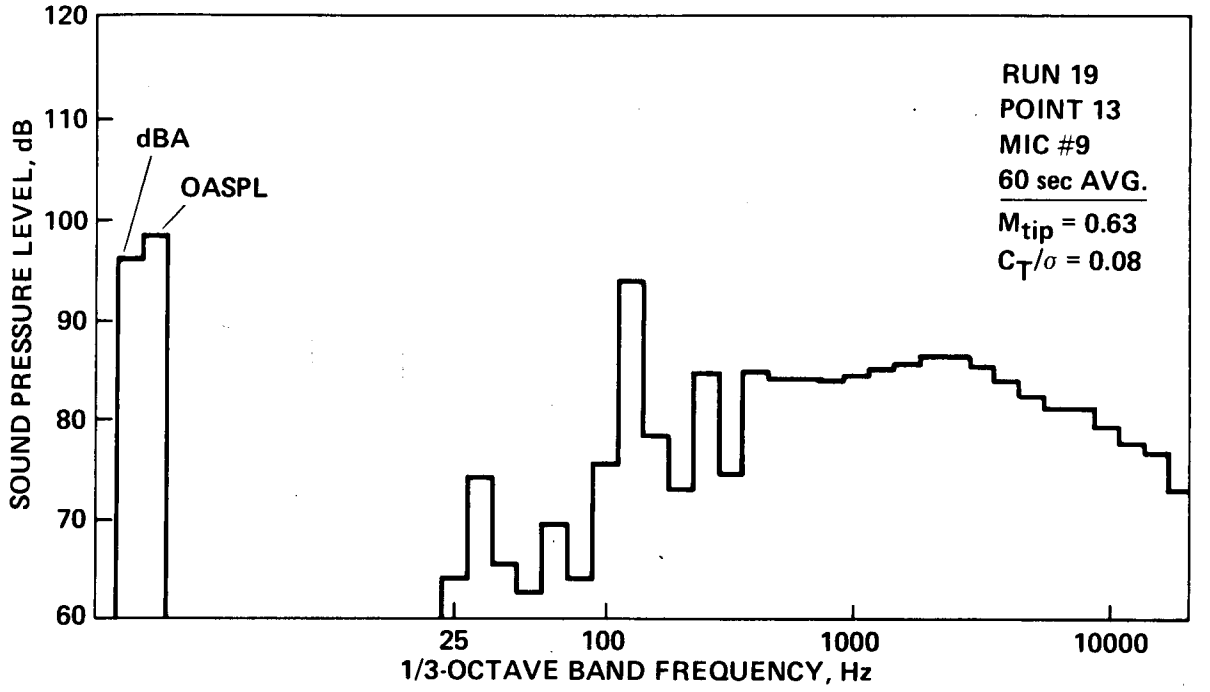

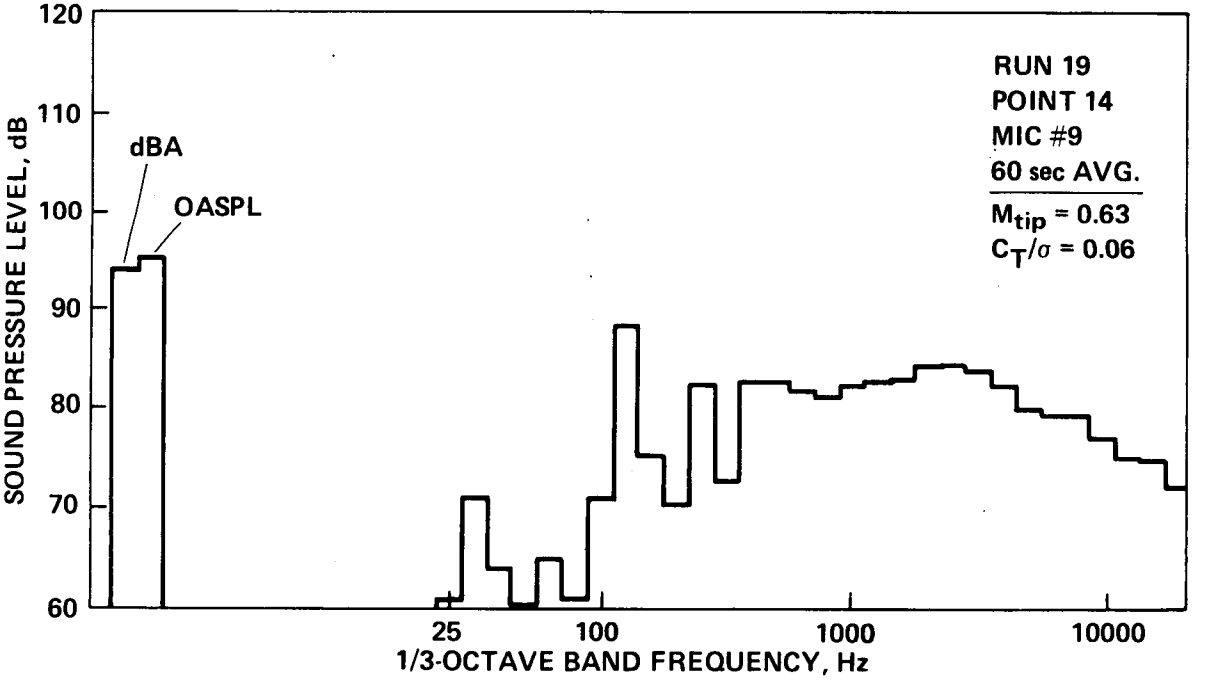

Figure A4.– Continued.

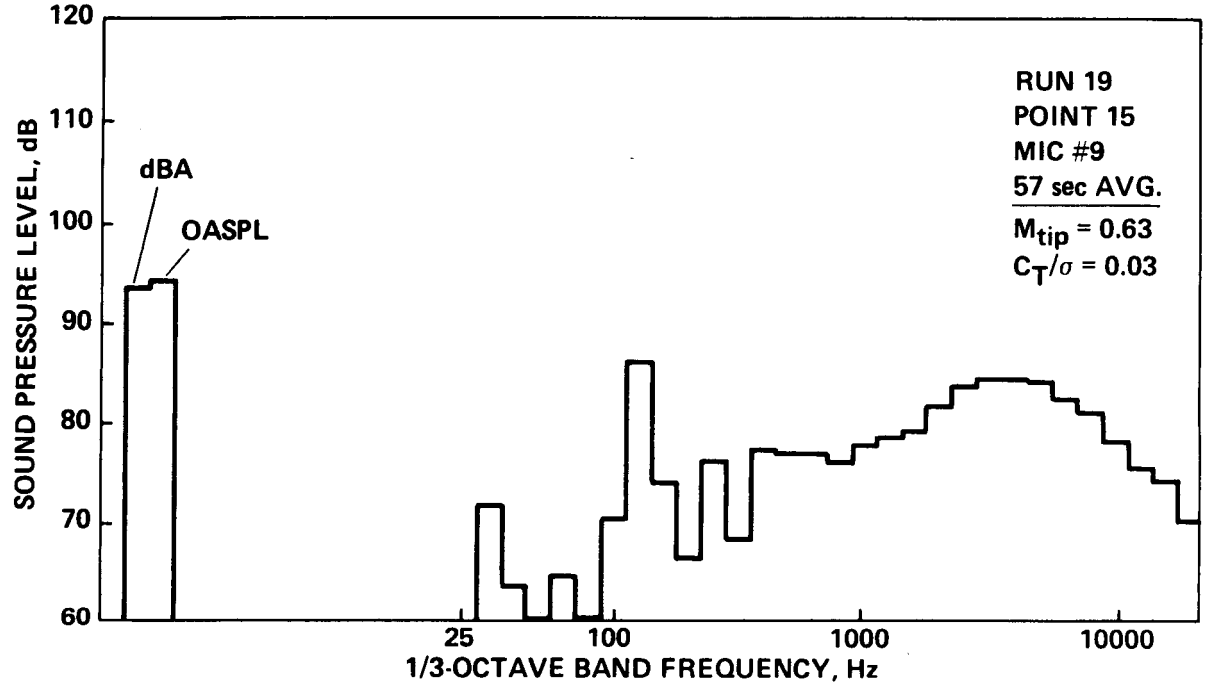

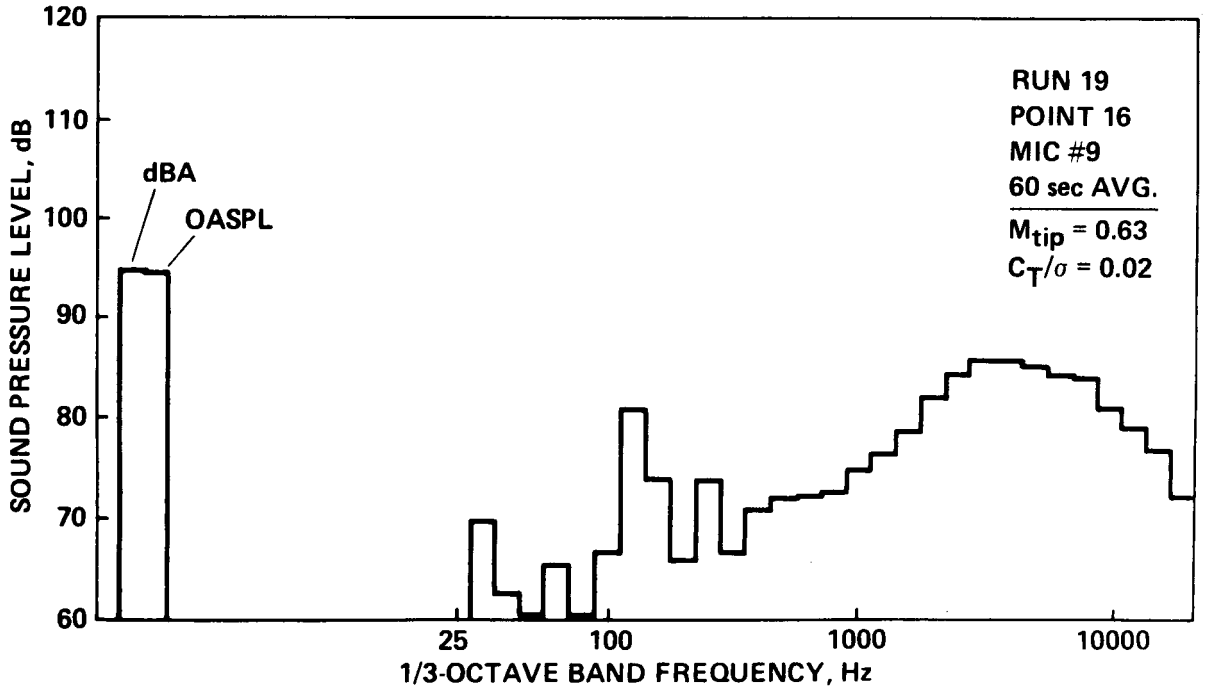

Figure A4.– Continued.

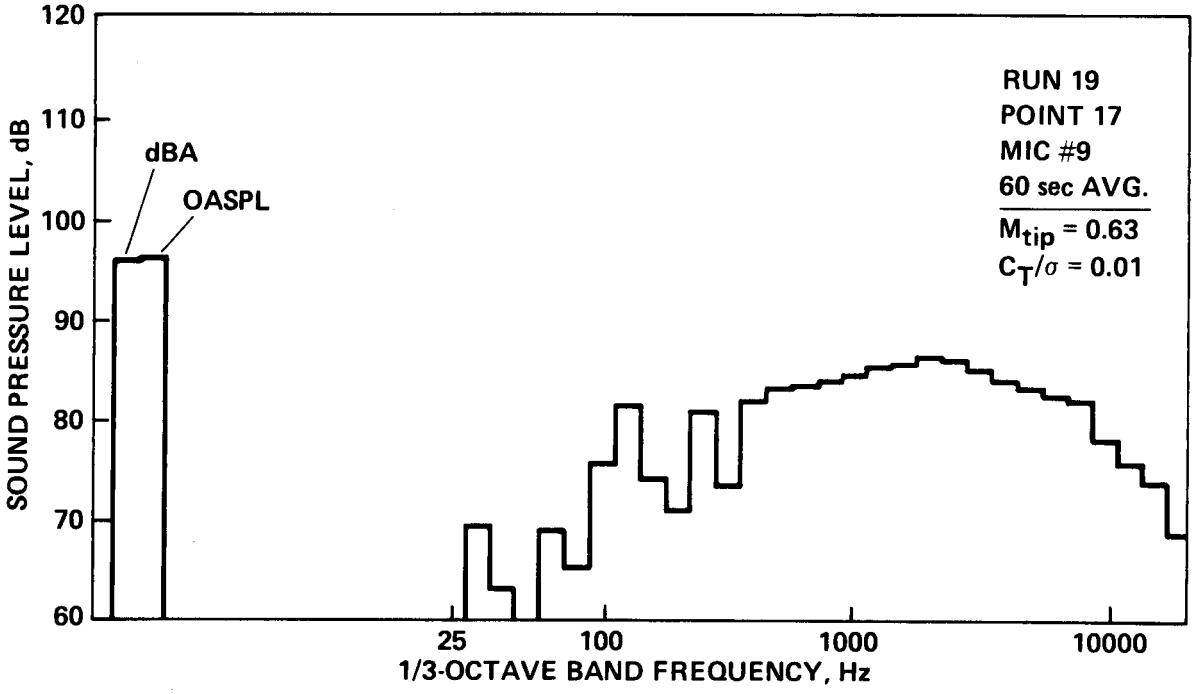

Figure A4.– Concluded.

APPENDIX B

EFFECT OF ROTOR PERFORMANCE ON ACOUSTICS

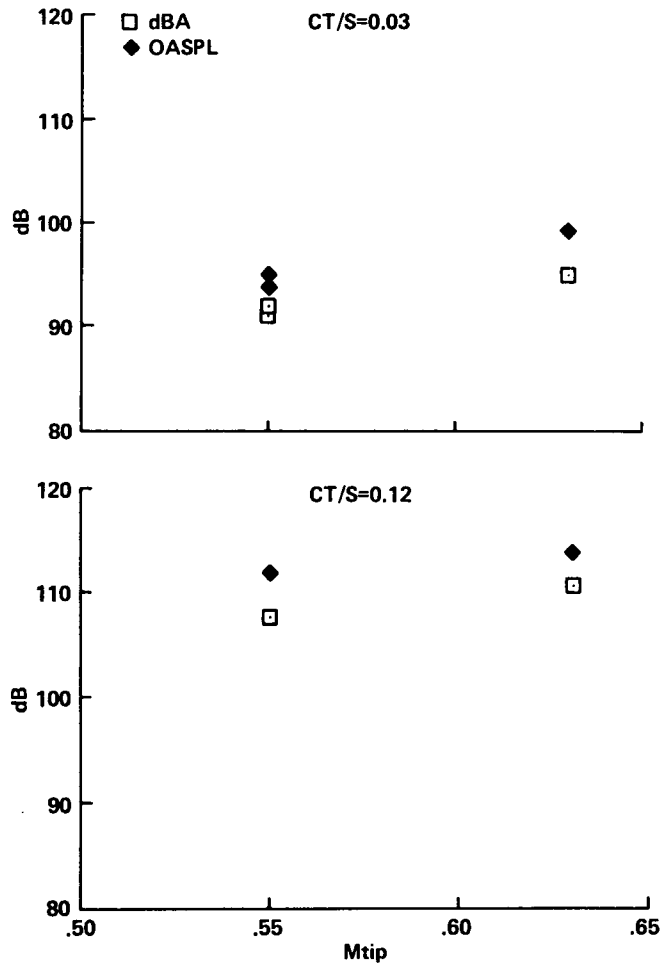

Figure B1.– Acoustic levels as a function of M_{tip}. Microphone No. 5: r/D = 1.0, ψ = 180°, θ = +10°.

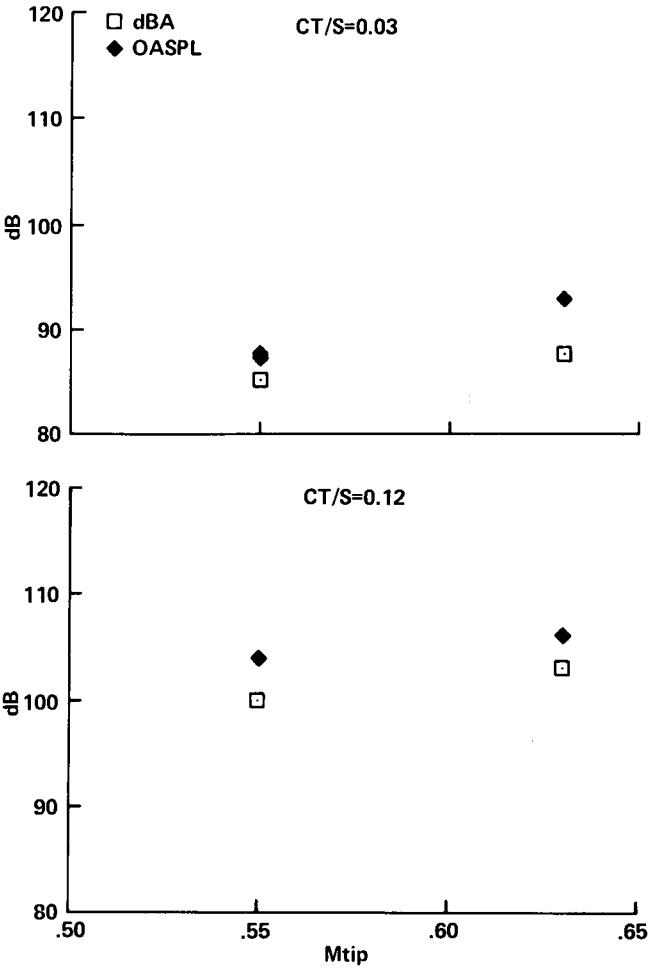

Figure B2.– Acoustic levels as a function of M_{tip}. Microphone No. 7: r/D = 2.0, ψ = 180°, θ = +10°.

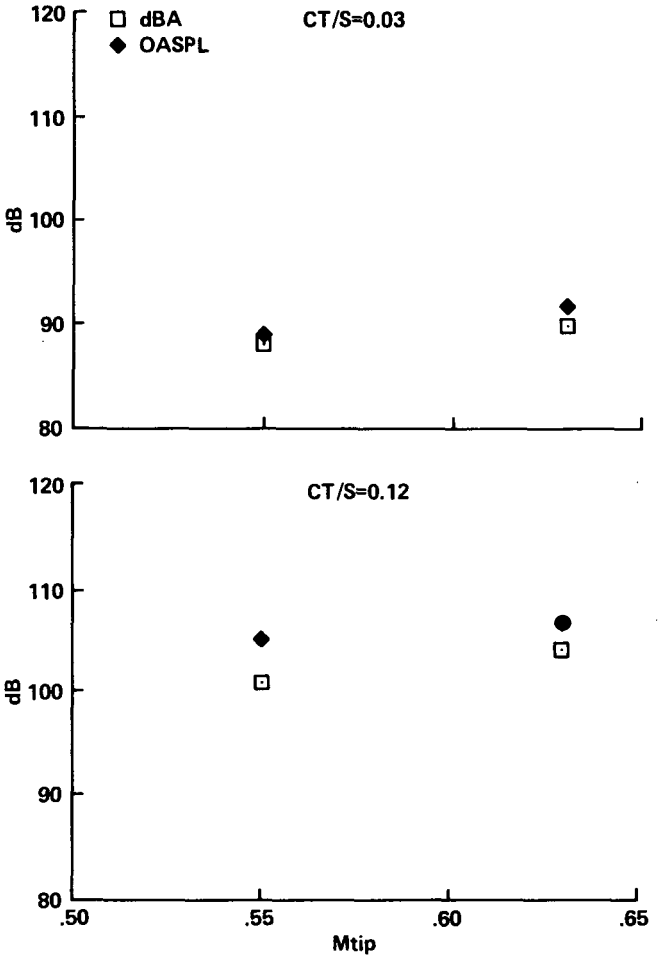

Figure B3.– Acoustic levels as a function of M_{tip}. Microphone No. 8: r/D = 2.0, ψ = 180°, θ = +30°.

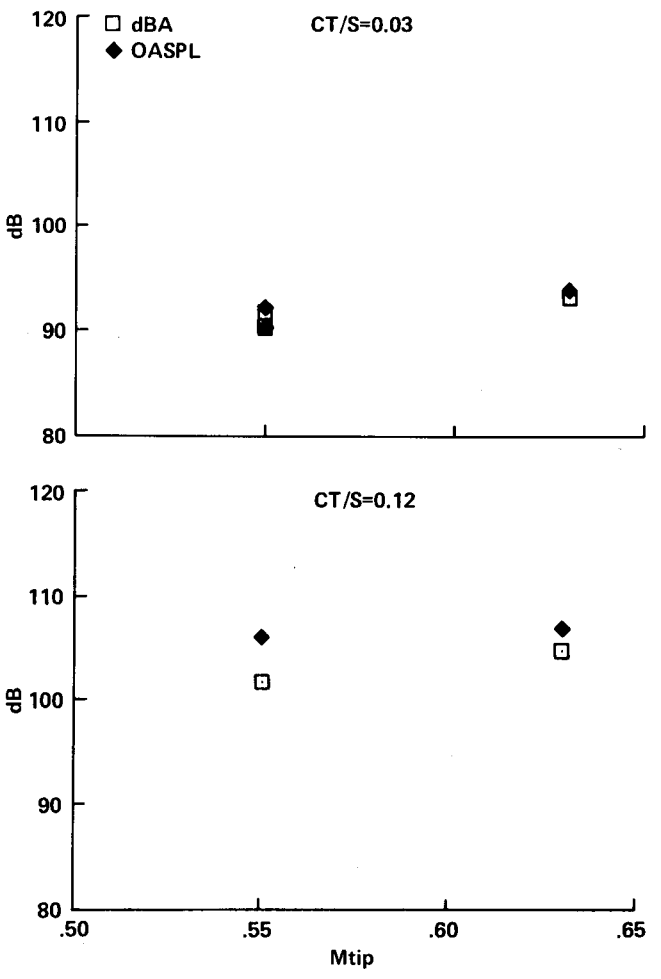

Figure B4.– Acoustic levels as a function of M_{tip}. Microphone No. 9: r/D = 2.0, ψ = 180°, θ = +45°.

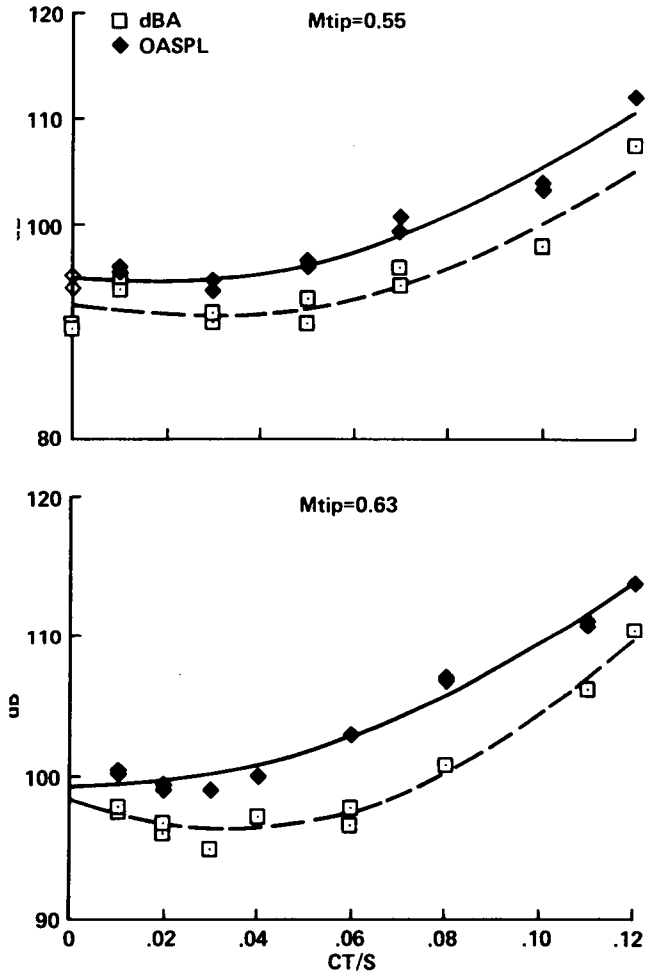

Figure B5.– Acoustic levels as a function of C_T/σ at two values of M_{tip}. Microphone No. 5: r/D = 1.0, $\psi = 180°$, $\theta = +10°$.

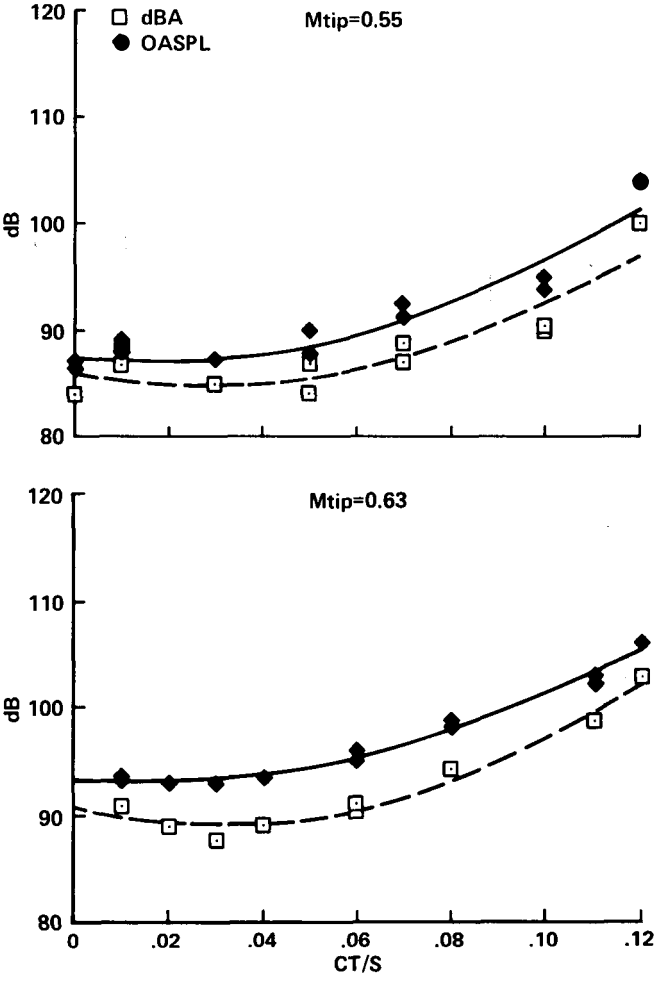

Figure B6.– Acoustic levels as a function of C_T/σ at two values of M_{tip}. Microphone No. 7: r/D = 2.0, $\psi = 180°$, $\theta = +10°$.

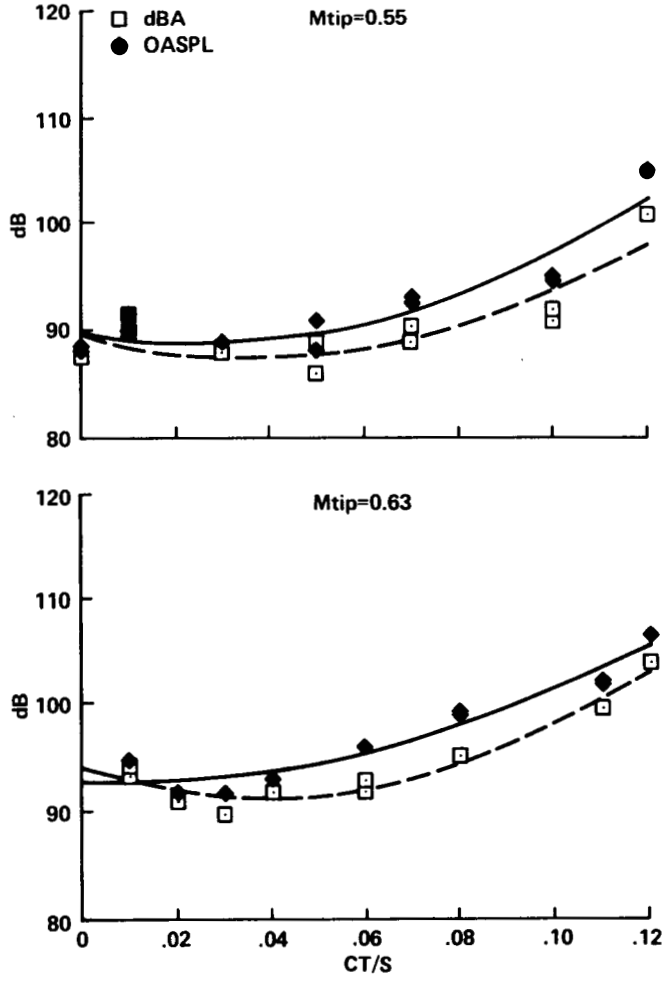

Figure B7.– Acoustic levels as a function of C_T/σ at two values of M_{tip}. Microphone No. 8: r/D = 2.0, $\psi = 180°$, $\theta = +30°$.

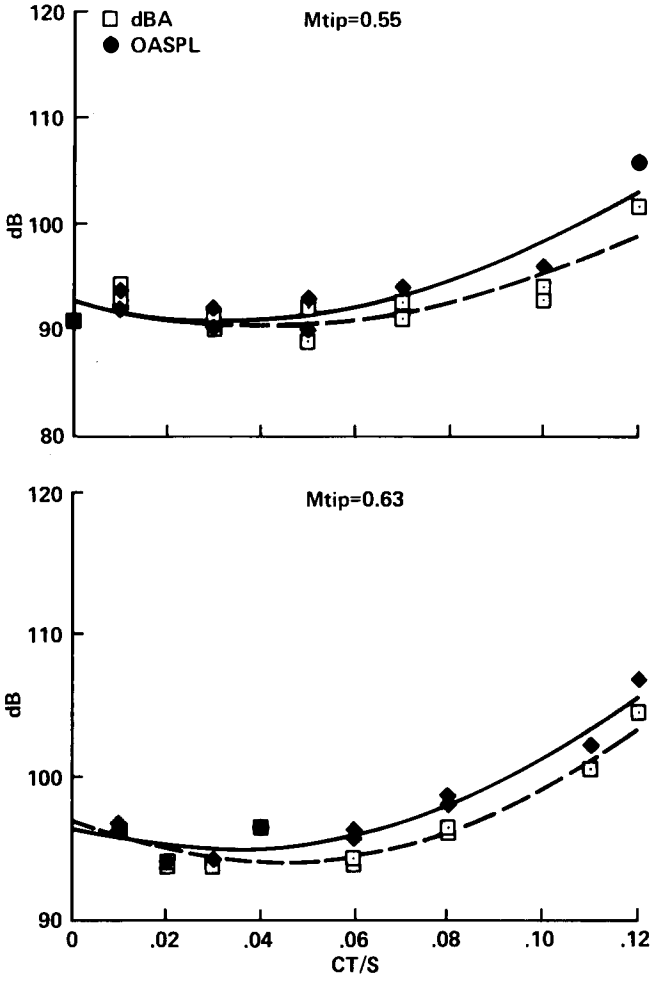

Figure B8.– Acoustic levels as a function of C_T/σ at two values of M_{tip}. Microphone No. 9: r/D = 2.0, $\psi = 180°$, $\theta = +45°$.

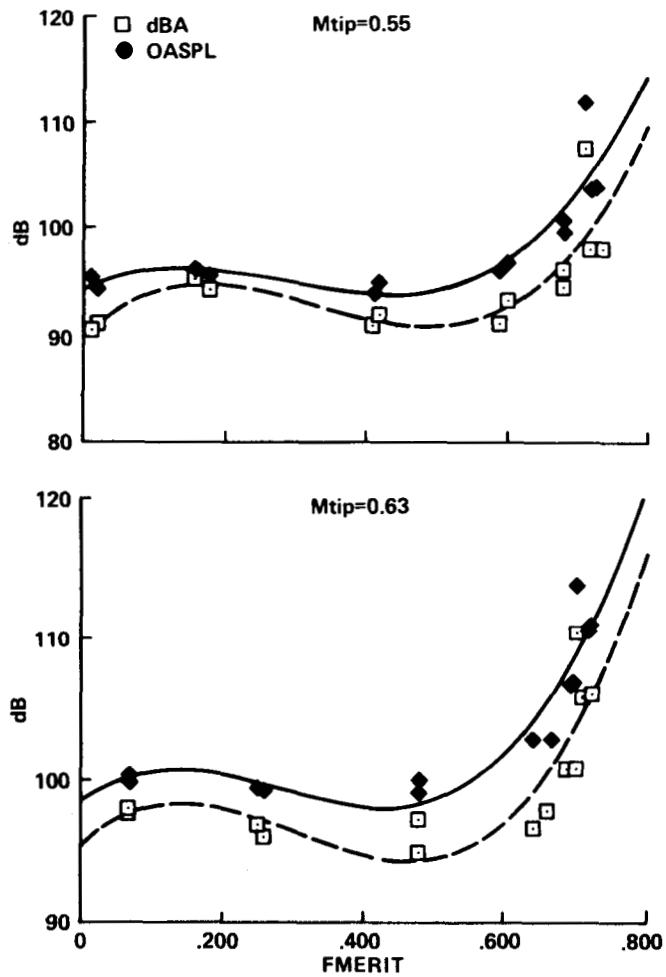

Figure B9.– Acoustic levels as a function of FMERIT at two values of M_{tip}. Microphone No. 5: r/D = 1.0, $\psi = 180°$, $\theta = +10°$.

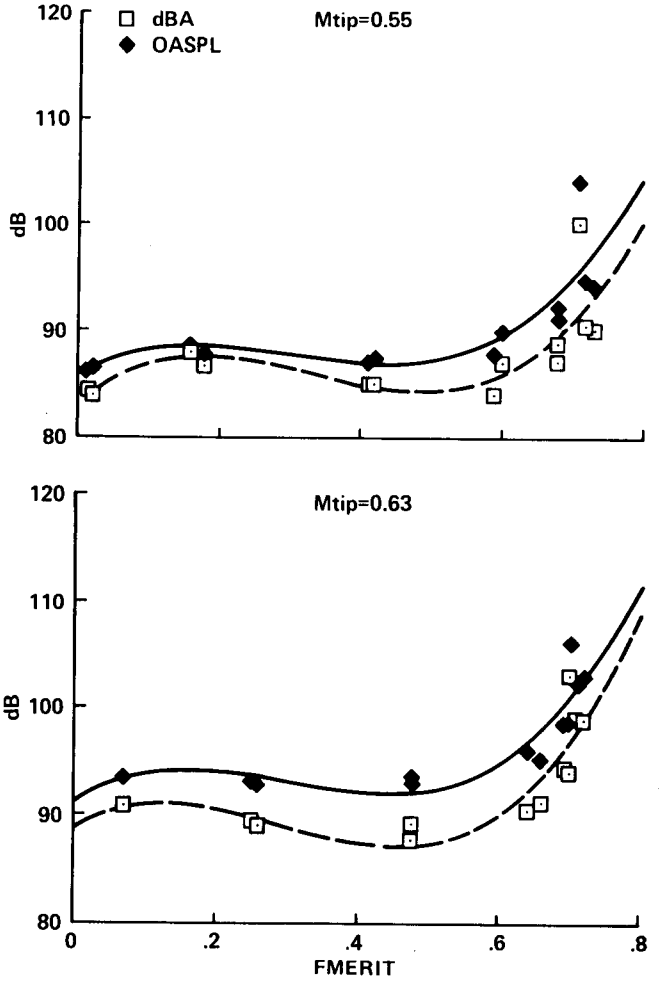

Figure B10.– Acoustic levels as a function of FMERIT at two values of M_{tip}. Microphone No. 7: r/D = 2.0, ψ = 180°, θ = +10°.

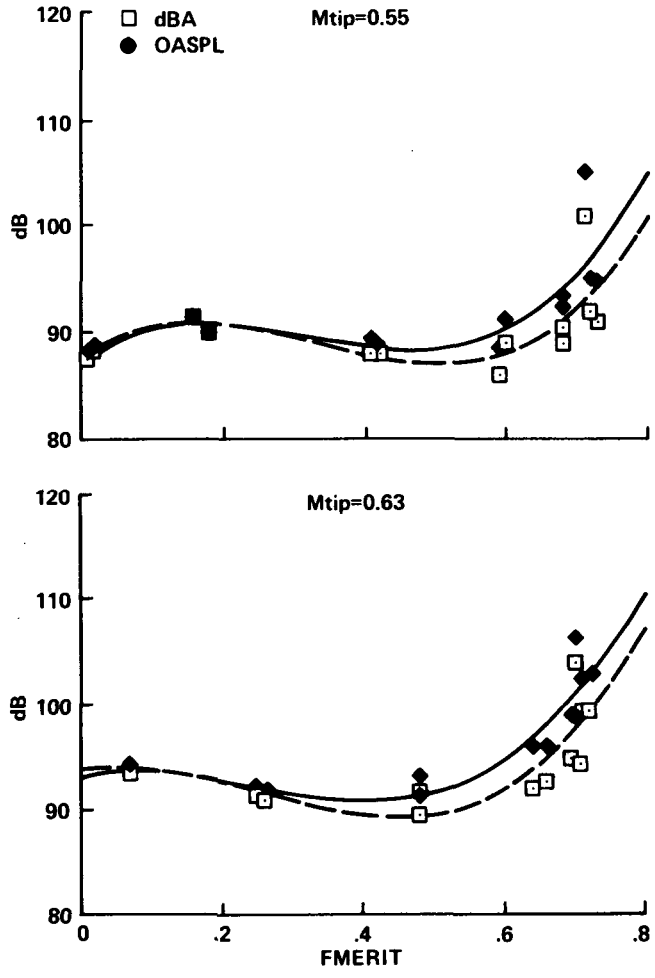

Figure B11.– Acoustic levels as a function of FMERIT at two values of M_{tip}. Microphone No. 8: r/D = 2.0, ψ = 180°, θ = +30°.

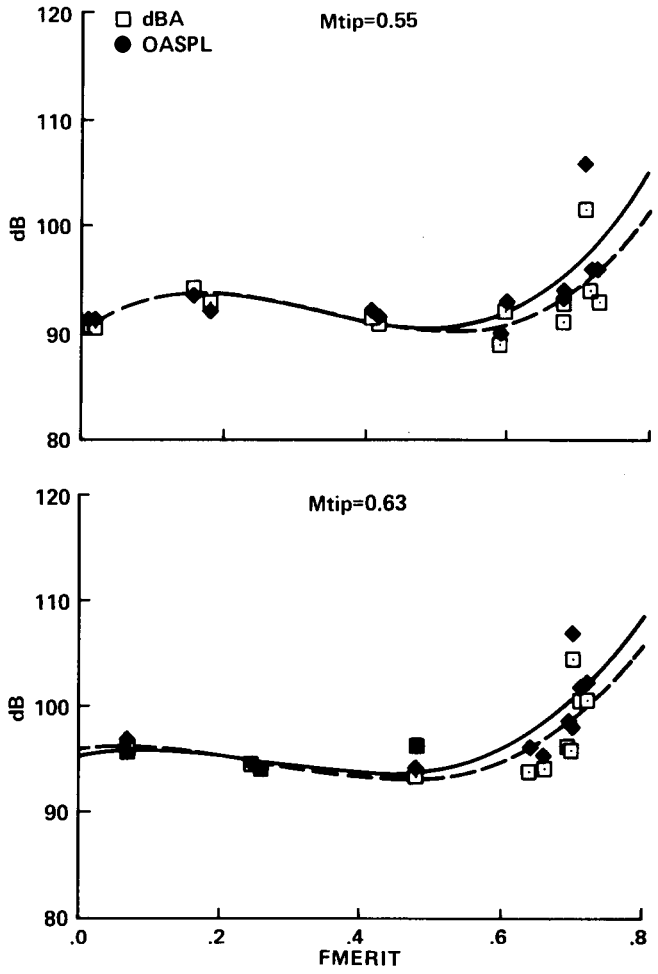

Figure B12.– Acoustic levels as a function of FMERIT at two values of M_{tip}. Microphone No. 9: r/D = 2.0, ψ = 180°, θ = +45°.

APPENDIX C

ACOUSTIC TRENDS AS A FUNCTION OF DISTANCE AND DIRECTIVITY ANGLE

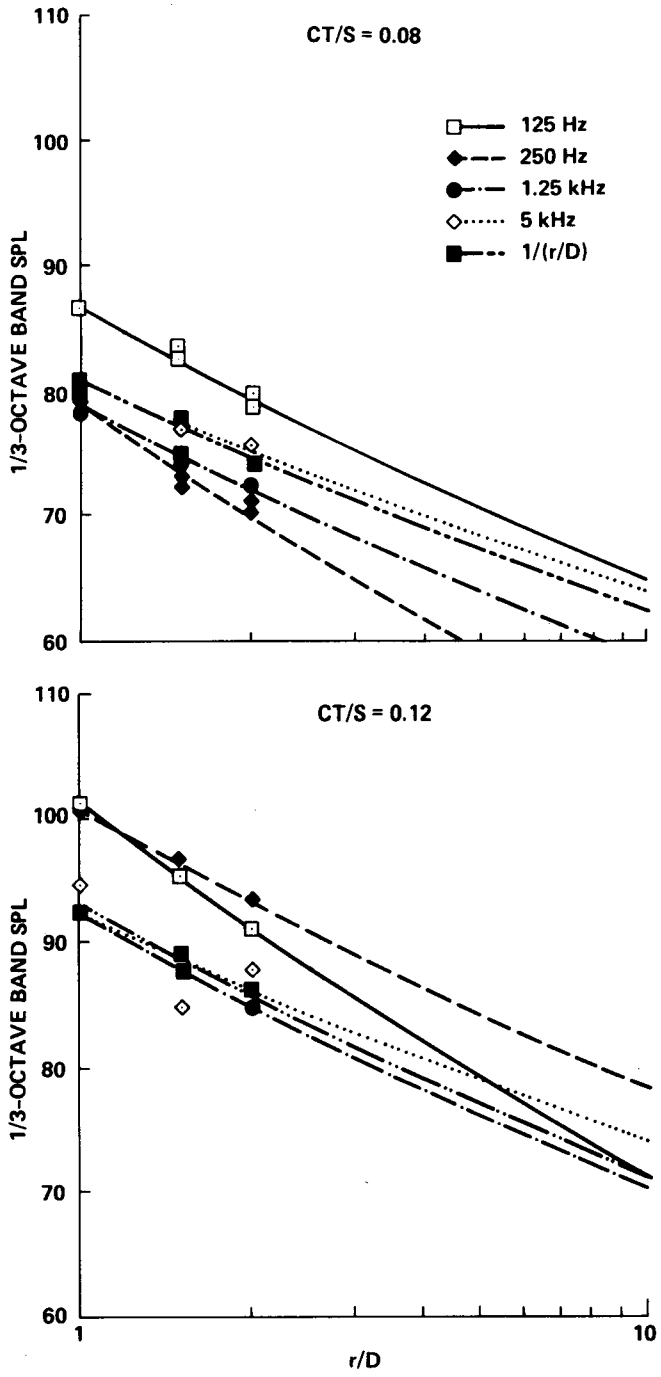

Figure C1.– Acoustic levels at four frequency bands as a function of microphone distance from the rotor hub: $M_{tip} = 0.55$, $\theta = +10°$.

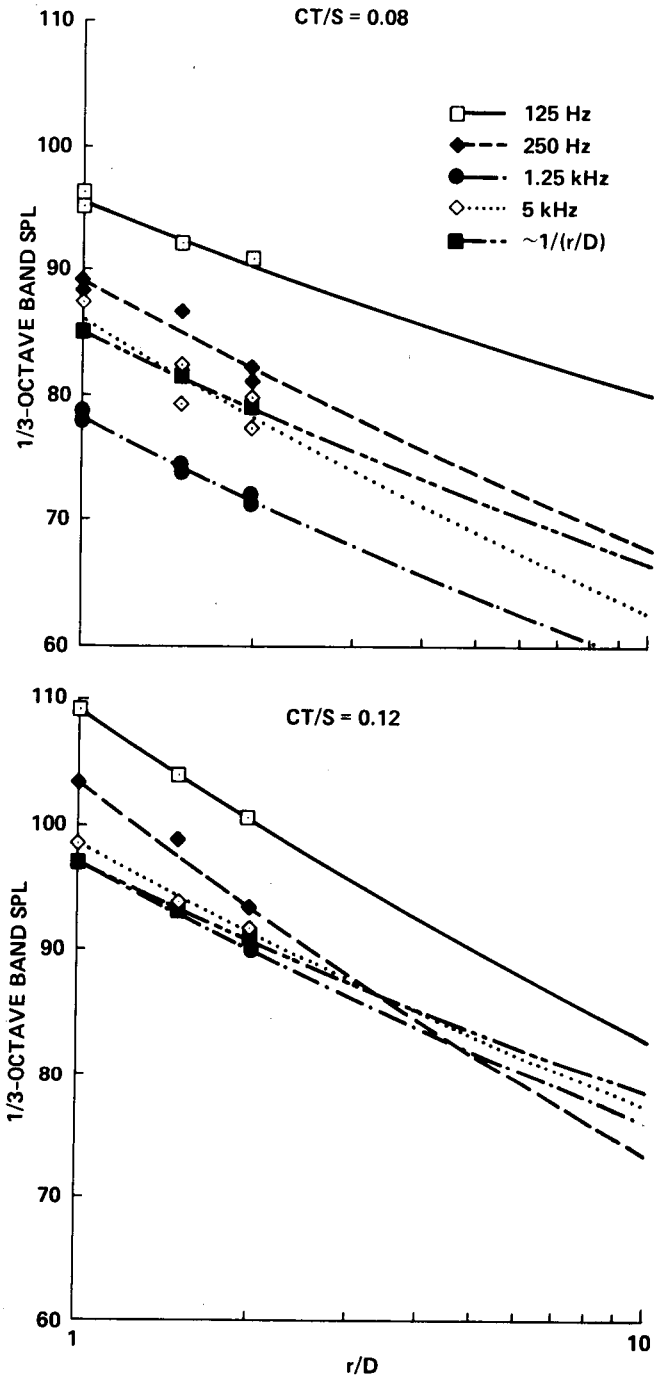

Figure C2.– Acoustic levels at four frequency bands as a function of microphone distance from the rotor hub: $M_{tip} = 0.63$, $\theta = +10°$.

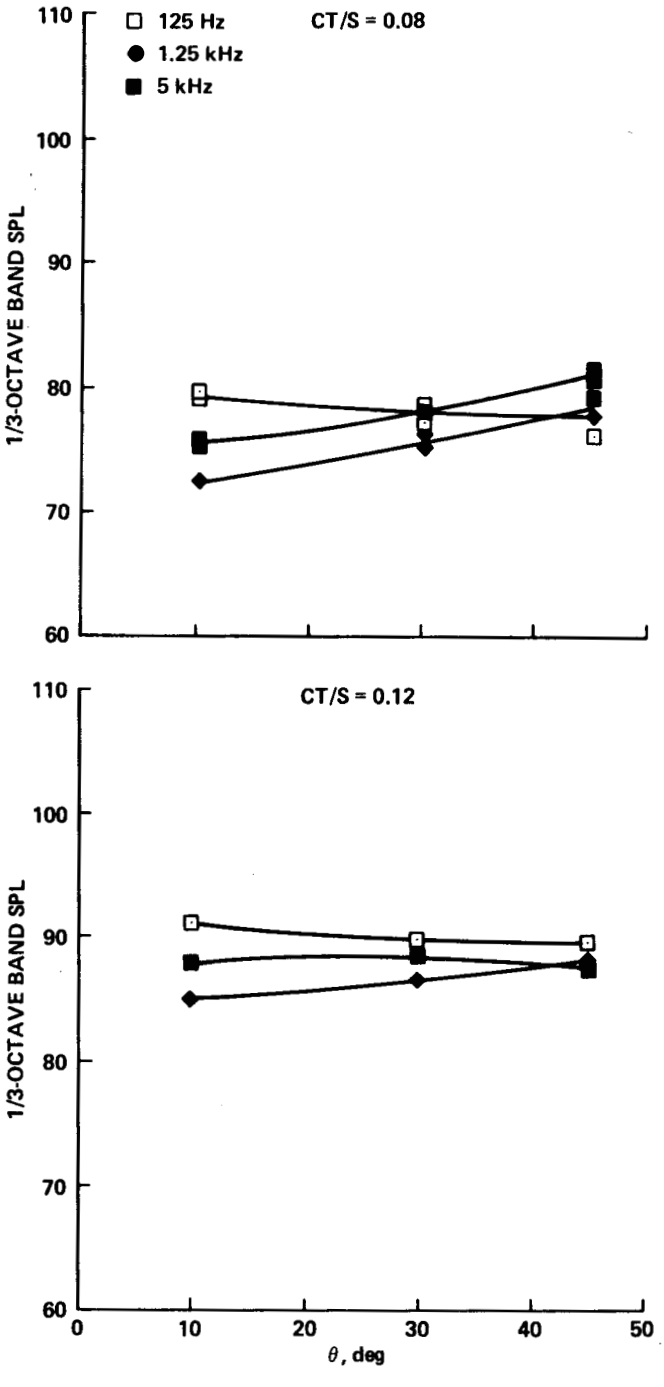

Figure C3.– Acoustic levels at four frequency bands as a function of elevation angle (directivity): $M_{tip} = 0.55$, r/D = 2.0.

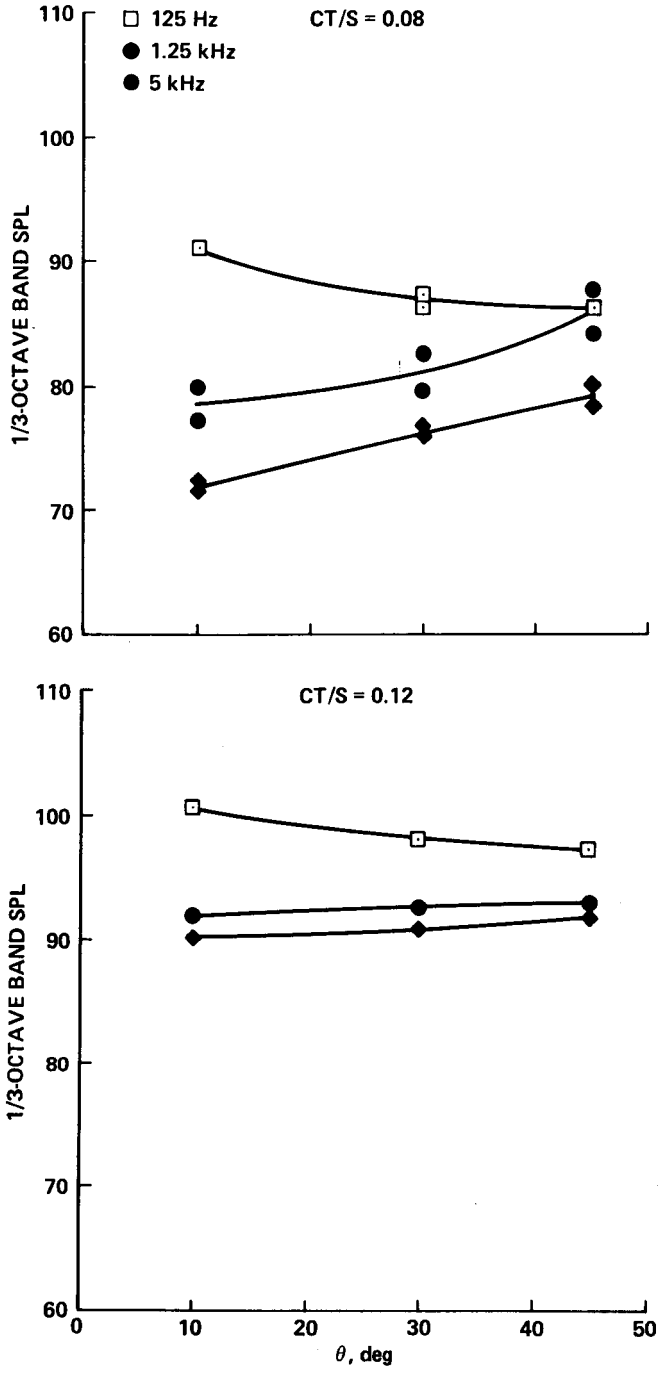

Figure C4.– Acoustic levels at four frequency bands as a function of elevation angle (directivity): $M_{tip} = 0.63$, r/D = 2.0.

NASA National Aeronautics and Space Administration

Report Documentation Page

1. Report No.	2. Government Accession No.	3. Recipient's Catalog No.
NASA TM-101058		

4. Title and Subtitle

The Acoustics of a Small-Scale Helicopter Rotor in Hover

5. Report Date

April 1989

6. Performing Organization Code

7. Author(s)

Cahit Kitaplioglu

8. Performing Organization Report No.

A-89015

10. Work Unit No.

505-61-51

9. Performing Organization Name and Address

Ames Research Center
Moffett Field, CA 94035

11. Contract or Grant No.

13. Type of Report and Period Covered

Technical Memorandum

12. Sponsoring Agency Name and Address

National Aeronautics and Space Administration
Washington, DC 20546 0001

14. Sponsoring Agency Code

15. Supplementary Notes

Point of Contact: Cahit Kitaplioglu, Ames Research Center, MS TR-031, Moffett Field, CA 94035
(415) 694-6679 or FTS 464-6679

16. Abstract

A 2.1-m diameter, 1/6-scale model helicopter main rotor was tested in hover in the test section of the NASA Ames 40- by 80-Foot Wind Tunnel. The primary objective of the test was to obtain performance and noise data on a small-scale rotor at various thrust coefficients and tip Mach numbers for comparison with existing data on similar full-scale helicopter rotors. These data form part of a data base to permit the estimation of scaling effects on various rotor noise mechanisms. A secondary objective was to contribute to a data base that will permit the estimation of facility effects on acoustic testing. Acoustic 1/3-octave-band spectra are presented, together with variation of overall acoustic levels with rotor performance, microphone distance, and directivity angle.

17. Key Words (Suggested by Author(s))	18. Distribution Statement
Rotor Noise Small-scale	Unclassified--Unlimited Subject Category: 02

19. Security Classif. (of this report)	20. Security Classif. (of this page)	21. No. of pages	22. Price
Unclassified	Unclassified	95	A05